Max-Planck-Institut
für Meteorologie

MAX-PLANCK-GESELLSCHAFT

International Max Planck Research School
on Earth System Modelling

Local and Nonlocal Biogeophysical Effects of Deforestation in a Climate Model

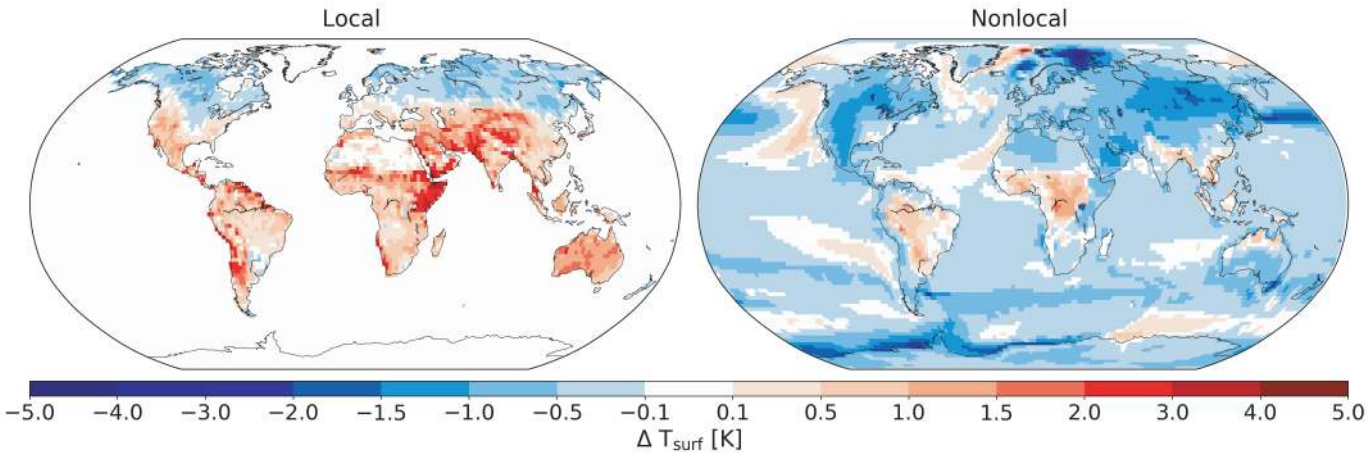

Johannes Winckler

Hamburg 2017

Berichte zur Erdsystemforschung
Reports on Earth System Science

201
2017

Hinweis

Die Berichte zur Erdsystemforschung werden vom Max-Planck-Institut für Meteorologie in Hamburg in unregelmäßiger Abfolge herausgegeben.

Sie enthalten wissenschaftliche und technische Beiträge, inklusive Dissertationen.

Die Beiträge geben nicht notwendigerweise die Auffassung des Instituts wieder.

Die "Berichte zur Erdsystemforschung" führen die vorherigen Reihen "Reports" und "Examensarbeiten" weiter.

Notice

The Reports on Earth System Science are published by the Max Planck Institute for Meteorology in Hamburg. They appear in irregular intervals.

They contain scientific and technical contributions, including Ph. D. theses.

The Reports do not necessarily reflect the opinion of the Institute.

The "Reports on Earth System Science" continue the former "Reports" and "Examensarbeiten" of the Max Planck Institute.

Anschrift / Address

Max-Planck-Institut für Meteorologie
Bundesstrasse 53
20146 Hamburg
Deutschland

Tel./Phone: +49 (0)40 4 11 73 - 0
Fax: +49 (0)40 4 11 73 - 298

name.surname@mpimet.mpg.de
www.mpimet.mpg.de

Layout

Bettina Diallo and Norbert P. Noreiks
Communication

Copyright

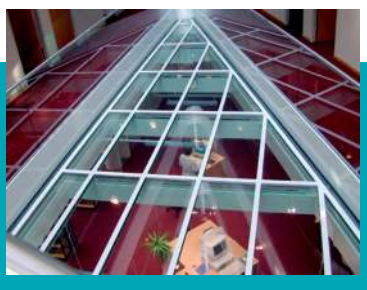

Local and Nonlocal Biogeophysical Effects of Deforestation in a Climate Model

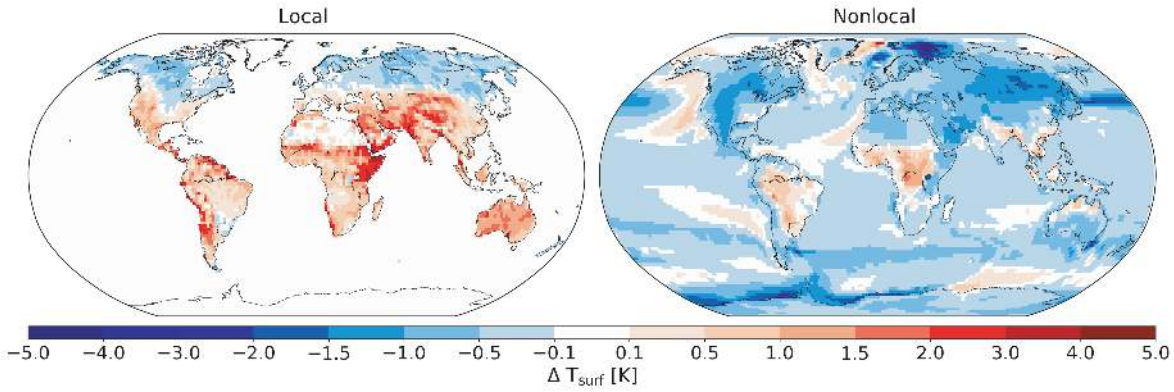

Dissertation with the aim of achieving a doctoral degree
at the Faculty of Mathematics, Informatics and Natural Sciences
Department of Earth Sciences of Universität Hamburg

submitted by

Johannes Winckler

Hamburg 2017

Johannes Winckler

Max-Planck-Institut für Meteorologie
Bundesstrasse 53
20146 Hamburg

Tag der Disputation: 09.11.2017

Folgende Gutachter empfehlen die Annahme der Dissertation:

Prof. Dr. Martin Claußen
Dr. Julia Pongratz

Berichte zur Erdsystemforschung / Max-Planck-Institut für Meteorologie 201
Reports on Earth System Science / Max Planck Institute for Meteorology 2017

ISSN 1614-1199

Contents

Abstract

Land cover change (LCC) influences surface temperature locally via biogeophysical effects by changing the water, energy, and momentum budget. In addition to these locally induced changes (local effects), LCC at a given location can cause changes in temperature elsewhere via advection and changes in circulation (nonlocal effects). This dissertation presents an approach to separate local and nonlocal effects in climate models. In three studies, the local and nonlocal effects on surface temperature are analyzed separately.

First, local and nonlocal effects are separated in the land-atmosphere model ECHAM6/JSBACH3 by simulating LCC in some model grid cells while leaving vegetation unchanged in others. The results show that the local effects do not depend on the number of LCC grid cells used in the separation approach. The local effects on surface temperature in the model agree reasonably well with observations. An energy balance decomposition reveals that the mechanisms differ strongly between the local and nonlocal effects.

In the second part, a new look-up approach is developed to investigate the local effects on historical LCC and LCC in future scenarios. Historically, biogeophysical changes in surface temperature are dominated by land use while in the future, the combination of warming background climate and subsequent natural shifts in the geographical distribution of forests may become of equal importance.

The third part focuses on the nonlocal effects. Simulations with the fully coupled climate model MPI-ESM reveal that the nonlocal cooling of large-scale LCC substantially contributes to the discrepancy between modeled and observed biogeophysical changes in surface temperature. When globally averaged, the deforestation-induced cooling from nonlocal effects outweighs the warming from local effects, and both local and nonlocal effects largely scale linearly with the spatial extent of LCC. The globally averaged nonlocal effects induce a cooling for deforestation in all latitudinal bands. In an inter-model comparison of plausible deforestation scenarios, the nonlocal effects induce a cooling also for most other investigated models.

This thesis bridges the gap between idealized studies on large-scale LCC and studies on more plausible LCC extents. Furthermore, the separate analysis of local and nonlocal effects reconciles previous model-based studies that found a negative radiative forcing from deforestation and a global mean cooling, and observation-based studies that found a deforestation-induced local warming in most regions.

Zusammenfassung

Eine Änderung in der Bedeckung der Landoberfläche ("land cover change", LCC) beeinflusst lokal die Wasser-, Energie- und Impulsbilanz durch biogeophysikalische Effekte. Zusätzlich zu diesen lokal verursachten veränderungen ("lokale Effekte") können Temperaturveränderungen auch durch LCC an anderen Orten ausgelöst werden ("nichtlokale Effekte"). In dieser Doktorarbeit wird eine Methode zum Auftrennen von lokalen und nichtlokalen Effekten in Klimamodellen vorgestellt. In drei Studien werden lokale und nichtlokale Effekte separat voneinander analysiert.

Zunächst werden lokale und nichtlokale Effekte im Land-Atmosphären-Modell ECHAM6/JSBACH3 aufgeteilt, indem in manchen Modell-Gitterzellen LCC simuliert wird, während die Vegetation in anderen Gitterzellen unverändert bleibt. Die Ergebnisse zeigen, dass die lokalen Effekte weitestgehend unabhängig sind von der Anzahl der Gitterzellen, die in der Separationsmethode verwendet werden. Der Einfluss der lokalen Effekte auf die Oberflächentemperatur stimmt im Modell im Großen und Ganzen mit Beobachtungen überein. Eine Zerlegung der Energiebilanz unterstreicht, dass sich die Mechanismen von lokalen und nichtlokalen Effekten stark unterscheiden.

Im zweiten Teil wird eine Methode entwickelt, um die lokalen Effekte für historische und zukünftige LCC zu untersuchen. Historisch werden biogeophysikalische Änderungen in der Oberflächentemperatur von Landnutzung dominiert, aber in der Zukunft kann die Kombination aus zwei Faktoren gleich wichtig werden: erstens das wärmere Hintergrundklima, und zweitens die dadurch bedingten räumlichen Umverteilungen in der Vegetationsbedeckung.

Der dritte Teil konzentriert sich auf die nichtlokalen Effekte. Simulationen im voll gekoppelten Klimamodell MPI-ESM zeigen, dass die nichtlokale Abkühlung im Fall von großflächigem LCC substantiell zur Diskrepanz zwischen modellierten und beobachteten Änderungen der Oberflächentemperatur beitragen. Im globalen Mittel überwiegt nach Entwaldung die Abkühlung durch nichtlokale Effekte gegenüber der Erwärmung durch lokale Effekte, und sowohl lokale als auch nichtlokale Effekte skalieren linear mit der räumlichen Ausdehnung von LCC. Die global gemittelten nichtlokalen Effekte sorgen bei Entwaldung in allen Breitengrad-Bändern für Abkühlung. Im Vergleich von plausiblen Entwaldungs-Szenarien über verschiedene Modelle hinweg bewirken die nichtlokalen Effekte eine Abkühlung auch in den meisten anderen untersuchten Modellen.

Diese Dissertation schließt die Lücke zwischen idealisierten Studien über großflächige LCC und Studien über eine realistischere Ausdehnung von LCC. Außerdem bringt die getrennte Untersuchung von lokalen und nichtlokalen Effekten frühere Studien in Einklang: modellbasierte Studien, in denen Entwaldung zu einem negativen Strahlungsantrieb und einer global gemittelten Abkühlung führte, und beobachtungsbasierte Studien, die in den meisten Regionen eine lokale Erwärmung feststellten.

Chapter 1

Introduction

1.1 Influence of land cover change on climate

Humans have substantially altered the land cover on the Earth's surface in particular via deforestation. More than $14\,\mathrm{M\,km^2}$ of forests (approximately 12% of the global ice-free land surface) have been cleared in the last millennium (Pongratz et al., 2008) mainly for agricultural use, and forest cover has continued to decrease in the 21^{st} century (Hansen et al., 2013). Forests provide a large range of ecosystem services which are put at risk when forests are lost (e.g., Foley et al., 2005). One key ecosystem service that forests provide is their potential to mitigate climate change (Bonan, 2008).

Changes in forest cover affect climate not only by changing the land carbon storage (e.g., Pongratz et al., 2010; Le Quéré et al., 2016) but can also affect the exchange of water, heat and momentum between the land surface and the atmosphere via biogeophysical effects (e.g., Mahmood et al., 2014). Surface albedo increases when dark forests are replaced by brighter grasslands, and thus more incoming solar radiation can be reflected back into space (e.g., Betts, 2000; Boisier et al., 2013). In addition, deforestation decreases the evapotranspiration efficiency –the capability of the land surface to release water to the atmosphere– for instance because forests have deeper roots and a higher leaf area index and thus can transpire more compared to grasslands (e.g., Boisier et al., 2014). Finally deforestation decreases the surface roughness and thus the ability of the land surface to exchange energy and momentum with the atmosphere (e.g., Rotenberg and Yakir, 2010). Changes in surface temperature from biogeophysical effects were found to be small in comparison to the carbon-related effects (Pongratz et al., 2010) but these changes were substantial in regions where deforestation happened (de Noblet-Ducoudré et al., 2012).

Changes in land cover comprise not only deforestation but also include changes between other land cover types such as conversions from grasslands to croplands. This thesis focuses on the conversion from forests to grasslands or vice versa, and throughout this

thesis the term 'land cover change' (LCC) refers to the conversion between these two land cover types. The physical surface properties of natural grasslands, croplands, shrubs and pastures are similar, and thus considering only the conversion between forests and grasslands is sufficient to cover the potential range of responses to land cover change (Gibbard et al., 2005).

A major achievement of this thesis is the development of a new method that enables the separation of effects that are induced by LCC locally and effects that extend beyond the deforested locations in climate models. The following sections provide a context for the local and nonlocal effects and outline the contribution of this work to a better understanding of both local and nonlocal effects.

1.2 Biogeophysical effects of LCC in climate models

1.2.1 Local and nonlocal impacts of LCC on the surface energy balance

Deforestation impacts surface temperature by changing the components of the surface energy balance (Figure 1.1). At the surface, the available energy (given as surface shortwave net radiation (SW_{net}) plus incoming surface longwave radiation ($LW_{\downarrow}$)) is on an inter-annual timescale partitioned into outgoing surface longwave radiation ($LW_{\uparrow}$), latent heat (LE), and sensible heat (H) (e.g., Luyssaert et al., 2014). Locally, a change in any surface property due to LCC may influence any component of the surface energy balance. For instance, an increase in surface albedo may decrease SW_{net}, and this may locally be balanced by a decrease in the turbulent heat fluxes LE and H, and/or by a decrease in $LW_{\uparrow}$ which is via the Stefan–Boltzmann law associated with a decrease in surface temperature (e.g., Boisier et al., 2014). These locally induced changes in the surface energy balance then influences the atmospheric conditions. For instance, a change in LE or H influences the humidity and temperature of the atmosphere above the deforested location.

Deforestation-induced changes in atmospheric moisture or temperature are then transferred to other regions via advection (e.g., West et al., 2011). There, the surface energy balance is in turn influenced by the changes in the atmospheric conditions. For instance, changes in precipitation may affect LE and H, or changes in atmospheric temperature and humidity may affect $LW_{\downarrow}$. Via such mechanisms, the surface energy balance and surface temperature may also be influenced at locations that experience no LCC.

Throughout this thesis, locally induced changes in surface temperature are referred to as 'local effects' whereas changes in surface temperature that also happen at locations where land cover does not change are referred to as 'nonlocal effects'. The sum of local and nonlocal effects is referred to as 'total effects'. The total effects were the subject of

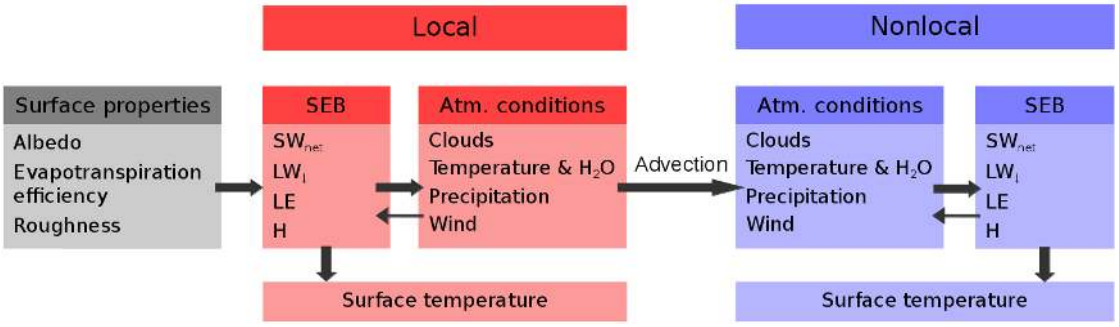

Figure 1.1: Surface temperature is affected by LCC via changes in components of the surface energy balance ("SEB"). Some changes happen only at the location of LCC ("Local", red) and some changes happen also at locations that are not deforested ("Nonlocal", blue).

most previous modeling studies on the biogeophysical effects of LCC because local and nonlocal effects could not be distinguished. Studies on the LCC effects can broadly be divided into two categories: idealized studies that simulate LCC in large areas and studies that simulate plausible areal extents and spatial distributions of LCC. One aim of this thesis is to establish a link between these two types of studies. The following subsections outline the context and the research objectives of the three main chapters.

1.2.2 Separating local and nonlocal effects in simulations of large-scale LCC

In order to investigate the biogeophysical effects of LCC, previous studies simulated global-scale deforestation (e.g., Bala et al., 2007; Brovkin et al., 2009; Davin and de Noblet-Ducoudré, 2010) or deforestation of large latitudinal bands (e.g., Claussen et al., 2001; Swann et al., 2012; Devaraju et al., 2015). One reference simulation was performed in which forests are prescribed over a specific region, and the climate in this reference simulation was compared to the climate in a simulation where vegetation in the respective region was replaced by grasslands. These studies revealed that boreal deforestation leads to a cooling because of a large increase in surface albedo (e.g., Bonan et al., 1992; Devaraju et al., 2015) while tropical deforestation leads to a regional warming because the grasslands can transpire less compared to forests (e.g., Lejeune et al., 2015) and cloud cover decreases (e.g., Claussen et al., 2001).

These studies share one notable limitation: The local and nonlocal effects mingle in these simulations, and thus it is impossible to distinguish between the two effects in regions of LCC. For two major reasons a separation of local and nonlocal effects in simulations of large-scale LCC may be desirable: First, observation-based datasets by construction only contain local effects (e.g., Li et al., 2015; Alkama and Cescatti, 2016; Bright et al., 2017), while model simulations can contain substantial nonlocal effects (Swann et al., 2012; Devaraju et al., 2015). Thus, an isolation of the local effects in the models is essential for a consistent comparison of modeled and observed LCC effects on

the global scale. Second, the physical mechanisms underlying the local and nonlocal effects differ strongly (Figure 1.1) and thus a separate assessment of the two effects may enable a deeper process understanding for both local and nonlocal effects. Without a deeper process understanding the biogeophysical effects can not be considered as a tool for adaptation at the locations of LCC or for climate change mitigation at regions far away from LCC. In **chapter 2**, a new method for the separation of local and nonlocal effects is developed and applied to simulations of global-scale LCC in the land-atmosphere model ECHAM6/JSBACH3 (Giorgetta et al., 2013; Reick et al., 2013) to close these existing research gaps:

- To enable an attribution of changes in surface temperature to local LCC in any climate model, and to assess whether the local effects in one location are influenced by LCC in other locations.
- To enable a consistent comparison of the local effects in climate models to global-scale observations.
- To gain process understanding about the mechanisms that trigger local and nonlocal effects.

1.2.3 Investigating the local effects in plausible LCC scenarios

While the idealized simulations of large-scale LCC provide process understanding, they do not represent LCC that may happen in reality. Both for historical LCC and plausible scenarios of future development, LCC does not happen in large latitudinal bands or globally but instead in smaller spatial extents. Furthermore, in plausible scenarios LCC is not distributed homogeneously in space but concentrates in specific areas, for instance in North America and Eurasia in the case of historical LCC. Because of these differences the climatic impacts may differ between scenarios of large-scale and plausible LCC.

Previous studies aimed at identifying robust impacts of the biogeophysical effects across models, both for historical land use (Pitman et al., 2009; de Noblet-Ducoudré et al., 2012; Boisier et al., 2012) and land use in plausible future scenarios (Brovkin et al., 2013a; Boysen et al., 2014). In regions in North America and Eurasia where land use was simulated, historical land use was found to exert a cooling of similar magnitude than the impact of elevated greenhouse gases (de Noblet-Ducoudré et al., 2012), but the inter-model spread was found to be large (e.g., Pitman et al., 2009). This inter-model spread may originate from several factors: First, models differ not only in their parameterizations but also in the distribution of land use regions (Boisier et al., 2012). Second, land use happens in each models' specific background climate which may substantially influence the land use effects (Pitman et al., 2011). Third, models differ

in their representation of natural shifts in the spatial distribution of vegetation (e.g., Sitch et al., 2008).

A thorough analysis of the inter-model spread, and thus process understanding, was further exacerbated by the poor signal-to-noise ratio of the total biogeophysical effects (e.g. Boysen et al., 2014). The isolated local effects, on the other hand, are by construction largely free of climate variability (e.g., Kumar et al., 2013; Malyshev et al., 2015). Thus, the local effects provide a testbed to understand differences across models (Lejeune et al., 2017b).

Not only models differ in the three factors described above, but also historical LCC differs from scenarios of future LCC. Thus, also within one model, process understanding may benefit from comparing the local effects of LCC across different scenarios. This is the focus of **chapter 3**, where the local effects for historical LCC and scenarios of future LCC are analyzed to achieve the following:

- To quantify the locally induced changes in surface temperature for three factors: land-use–induced LCC, warming background climate, and natural changes in the spatial distribution of forests.
- To consistently compare these factors across scenarios within one model and using one set-up.

In order to assess the local effects in the LCC scenarios, a newly developed look-up approach serves to convert changes in forest fraction within a grid cell into a change in surface temperature. For this approach, an investigation is required whether surface temperature within any model grid cell responds nonlinearly to local changes in forest cover. Such a nonlinearity may affect the results because the pre-LCC forest fractions differ across scenarios. Thus, chapter 3 investigates to what extent such a nonlinearity contributes to differences of the local effects across scenarios.

1.2.4 Investigating the nonlocal LCC effects

Deforestation may substantially influence climate far away from the region where LCC happens. For instance, deforestation may shift precipitation bands (Swann et al., 2012), and the shifts in precipitation may even be large for deforestation in remote regions (Devaraju et al., 2015). Furthermore, deforestation may substantially cool sea surface temperatures (e.g., Ganopolski et al., 2001) and this may even switch the sign of the deforestation response from warming to cooling (Davin and de Noblet-Ducoudré, 2010). However, despite their possible importance the nonlocal effects could not be investigated in previous studies, at least not in regions where also LCC happened, because the local and nonlocal effects could not be distinguished.

It stands to reason that the nonlocal effects may differ strongly between the studies of large-scale LCC and plausible LCC. The nonlocal effects may be stronger if more

area is deforested. Furthermore, the nonlocal effects might be different in simulations where LCC is geographically homogeneously distributed, concentrated in latitudinal bands or in plausible LCC scenarios. However, because the nonlocal effects could not be isolated, the link between studies of large-scale and plausible LCC could previously not be established. In **chapter 4**, this research gap is closed and the nonlocal effects are analyzed in simulations with the fully coupled MPI-ESM (Giorgetta et al., 2013) to achieve the following:

- To investigate to what extent the nonlocal effects contribute to differences between the biogeophysical effects in models and observations.
- To assess the dependence of the nonlocal effects on the areal extent and spatial distribution of LCC.
- To explore the role of changes in surface albedo for the nonlocal effects.
- To integrate the biogeophysical effects into a broader context by comparing the magnitudes of the globally averaged temperature changes from local and nonlocal effects to temperature changes from LCC-induced changes in land carbon storage.

Chapter 4 focuses on the nonlocal effects in the MPI-ESM. The analysis within this one model is beneficial for gaining process understanding, but the exact quantification of the nonlocal effects may be different in other models. Thus, for an overview over the nonlocal effects of plausible LCC in other fully coupled climate models, chapter 4 also provides an inter-model comparison.

Chapter 2

Robust identification of local biogeopysical effects of land cover change in a global climate model[1]

Land cover change (LCC) happens locally. However, in almost all simulation studies assessing biogeophysical climate effects of LCC, local effects (due to alterations in a model grid cell) are mingled with nonlocal effects (due to alteration in wide-ranging climate circulation). This study presents a method to robustly identify local effects by changing land surface properties in selected "LCC cells" (where local plus nonlocal effects are present), while leaving others unchanged (where only nonlocal effects are present). While this study focuses on climate effects of LCC, the method presented here is applicable to any land surface process that is acting locally but capable of influencing wide-ranging climate when applied on a larger scale. Concerning LCC, the method is more widely applicable than methods used in earlier studies. The study illustrates the possibility of validating simulated local effects by comparison to observations on a global scale, and contrasts the underlying mechanisms of local and nonlocal effects. In the MPI-ESM, the change in background climate induced by extensive deforestation is not strong enough to influence the local effects substantially, at least as long as sea surface temperatures are not affected. Accordingly, the local effects within a grid cell are largely independent of the number of LCC cells in the isolation approach.

2.1 Introduction

Humans have altered the land surface extensively by changing land cover, e.g., by replacing forests with grasslands (e.g., Pongratz et al., 2008). Such land cover change

[1]This chapter has been published with minor modifications as "**Winckler, J.**, C. H. Reick and J. Pongratz (2017), Robust identification of local biogeopysical effects of land cover change in a global climate model, J. Clim., **30**(3), 1159-1176, doi:10.1175/JCLI-D-16-0067.1."

(LCC) not only affects the carbon balance (IPCC, 2013), but also disturbs the energy and hydrological balance of the land surface via biogeophysical effects: First, surface albedo increases when replacing a forest with a typically brighter grassland, reflecting more sunlight and altering the surface shortwave radiation budget (e.g., Bonan, 2008); Second, LCC induces changes in non-radiative properties, such as evapotranspiration efficiency (as defined in the study by Davin and de Noblet-Ducoudré (2010)) and surface roughness. These biogeophysical effects can alter climate within a grid cell undergoing LCC, which we refer to as the "local effects". However, additionally to these locally induced effects, climate within a grid cell can also be altered by LCC in nearby or remote grid cells, which we refer to as "nonlocal effects".

In the past, two types of studies have been performed to quantify and understand the effects of LCC: Studies investigating plausible LCC scenarios and studies investigating idealized extensive LCC. The first type investigated the climate effects of plausible LCC scenarios such as the historical evolution of land-use–induced LCC or future LCC (e.g., Pitman et al., 2009; Boysen et al., 2014), based on scenarios derived from socio-economic models (e.g., Hurtt et al., 2011). Considering temperature on the local scale, the biogeophysical (BGP) effects of historical LCC have been simulated to have similar magnitude as the effect of the increase in greenhouse gases since the preindustrial period (de Noblet-Ducoudré et al., 2012). However, models do not agree in sign and amplitude of temperature changes following land-use–induced LCC, neither regionally nor globally (e.g., Pitman et al., 2009; Boysen et al., 2014). Part of the uncertainty in studies on plausible LCC scenarios originates from the fact that in most grid cells, these scenarios alter only a small fraction of the vegetation cover. This results in a climatic signal that is small compared to weather-related noise, especially as regions with a large historical land-use–induced LCC are located in the northern temperate latitudes, where weather-related noise is high (e.g., Mahlstein et al., 2011).

The second type of LCC study investigated the effects of idealized extensive (instead of plausible) LCC, such as complete deforestation of wide latitudinal bands (e.g., Claussen et al., 2001; Bala et al., 2007; Bathiany et al., 2010), with a focus on understanding the more general role of vegetation changes in the Earth system. While such idealized simulations improve the signal/noise ratio, they also feature substantial nonlocal effects, because extensive changes in surface properties can alter global circulation (e.g., Goessling and Reick, 2011; Swann et al., 2012). Within a region, the nonlocal effects can even be larger than the local effects of deforestation (Devaraju et al., 2015). However, in the traditional approach of simulating spatially homogeneous LCC in *every* grid cell within a large region, local and nonlocal effects are mingled and cannot be distinguished. This brings complications: Observations of LCC effects only comprise the local LCC effects because they compare climate in forested areas with nearby open land, and thus both weather-related noise and nonlocal effects cancel. Thus, the total (local plus nonlocal) simulated effects cannot be compared to observations consistently. In addition, simulations of idealized extensive LCC cannot represent the effects of any plausible LCC scenario due to substantial nonlocal effects. In particular, with the

model set-up used in most previous studies, the results within a grid cell are not only determined by the extent of LCC within that grid cell, but also strongly dependent on LCC in neighboring or remote grid cells, see e.g. the boreal cooling simulated for tropical deforestation due to a reduction in atmospheric water vapor (Claussen et al., 2001). Therefore, the total effect of LCC within a grid cell strongly depends on the chosen geographical distribution of LCC cells, impeding inference of the climatic relevance of LCC in a specific grid cell from one global LCC distribution to the other.

The local effects have been implicitly isolated for historical and future projected LCC (Kumar et al., 2013) in order to deal with the problem of low signal/noise-ratio in plausible LCC scenarios. Similar to observational studies, they compare climatic changes in grid cells with LCC to climatic changes in grid cells without LCC within a region where changes in climatic conditions are assumed to be homogeneous, and thus both weather-related noise and nonlocal effects cancel. Malyshev et al. (2015) isolate local effects in a model that calculates canopy air temperature separately for each land use type within a grid cell. They calculate local effects as the temperature difference between the different land use types within a grid cell. Furthermore, they compare their local effects with the total effects that result from the typical model set-up of earlier studies comparing a simulation with LCC to a reference with undisturbed vegetation. Here, we present a method to isolate the local effects by specifying regularly spaced "LCC cells" (where both local plus nonlocal effects are present) and "no-LCC cells" (where only nonlocal effects are present). The presented approach goes beyond the previous approaches in several respects: First, it provides information on the local effects in every land grid cell globally, and avoids applying ad-hoc thresholds in the amount of LCC to identify areas of LCC as in the study by Kumar et al. (2013). Second, our set-up captures all simulated land-atmosphere feedbacks within a grid cell, even via local changes in clouds and precipitation. This complements previous studies calculating local effects using offline models (e.g., West et al., 2011) or a subgrid tile approach as in the study by Malyshev et al. (2015). Third, our method is applicable to all DGVMs, even if they do not calculate temperature for each subgrid tile separately, as in the study by (Malyshev et al., 2015).

In this study, we examine the sensitivity of the local effects to the number of LCC cells used in this separation method. Potentially, a high number of LCC cells could change background climate strong enough to influence the local effects (Pitman et al., 2011). We assess if the change in background climate via the nonlocal effects is strong enough to influence the local effects substantially, or whether we can still robustly identify the local effects. To this end, we compare the local effects in two extreme cases: LCC only at a few grid cells, similar to plausible LCC scenarios, and LCC in almost all grid cells, representative for idealized extensive LCC. If the local effects can be identified irrespective of the number of LCC cells, this isolation is a step towards consistent comparison of LCC effects between models and observational datasets. The presented method allows for isolating the local, but also to additionally quantify the nonlocal effects. This separation of local and nonlocal effects opens ways for a better

understanding of the processes underlying the climatic effects of LCC and related interactions with local and large-scale climate.

2.2 Methods

2.2.1 Model and set-up

We use the Max-Planck-Institute Earth System Model (MPI-ESM), which has been validated in depth with respect to the energy and hydrological balance at the land surface by Hagemann et al. (2013). Deforestation effects in an offline land surface model differ substantially from the results in a set-up accounting for atmospheric feedbacks (Gibbard et al., 2005). Thus, we choose a configuration with the land surface model JSBACH (Reick et al., 2013) coupled to the atmospheric model ECHAM6 (Giorgetta et al., 2013) with horizontal resolution T63 (approximately 2° at the equator) and 47 vertical layers. In each simulation, we use the last 30 out of 35 years (1976-2005) for analysis. To exclude carbon effects of LCC and thus isolate the BGP effects, we prescribe CO_2 from the historical simulation performed within the Coupled Model Intercomparison Project, Phase 5 (CMIP5) by the fully coupled MPI-ESM. From this simulation, we also prescribe 1976-2005 inter-annually varying SSTs and sea ice in order to reduce weather-related noise induced by ocean variability. A similar set-up has been used in an intercomparison of the BGP effects of historical land-use–induced LCC, where ECHAM5/JSBACH was within the range of the other models, both for radiative and non-radiative processes (Boisier et al., 2012). Prescribing SST substantially influences simulated LCC effects (Davin and de Noblet-Ducoudré, 2010). Nevertheless, SSTs are prescribed by purpose in our study in order to identify the local effects of LCC more clearly – its only the nonlocal effects that are affected by land-ocean interactions. This issue is further discussed in the "Discussions and Conclusions" section.

As described in the next paragraph, we choose two set-ups, in each of which land cover is changed in some grid cells ("LCC cells"), and land cover remains unchanged at other grid cells. For each of the two spatial distributions of LCC cells described below, we perform two simulations: In the first simulation, we set the vegetated part in the LCC cells to 100% forest cover. In the second simulation, we set the vegetated part of the LCC cells to 100% grass cover. When scaling to 100% grass cover, we keep the ratio between C3 and C4 grasses, and when scaling to 100% forest cover, we keep the ratio between the four forest PFTs in JSBACH (tropical broadleaf evergreen, tropical broadleaf deciduous, extratropical evergreen, extratropical deciduous). In the remaining "no-LCC cells" we do not change land cover, but prescribe present-day land cover (the CMIP5 mean state of 1976-2005) in both simulations. We calculate the total deforestation effect as the difference between these two simulations.

2.2.2 Definition of sparse and extensive LCC

We are interested in the local LCC effects. The most accurate way to directly simulate these local effects at a given grid cell would be to simulate LCC at only this one grid cell. However, this would require one "forest" and one "grass" simulation for each land grid cell. Our approach to reduce the number of required simulations is to change land cover in more than one land grid cell per simulation pair. First, we deforest one out of eight grid cells (gray grid cells in Fig. 2.1*b*), which we define as *sparse LCC*. The local effects can then be separated as described in the next subsection. This scheme of sparse LCC is a trade-off: By deforesting only a small number of grid cells, we can assume that the deforestation effects of any two cells do not influence each other substantially, but we can still get information about the local effects on a global scale.

The choice of 1 out of 8 LCC cells seems arbitrary. To test the sensitivity of the local effects to the number of LCC cells, we choose an additional scheme of deforestation in 7 out of 8 grid cells (gray grid cells in Fig. 2.1*g*), which we define as *extensive LCC*. This choice of the extensive LCC scheme is again a trade-off: It approximates the case of the maximal possible number of LCC cells, but still allows us to separate local and nonlocal effects, as explained below. The two LCC schemes only differ in the number of LCC cells. We prescribe the same SSTs as in the sparse LCC case in order to ensure comparability of the results.

2.2.3 Separation of local and nonlocal effects

We define the local effects within a grid cell as the changes that are present only due to changes in surface properties of only this one grid cell. We define the nonlocal effects as LCC-induced changes that arise remotely from the location of LCC, mediated e.g. by induced changes in circulation. In our set-up of introducing LCC only in the LCC cells, nonlocal effects may be active in both LCC cells and no-LCC cells. In the following, we assume that the total effects in LCC cells consist of the sum of local and nonlocal effects, while the total effects in no-LCC cells consist of only nonlocal effects.

Several computational steps are necessary to separate local and nonlocal contributions to the total effect of LCC. These steps are illustrated in the subfigures of Fig. 2.1:

(a) From the described pair of simulations we identify the total effects of LCC.

(b) The nonlocal effects can be seen in the no-LCC cells (colored grid cells in Fig. 2.1*b*).

(c) We assume that these nonlocal effects are present also *at the LCC cells*. We obtain the nonlocal effects at the LCC cells by horizontal interpolation.

(d) We then calculate the local effects at the LCC cells. To this, we assume that both local and nonlocal effects are present within LCC cells. Consequently, in order

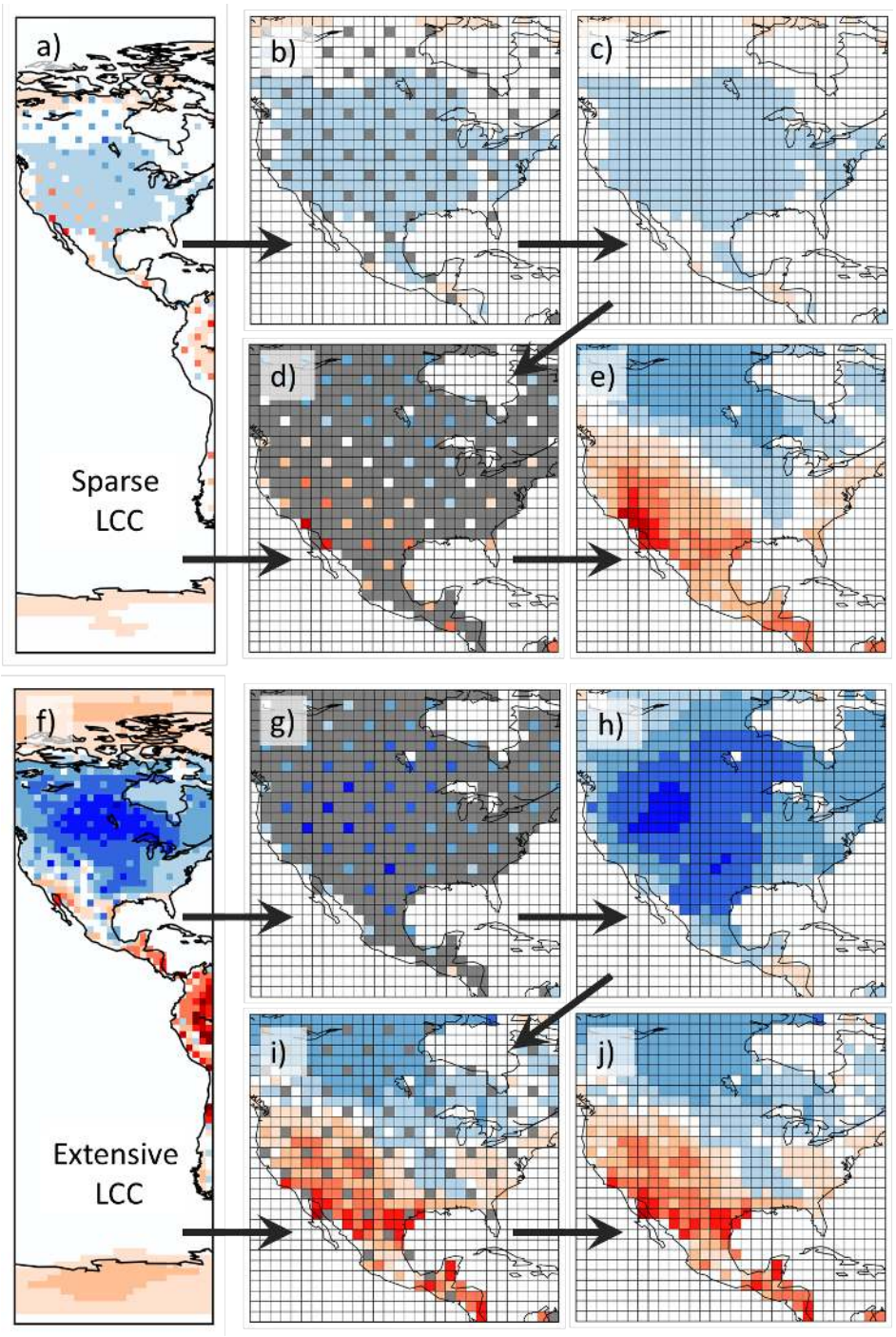

Figure 2.1: Sketch illustrating the separation approach (arbitrary color scale). The simulation result, the total effects, is depicted in subfigure a. The LCC grid cells stand out because there, the total effects (local plus nonlocal) are mostly stronger than in the surrounding no-LCC grid cells (only nonlocal). The nonlocal effects at no-LCC cells can be seen in b. The nonlocal effects are interpolated to LCC cells c. The difference at the LCC cells between total effects a and interpolated nonlocal effects c is shown in d, which we then interpolate in order to obtain global information on the local effects e. This approach works analogously for extensive deforestation $f - j$. Grid cells whose information is not used for interpolation in b, d, g, and i are shown in gray. For results on local and nonlocal effects see Fig. 2.2.

to obtain the local effects *at the LCC cells*, we substract the nonlocal effects, as calculated in the previous step, from the total effects (local plus nonlocal).

(e) Finally, we obtain a global map of the local effects by interpolation of the identified local effects from the LCC cells to all land grid cells.

The local contribution to the total effects of LCC is in a statistical sense "cleaner" than the simulated total effects: for the total effects a longer simulation period is needed to decrease the signal/noise ratio compared to the signal/noise ratio of the local effects (Fig. A.1.1), because climate variability (e.g., Deser et al., 2012) is by construction mostly contained in the nonlocal effects. Simulating longer time periods than 30 years does not increase the signal/noise ratio for the local effects, as demonstrated in Appendix A.1.

Both approaches, sparse and extensive LCC, include horizontal interpolation from one out of eight grid cells (for the interpolation of local or nonlocal effects, respectively). The error associated with interpolation depends on the distance between the interpolation knots, so the distance between the grid cells that the values are interpolated from. In order to assess the interpolation errors in the performed simulations, and to decrease dependence on the location of the LCC cells, we repeat all simulations with the LCC cells shifted by two. For the further analysis, we average local effects obtained from the unshifted and shifted simulations, and apply the same averaging to the nonlocal effects. Details on the interpolation method and interpolation errors are presented in Appendix A.4.

2.2.4 Energy balance decomposition

In the presented results, we contrast the mechanisms underlying local and nonlocal effects. For the exploration of these mechanisms, we employ an energy balance decomposition approach as in, e.g., the study by Luyssaert et al. (2014). Here, we provide a short introduction to this method, in which a change in simulated surface temperature can be split into contributions from the individual terms of the surface energy balance.

The surface energy budget is balanced between shortwave and longwave net radiation ($\mathrm{SW_{net}}$ and $\mathrm{LW_{net}}$), latent heat (LE), sensible heat (H) and a residual term (G, mainly consisting of ground heat flux):

$$\mathrm{SW_{net}} + \mathrm{LW_{net}} = \mathrm{LE} + \mathrm{H} + \mathrm{G}. \tag{2.1}$$

The component $\mathrm{LW_{net}}$ can be rewritten by applying the Stefan-Boltzmann law:

$$\mathrm{LW_{net}} = \epsilon \mathrm{LW_{down}} - \mathrm{LW_{up}} = \epsilon \mathrm{LW_{down}} - \sigma \epsilon \mathrm{T^4_{surf,}} \tag{2.2}$$

where σ is the Stefan-Boltzmann constant, ϵ is emissivity and is set to 1, and $\mathrm{T_{surf}}$ is surface temperature. Inserting (2.2) into (2.1), we obtain

$$\sigma T^4_{\mathrm{surf}} = \mathrm{SW_{net}} + \mathrm{LW_{down}} - \mathrm{LE} - \mathrm{H} - \mathrm{G}.$$

Applying the total derivative, we obtain

$$\Delta T_{surf} = \frac{1}{4\sigma T_{surf}^3}\left(\Delta SW_{net} + \Delta LW_{down} - \Delta LE - \Delta H - \Delta G\right).$$

Because the multi-year mean ground heat flux is largely unaffected by deforestation (not shown), we omit the residual term ΔG in the further analysis. Note that the energy balance decomposition approach does not allow us to attribute changes in the energy balance to changes in surface properties. As an example, a simulated change in LE could originate from a change in surface albedo, evapotranspiration efficiency, surface roughness, or a combination of all three (Davin and de Noblet-Ducoudré, 2010). However, the surface energy balance decomposition (see Fig. 1.1) illustrates the importance of changes in the individual flux terms that each are influenced by changes in various surface properties and include feedbacks.

2.3 Contrasting local and nonlocal effects of global deforestation

2.3.1 Mechanisms underlying local and nonlocal effects differ

To study the effects of global deforestation, we contrast the local and nonlocal effects from the extensive LCC experiment. The local effects of deforestation on surface temperature in ECHAM6/JSBACH are a warming in the tropics and a cooling in the northern high latitudes (Fig. 2.2 *b*). This is in accordance with the local effects shown in the study by Malyshev et al. (2015) and qualitatively also in accordance with previous idealized extensive LCC studies that considered the total (local plus nonlocal) effects (e.g. Claussen et al., 2001; Davin and de Noblet-Ducoudré, 2010). The dynamic global vegetation model JSBACH is known to underestimate bare land fraction in subtropical deserts (Brovkin et al., 2013b), which explains why there are still substantial local effects in these regions. Note that 2m-air temperature responds much weaker to LCC as compared to surface temperature, see Appendix A.3. Precipitation decreases in the local effects in the northern temperate and boreal regions, and even more strongly in the humid tropics (Fig. 2.3 *b*). Concerning the total effects, most previous studies hinted at a decrease in rainfall, e.g., for deforestation of the Amazon rainforest (Lejeune et al., 2015).

The nonlocal effects for surface temperature (Fig. 2.2 *d*) and precipitation (Fig. 2.3 *d*) are similar in magnitude as compared to the local effects. While for both effects, temperature is increased and precipitation is reduced in the Amazon region and central Africa, there are also regions where local and nonlocal effects disagree significantly in sign (Fig. 2.2 *b* versus 2.2 *d* and 2.3 *b* versus 2.3 *d*). These are, e.g., the southern part of Australia, where the local effects show a warming while the nonlocal effects are cooling,

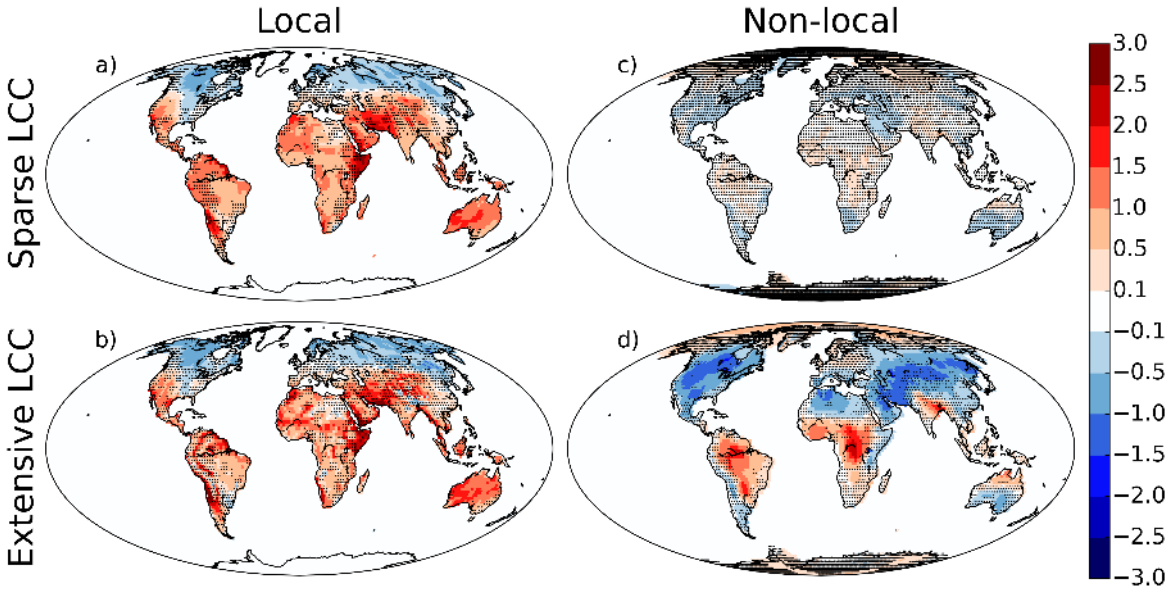

Figure 2.2: Change in mean surface temperature [K] due to *a*,*c* sparse and *b*,*d* extensive deforestation. *a*,*b* local effects, *c*,*d* nonlocal effects. Mean over 30 years and another 30 years from a simulation with LCC cells shifted by two. Statistical significance is calculated according to a 5 % level in a Student's t-test accounting for autocorrelation (Zwiers and von Storch, 1995). Note that we mark grid cells that are *not* statistically significant.

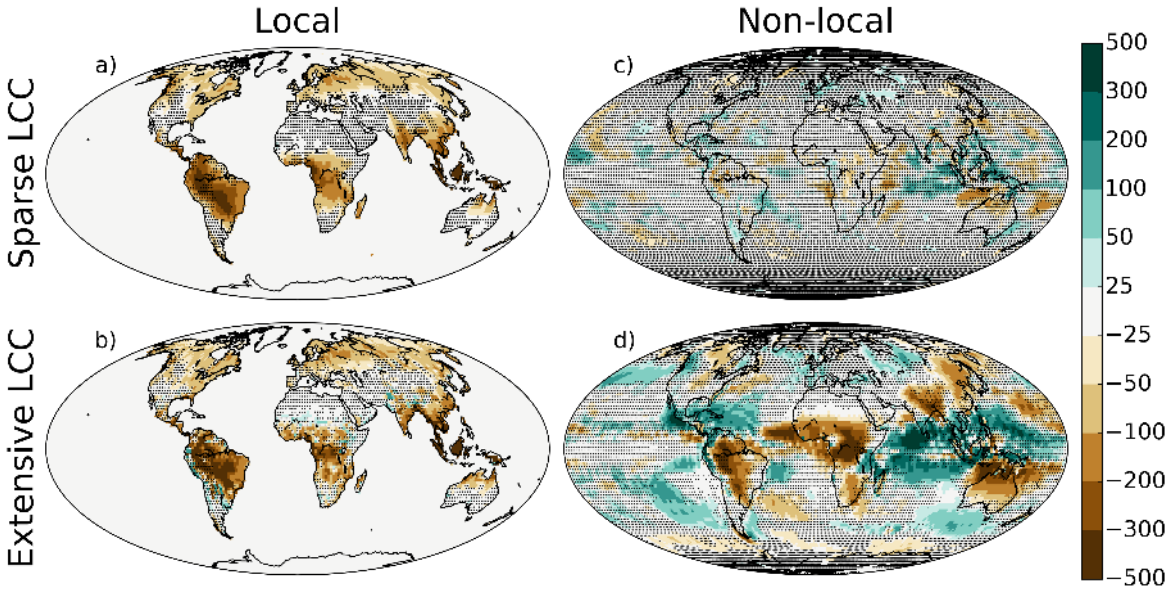

Figure 2.3: Difference in mean precipitation [mm/y] for *a*,*c* sparse and *b*,*d* extensive deforestation. *a*,*b* local effects, *c*,*d* nonlocal effects. Statistical significance is calculated according to a 5 % level in a Student's t-test accounting for autocorrelation (Zwiers and von Storch, 1995). Note that we mark grid cells that are *not* statistically significant.

or the Malay Archipelago, where the local effects show a decrease in precipitation while the nonlocal effects show an increase in precipitation.

Not only the spatial patterns, but also the mechanisms underlying local and nonlocal effects differ. Considering, for example, the local effects in the boreal winter months DJF (Fig. 2.4 *b* for extensive LCC), we obtain an increase in surface temperature south of 40°N. In the arid tropics (e.g., Fig. A.2.5 *d*), this warming can be attributed to changes in surface sensible heat flux, probably triggered by a reduction in surface-atmosphere exchange of heat because of a decreased surface roughness, consistent with the study by Rotenberg and Yakir (2010). In the humid tropics (e.g., Fig. A.2.5 *e*), the response is dominated by changes in latent heat flux, probably triggered by a changes in evapotranspiration efficiency. North of 40°N, the surface cooling of the local effects is partly originating from a strong decrease in surface shortwave net radiation due to the albedo increase after deforestation, which is especially strong in the presence of snow (not shown). Considering the nonlocal effects (Fig. 2.4 *d*), we see that the underlying mechanisms differ from the local effects: The changes in latent and sensible heat in the tropics indicate a southward shift of the tropical rain bands (not shown). In contrast to the local effects, increased surface shortwave and decreased longwave net radiation hint at a reduction in atmospheric water vapor and cloud cover.

The processes underlying local and nonlocal effects are inherently different. While nonlocal effects are driven by changes in global or regional climatic conditions, local effects result from changes in local surface properties and are only enhanced by changes in local climate conditions. Both for local and nonlocal effects, the mechanisms vary between regions and seasonally (see Appendix A.2). This analysis is not meant to be exhaustive but demonstrates that the mechanisms underlying local and nonlocal effects differ. Thus, it is important to distinguish local and nonlocal effects of LCC in Earth system simulations aimed at process understanding.

2.3.2 Local effects enable consistent comparison with observations

Due to the limited availability of time series covering LCC, observational studies often approximate LCC effects from a "paired-site set-up", i.e. from the difference in climate variables in adjacent locations with the same background climate but different land cover (e.g., Lee et al., 2011; Li et al., 2015; Alkama and Cescatti, 2016). Thus by construction, these observational studies cover only the local effects. The presence of nonlocal effect has impeded validation of the effects of simulated extensive deforestation with observational datasets in past studies (Zhang et al., 2014b). Thus, isolation of local effects enables a more consistent comparison of deforestation effects against observations, as noted by Malyshev et al. (2015).

In Fig. 2.5, we compare the local effects from the extensive LCC set-up with remote-sensing based paired-site observations from Li et al. (2015). In their observational

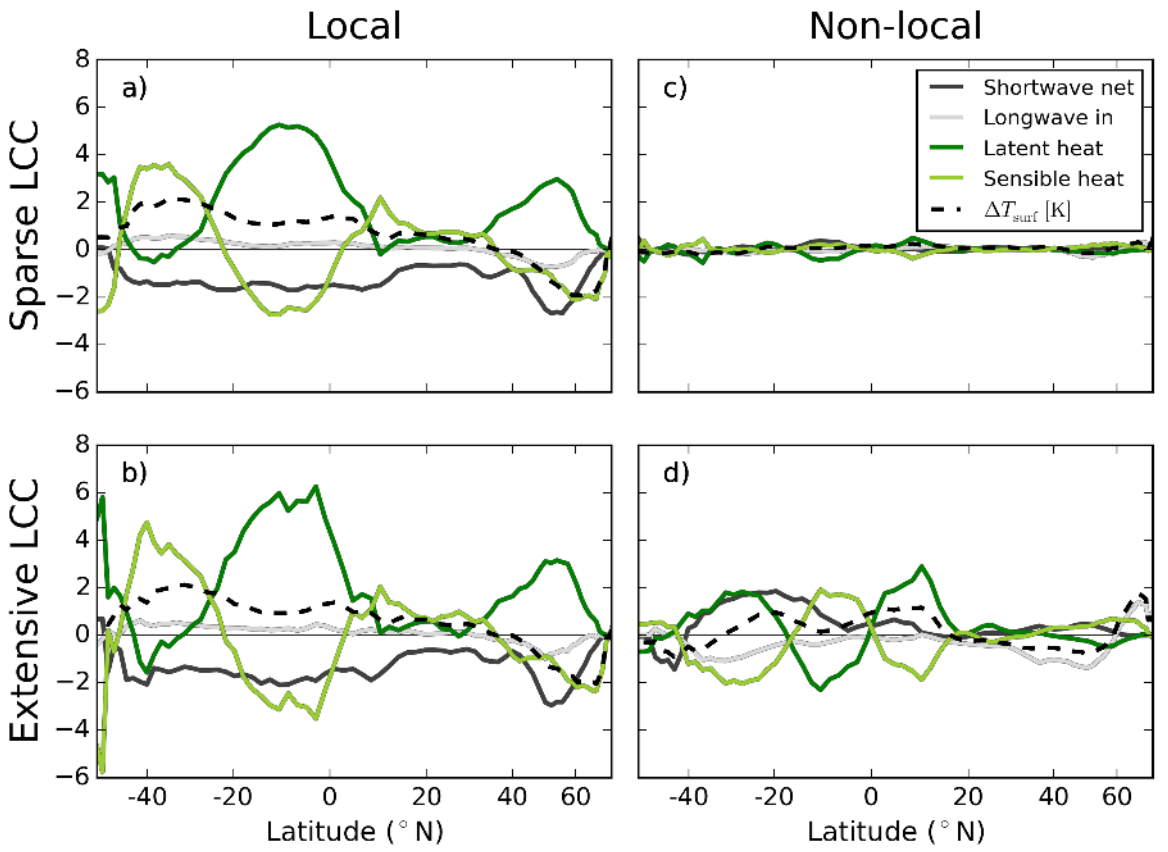

Figure 2.4: Energy balance decomposition for the boreal winter months (DJF). The dashed line denotes changes in surface temperature T_{surf} [K], caused by *a*,*c* sparse and *b*,*d* extensive deforestation, *a*,*b* local effects and *c*,*d* nonlocal effects. The solid lines, which approximately add up to the dashed line, represent surface temperature changes due to changes in components of the surface energy budget. All values are latitudinally averaged over land areas. The horizontal axis is scaled with the area that the respective latitude occupies.

study, they investigate the local effects of deforestation on a global scale by comparing surface temperature of forest with that of open land within a small region (approximately 50 km × 28 km based on MODIS satellite imagery). In the model, the simulated local response (Fig. 2.5 *c*) is weaker than in the observations (Fig. 2.5 *d*) in most seasons and latitudes, part of which can be explained by the fact that the observational dataset only captures clear-sky conditions (Li et al., 2015). Nevertheless, local effects in ECHAM6/JSBACH and observations generally agree with respect to the seasonal pattern in the extratropics. However, in the tropics, seasonal cycles do not match, which becomes evident in low temporal correlations (northern tropics) or even negative temporal correlations (southern tropics) between simulated local effects and observations (Fig. 2.5 *e*). Both the high correlation in the extratropics (at around 30 to 45°N) and the low correlation in the tropics (at around 5 to 15°S) are less evident when comparing observations to the total (local plus nonlocal) effects, and thus a more thorough assessment is enabled by isolation of the local effects. This once more puts

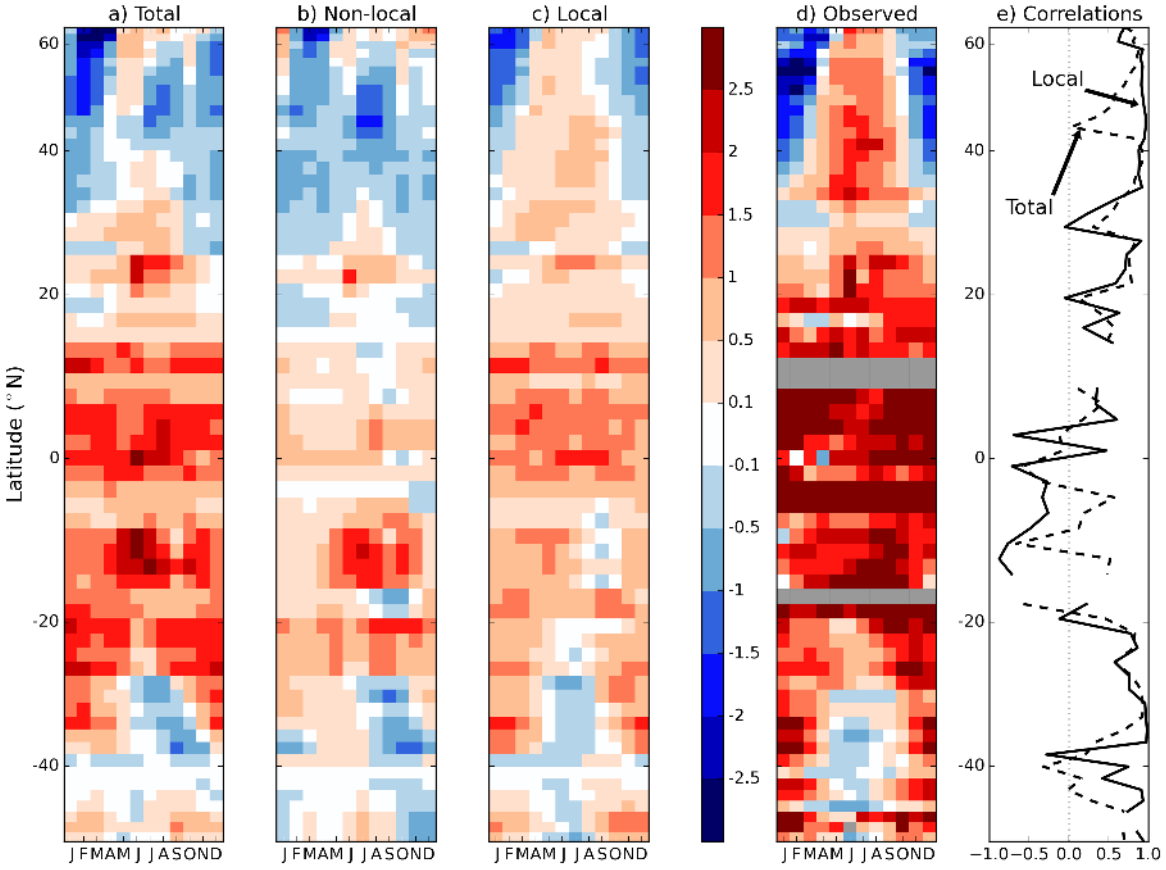

Figure 2.5: Surface temperature change [K] of deforestation, for *a* the total (local plus nonlocal effects), *b* the nonlocal effects, *c* the local effects, evaluated where observations were available, *d* remote sensing observations from Li et al. (2015) (their Fig. 2*c*), with the latitudes regridded to our model resolution, and *e* correlation coefficient of the monthly means (averaged over the available time period) in the respective latitudes for observations versus local (solid line) and observations versus total effects (dashed line). The vertical axis is scaled with the area that the respective latitude occupies.

emphasis on the importance of isolating the local effects when comparing simulated deforestation effects to observational datasets.

2.3.3 Dependence of nonlocal and local effects on the number of LCC cells

The comparison of sparse and extensive LCC shows that nonlocal effects strongly depend on the areal extent of LCC. For sparse LCC, the nonlocal effects have the order of magnitude of weather-related noise in almost all regions, as shown by the small number of significant grid cells (Fig. 2.2 *c* and 2.3 *c*). For extensive LCC, the nonlocal effects have the same order of magnitude as the local effects. In contrast, the local effects within this set-up do not differ substantially between sparse and extensive LCC

(Fig. 2.2 *a* versus 2.2 *b*). This is not only the case for changes in surface temperature, but also precipitation (Fig. 2.3 *a* versus 2.3 *b*) and 2m-air temperature (Fig. A.3.1 *a* versus A.3.1 *b*).

To quantify the similarity of the local effects in the two LCC cases, we determine the mean absolute difference of surface temperature over land between local effects from extensive and sparse LCC, respectively. We compute the numbers below only from values at the sparse LCC cells in both cases in order to reduce differences due to the different number of LCC cells. The mean absolute difference between the two local effects is 0.15K, and thus of secondary importance as compared to the effect itself (the mean absolute change in surface temperature on land for the local effects in the sparse LCC is 0.69K). There is no systematic bias: the mean difference between local effects for sparse versus extensive LCC is 0.05 K. At the same time, spatial correlation between the two is 0.96, so also the spatial pattern of the local effects is practically identical for the two LCC cases.

Not only the spatial pattern, but also the mechanisms underlying the local effects are identical for sparse and extensive LCC, as can be seen in Fig. 2.4 *a* versus 2.4 *b*. The peaks are more pronounced for extensive LCC (Fig. 2.4 *b*) due to the different number of LCC cells that the local effects are interpolated from. Still, the latitudinal patterns of the energy balance decompositions match well for the local effects from sparse and extensive LCC, illustrating that the underlying mechanisms are the same. Therefore, on the grid cell level, the local effects are largely independent of the number of LCC cells in the separation approach, although background climate is strongly influenced by the nonlocal effects due to the grossly differing areal LCC extent. While an even stronger change in background climate than can be induced by LCC might be capable of influencing the local effects, our results suggest that – at least in the case of unaffected SSTs – the local effects on a grid cell level will be robust for a wide range of chosen numbers of LCC cells in the separation approach.

2.4 Discussion and conclusions

In simulations of idealized extensive LCC, local effects are masked by the strong presence of nonlocal effects. The results presented here confirm previous studies (e.g., Swann et al., 2012; Devaraju et al., 2015) that illustrate that the sum of LCC on a larger scale can trigger substantial nonlocal effects. However, the effects of deforestation of a single model grid cell are initially local. Thus, the total simulated effects of *large-scale* LCC are not representative for the effects of deforestation in *plausible* LCC scenarios, in which nonlocal effects are less pronounced. Previous studies have focused on isolating the local –that is, locally induced– biogeophysical climate effects of LCC, either in plausible LCC scenarios (Kumar et al., 2013) or in models with climate information on subgrid vegetation tiles (Malyshev et al., 2015). Here, we present a

method that is capable of robustly isolating the local effects, accounting for local atmospheric feedbacks. Our results based on two extreme cases of sparse and extensive LCC, respectively, suggest that the local effects in the MPI-ESM can be robustly isolated irrespectively of the number of LCC cells. Thus, follow-up studies that require an isolation of the local effects may use a a chessboard-like pattern of one out of two LCC cells (see Appendix A.4) in order to only rely on interpolation from directly adjacent grid cells and thus reduce the horizontal interpolation errors.

Interpretation of the nonlocal effects is more complex than interpretation of the local effects for several reasons: First, for the nonlocal effects of one concrete geographical distribution of LCC, we cannot determine the relative importance of LCC of each grid cell for triggering those nonlocal effects. Second, while the nonlocal effects are determined by a modification of wide-ranging meteorological relationships, the local effects within a grid cell can be largely explained directly by changes in local surface properties. Thus, we can understand the mechanisms underlying the local effects better than those underlying the nonlocal effects. Third, the nonlocal effects depend not only on the spatial extent, but also strongly on the concrete geographical LCC distribution because LCC changes atmospheric circulation. This impedes inference of the climatic relevance of LCC from one LCC distribution to the other. We have shown that the local effects within a grid cell can be robustly isolated using a wide range of spatial LCC patterns, even in the presence of substantial nonlocal effects. This is a step towards a better attribution of climatic changes to local LCC. This attribution is important, as there are various plausible scenarios for future LCC (Hurtt et al., 2011). Independent of the investigated scenario, the local effects thus allow for an assessment in an adaptation/mitigation context.

Changes in background climate can influence the effects of LCC (Pitman et al., 2011). In order to isolate the local effects, we want to keep LCC-induced changes in background climate small, and thus we prescribe SSTs. In this set-up of prescribed SSTs, the local effects are very similar for sparse and extensive LCC, indicating that changes in background climate by extensive LCC are not strong enough to substantially influence the local effects. It is not clear if this conclusion still holds with an interactive ocean: accounting for oceanic feedbacks in a global deforestation experiment has been simulated to substantially influence deforestation effects (1K less tropical warming and about 2K more northern-hemispheric cooling in one climate model (Davin and de Noblet-Ducoudré, 2010)). We speculate that, if we used interactive SSTs in our simulations, most of these feedbacks would be included in the nonlocal effects, as they would also be seen in hypothetical no-LCC cells. The oceanic feedback strength from the study by Davin and de Noblet-Ducoudré (2010) could thus lead up to a doubling of the nonlocal effects in terms of surface temperature changes. In order to avoid an influence of these amplified nonlocal effects on the local effects, we recommend prescribing SSTs for applications that aim at a robust isolation of the local effects.

We acknowledge that land surface models differ in their methods of implementing LCC

(Pitman et al., 2009). Thus, the results presented here, both for local and nonlocal effects, are specific for our model (MPI-ESM), in particular for exact quantifications. However, the approach presented in this study opens ways to an intercomparison of local and nonlocal effects across climate models. If models disagree mainly with respect to the nonlocal effects, this would hint at large-scale advective processes and changes in global circulation to be responsible for inter-model differences. However, an inter-model spread in the local effects would suggest a different representation of processes relevant within a grid cell to be responsible for the inter-model uncertainties. Thus, due to their different nature, analyzing local and nonlocal effects separately allows for a deeper process understanding of LCC effects in climate models.

An isolation of the local effects has a wide range of applications in the LCC context. As we illustrated, isolation of the local effects enables a consistent comparison to observed climate effects of LCC, such as ground-based (e.g., Lee et al., 2011; Zhang et al., 2014b) or remote-sensing studies (e.g., Li et al., 2015). Further studies can investigate whether night-time and day-time effects of LCC (e.g., Lee et al., 2011; Li et al., 2015) are well represented in climate models, and whether models correctly capture the effects on temperature and precipitation during extreme events, as in the study by Teuling et al. (2010). As weather-related noise and advection processes are largely excluded from the local effects, they can be employed to determine the influence of land-atmosphere coupling strength on the LCC effects, as performed for the total biogeophysical effects by Lorenz and Pitman (2014).

In a broader context, the method described here of separating local and nonlocal effects is not restricted to LCC studies but can be employed in studies focusing on any land surface process that is mainly acting locally but capable of influencing wide-ranging climate when applied on a larger scale. For instance, this method could be used in studies on the climate effects of irrigation or wildfires. Analogous to the findings in our study, isolating local effects can improve signal/noise ratio in realistic scenarios. Additionally, the method of separating local and nonlocal effects can be used in idealized large-scale studies, and enhance understanding in processes influencing local and large-scale climate.

Chapter 3

Why does the locally induced temperature response to land cover change differ across scenarios?[1]

Land cover change (LCC) affects temperature locally. The underlying biogeophysical effects are influenced by land use (location and extent), but also by natural biogeographic shifts and background climate. We examine these three factors' contribution to surface temperature changes upon LCC and compare them across CMIP5 scenarios. To this end, we perform global deforestation simulations with an Earth system model to deduce locally induced changes in surface temperature for historical and projected forest cover changes. We find that the dominant factors differ between historical and future scenarios. The local temperature response is historically dominated by the factor land use change, but the two other factors become just as important in scenarios of future land use and climate. An additional factor contributing to differences across scenarios is the dependence on the extent of forests before LCC happens. For most locations, the temperature response is strongest when starting deforestation from low forest cover fractions.

3.1 Introduction

Land cover change (LCC), such as a conversion from forests to grasslands, perturbs the local surface energy and water balance. Historically, these biogeophysical effects have been found to cool global climate (e.g., de Noblet-Ducoudré et al., 2012; Boisier et al., 2012). For future LCC in the Representative Concentration Pathway (RCP) scenarios (Moss et al., 2010), the simulated biogeophysical effects were found to be

[1]This chapter has been published with minor modifications as "**Winckler, J.**, C. H. Reick and J. Pongratz (2017): Why does the locally induced temperature response to land cover change differ across scenarios?, Geophys. Res. Lett., **44**, 3833-3840, doi:10.1002/2017GL072519."

substantially weaker (Brovkin et al., 2013b; Boysen et al., 2014; Davies-Barnard et al., 2015). The overall sign of the future response depends of course on the type of LCC (de- or afforestation dominating (Davies-Barnard et al., 2015)), but even scenarios with the same general direction of LCC, such as the deforestation scenarios of RCP2.6 and RCP8.5, differ in their climatic effects (Brovkin et al., 2013b). Several factors have been proposed that are responsible for differences in LCC effects across scenarios (e.g., Brovkin et al., 2013b; Zhang et al., 2014b; Pitman et al., 2011). In this chapter, we explore three factors (see next paragraph) that are relevant for the locally induced effects in past and future scenarios, and we compare their relative importance. We focus our analysis on the locally induced changes in surface temperature (e.g., Kumar et al., 2013; Malyshev et al., 2015). Additionally, LCC may affect climate by nonlocal effects, such as advection of local changes in air temperature and humidity to neighboring regions. However, these nonlocal effects are triggered locally, such that a better understanding of inter–scenario differences should begin at a local level. Furthermore, local temperature changes are directly relevant for local living conditions.

The relative importance of the following three factors is assessed in our study: First, the effects of LCC vary strongly across regions (Pongratz et al., 2011), and thus past and future effects may differ because of differences in areal extent and geographical distribution of *land-use–induced land cover change (LULCC)* in the scenarios (Brovkin et al., 2013b). Second, the effects of LCC at a given location will be modified by a *warming background climate (WARM)*, which may lead to a reduction in snow cover and changing evapotranspiration (Pitman et al., 2011). While the change in background climate between pre-industrial and present-day conditions did not influence the LCC effects substantially (de Noblet-Ducoudré et al., 2012), the influence of a warming background climate may be substantial in future scenarios. Third, any change in background climate might cause natural biogeographic shifts, which we refer to as *climate–induced land cover change (CILCC)*; for instance, due to global warming, the tree-line in boreal regions is shifting northwards (ACIA, 2004), and effects of this tree-line shift might accelerate warming locally (e.g., Zhang et al., 2014b). While the factors LULCC, CILCC and WARM have been investigated individually in previous studies (e.g., Brovkin et al., 2013b; Zhang et al., 2014b; Pitman et al., 2011), our approach enables us to determine their relative contribution within one set of simulations. This assessment of their relative contribution is essential to understand differences in the climate effects of LCC across scenarios.

In addition to the above factors, past and future scenarios differ in their initial forest cover fraction: In some areas that where partially deforested historically, deforestation or afforestation might take place in the future, but starting from a lower initial forest cover fraction. Further, depending on the scenario, LCC happens in different regions showing more or less forest cover. These differences in initial forest cover fractions would not affect the results if, on a grid cell level, climate responds linearly to deforestation. However, if climate responds nonlinearly to deforestation, this difference in initial forest cover fractions will contribute to the difference of the deforestation effects

across the scenarios. Such a nonlinearity has been demonstrated in simulations by Li et al. (2016) for the total effects (locally induced plus remotely induced). We examine if this nonlinearity is also present for the locally induced changes in surface temperature, and to what extent this nonlinearity contributes to the differences in the temperature response across LCC scenarios.

3.2 Methods: Look-up approach for the local effects

To infer locally induced changes in surface temperature from LCC –modeled here as a replacement of forests by grasslands– we proceed as follows (Fig. 3.1*a*): We simulate changes in surface temperature following a step-wise reduction in the fraction that is covered with forest within each grid cell ('forest fraction'). Then, we isolate the local effects as described in chapter 2. In each grid cell, we interpolate the values that we obtained from the step-wise deforestation. The resulting curves then serve as look-up tables to infer temperature change from different LCC scenarios without the need for additional simulations: We insert the forest fractions at the start and the end of a scenario, and we obtain the change in surface temperature that is locally induced by this change in forest fraction (black arrow in Fig. 3.2).

3.2.1 From simulations to look-up tables

First, we simulate changes in surface temperature following a reduction of forest fraction. We use the coupled land–atmosphere model ECHAM6/JSBACH (Giorgetta et al., 2013; Reick et al., 2013) at horizontal resolution T63 (about 1.9°). In each experiment, we simulate 30 years after a 5-year spin-up. We impose present-day background climate: we prescribe sea surface temperatures, sea ice, and CO_2 for the years 1976 - 2005 from the MPI-ESM CMIP5 (Coupled Model Intercomparison Project, phase 5) historical simulation (Giorgetta, 2012a). Following the approach of 'sparse' deforestation described in chapter 2, the conversion from forests to grasslands is performed in 1 out of 8 grid cells arranged in a regular spatial pattern (see Fig. 1 there). In the remaining cells, present-day vegetation is left unchanged. This way, we ensure that background climate (the influence of which we investigate separately, see section 3.2.3) is not altered substantially by deforestation. To decrease the dependence of our results on the exact location of the deforestation grid cells, we additionally simulate deforestation in 1 out of 8 grid cells in a spatial pattern that is shifted by two grid cells. For both the 'shifted' and 'unshifted' simulations, we then isolate the local effects by removing non-local effects and noise related to climate variability (for details see chapter 2). In the following, we consider the mean of the local effects from the 'shifted' and 'unshifted' simulations. Going beyond the simulations described in chapter 2, we isolate the local

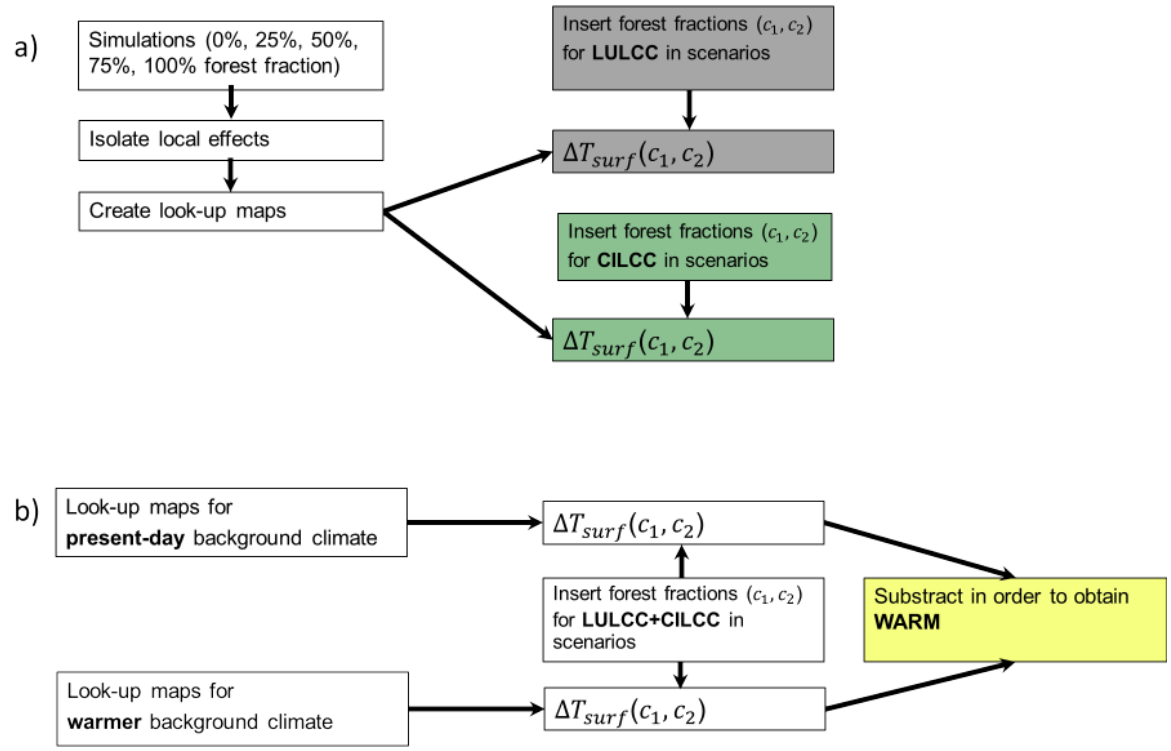

Figure 3.1: Conceptual diagram illustrating how changes in surface temperature are obtained for a given scenario of changes in forest fraction. See also section 3.2 for a methodological overview of the look-up approach. *a*) We insert forest fraction for land-use (LULCC) or climate–induced land cover change (CILCC) into the look-up tables (see Fig. 3.2) to obtain the corresponding temperature changes. The change in surface temperature ΔT_{surf} depends on the forest fractions at the beginning (c_1) and end (c_2) of the scenario. *b*) We obtain the effect of warmer background climate (WARM) by comparing the effects in present-day background climate to the effects in a warmer background climate. To this end, we insert changes in LULCC+CILCC into two look-up tables that were obtained for different background climates. The colors correspond to the colors in Fig. 3.

effects not only for complete deforestation within a grid cell, but deforest in steps of 25% starting from 100% forest cover in the vegetated part of each grid cell. The bare land part of each grid cell is left unchanged. We have then 5 forest fractions $\times$ 2 (shifted and unshifted) = 10 simulations.

For each land grid cell, we compute 30-year means for each of the five experiments (illustrated by the red dots in Fig. 3.2). We interpolate these means with a cubic spline. Using this curve $s()$ as a look-up table, we can convert a given change in forest fraction within the respective grid cell (induced by LULCC, CILCC or both) into a locally induced change in surface temperature (black arrow):

$$\Delta \mathrm{T}_{surf}(c_1, c_2) = s(c_2) - s(c_1), \tag{3.1}$$

where c_1 and c_2 denote the forest fractions in the start and end of the LCC scenario.

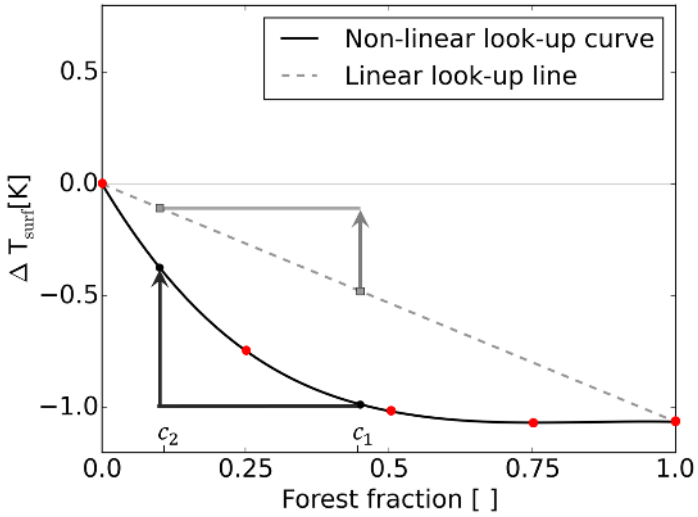

Figure 3.2: Illustration of the look-up approach for one selected grid cell. Shown are the local effects from the five simulations with different forest fractions (red dots), the resulting interpolated look-up curve (black) and an artificial look-up line interpolating linearly between 100% and 0% forest cover (gray). The vertical axis denotes locally induced changes in surface temperature with respect to zero forest fraction. The arrows show the respective changes in surface temperature for a change in forest fraction from c_1 to c_2. In this example, the calculated change in surface temperature would be underestimated when using the linear look-up line.

3.2.2 Forest fraction scenarios

We calculate the locally induced changes in surface temperature for various LCC scenarios: The historical scenario (between 1850 and 2005) and the future scenarios RCP2.6, RCP4.5, and RCP8.5 (between 2006 and 2099) of CMIP5. To determine the respective temperature response, we require the initial and final forest fractions (see equation 3.1). These forest fractions are based on the land-use transitions dataset by Hurtt et al. (2011), which is translated into geographical distributions of the plant functional types of the MPI-ESM for CMIP5 as described in the paper by Reick et al. (2013) (see Fig. 3.4 for LULCC–induced forest fraction changes in the respective scenarios). While we change the forest fractions within the vegetated part of a grid cell, we keep this vegetated fraction fixed (see Appendix section B.1).

For calculating forest fraction changes due to CILCC in the respective scenarios, we follow the approach by Schneck et al. (2015) and use the cover fractions from two existing simulations: The changes in forest fractions in the MPI-ESM simulations for CMIP5 (Giorgetta, 2012a,b,c,d) include both LULCC from the land-use transitions by Hurtt et al. (2011), and CILCC from JSBACH's dynamic vegetation module (Reick et al., 2013) for the respective background climate. In a second dataset, forest fraction changes are derived from the transitions by Hurtt et al. (2011), but the dynamic vegetation module is switched off (Schneck et al., 2015). We calculate CILCC as the

difference in forest fraction change between these two datasets (see Fig. 3.5 for CILCC–induced forest fraction changes in the respective scenarios). The forest fraction changes can then be applied to the look-up tables to assess the impacts of LULCC and CILCC on surface temperature. In the case of a nonlinear response of surface temperature to deforestation, it matters whether LULCC or CILCC are applied first. However, in our study this is irrelevant, as LULCC and CILCC are affecting different regions, and thus the synergies between them are negligible (see Appendix Fig. B.1).

3.2.3 Determining the influence of a warmer background climate

In different background climates, a given change in land cover may affect surface temperature differently. While in reality, background climate varies transiently, we consider the difference between the effects in two distinct background climates: present-day and the warmer RCP8.5 background climate. In addition to the look-up tables for present-day background climate (described in section 3.2.1), we create separate look-up tables for the warmer RCP8.5 background climate. For this, we repeat all 10 simulations described in section 3.2.1, but we prescribe SSTs, sea ice and CO_2 from the years 2070-2099 from an MPI-ESM RCP8.5 simulation (Giorgetta, 2012d). Instead of RCP8.5, we could also assess the effect of the climate change projected under RCP2.6 or RCP4.5. However, for comparability across scenarios, we want to assess how one given change in background climate influences the results for the respective LCC scenarios. We choose the RCP8.5 forcing scenario because it exhibits the strongest warming of the RCP scenarios, and thus can be seen as an upper bound for the relevance of background warming.

We calculate the influence of the warmer background climate as follows (see Fig. 3.1 *b*): The LCC effects are calculated seperately for the look-up table corresponding to the warmer background climate $\tilde{s}()$ and the present-day background climate $s()$. Then, we define the influence of the warming background climate as the difference between these two results:

$$\Delta \mathrm{T}_{surf}^{WARM}(c_1, c_2) = [\tilde{s}(c_2) - \tilde{s}(c_1)] - [s(c_2) - s(c_1)]. \tag{3.2}$$

Here, c_1 and c_2 are the forest fractions within a grid cell in the years 1850 and 2099. We choose to include LCC since 1850 (and not only LCC in the RCP scenarios starting in 2006) in the analysis of warming background climate for the following reasons: Background warming (mainly warming SSTs) is projected to occur only in the future. However, the resulting change of surface temperature within a land grid cell is not only determined by LCC in the future, but also by the forest fraction before the background warming. For instance, a given decrease in snow cover might cause warming in a fully forested grid cell. However, if this grid cell was deforested before the year 2005, this

warming might be even more pronounced: The albedo in the grassland grid cell (now without snow masking of trees) might respond stronger to the change in snow cover. Thus, the response of a grid cell to post-2005 background warming also depends on pre-2005 LCC. Consequently, for calculating the effect of warming background climate, we also account for LCC prior to the year 2005. Since our LCC scenario starts in the year 1850, we do not account for LCC prior to the year 1850.

3.3 Causes of differences in temperature response to LCC across scenarios

3.3.1 Land-use–induced and climate–induced land cover change

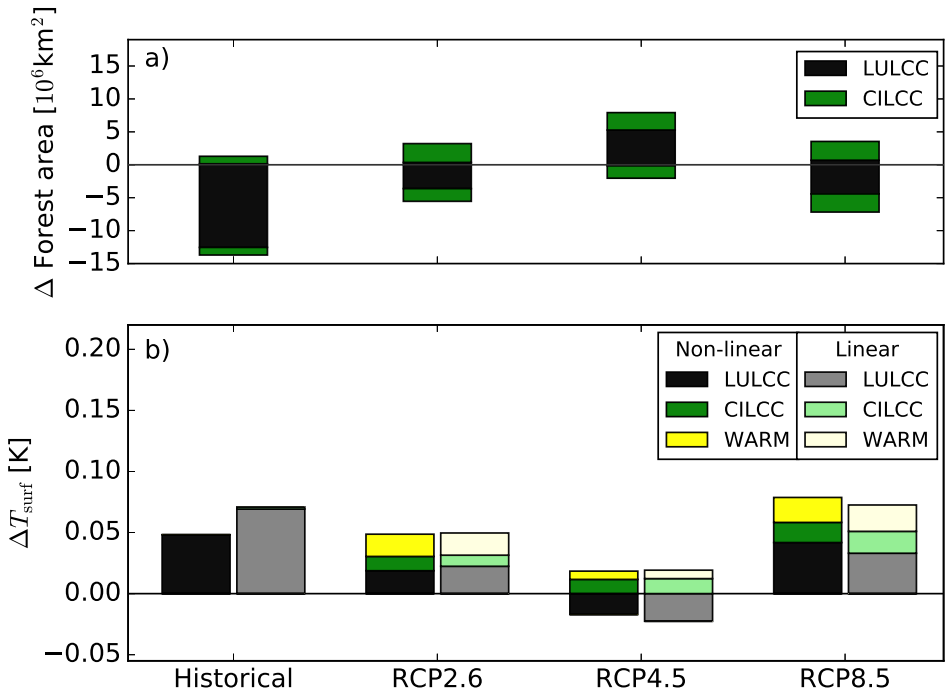

Figure 3.3: Comparison of LCC effects across scenarios. *a*) Changes in global forest area. Within a scenario, there can be both areas of forest gain (positive values) and forest loss (negative values). *b*) Contributions to local surface temperature changes from land-use–induced LCC, climate–induced LCC, and warming background climate. The vertical axis denotes surface temperature change averaged over land. For each scenario, the left bars account for the nonlinear response, the right bars assume a linear response to deforestation.

When averaged over land, the locally induced changes in surface temperature of LULCC cause a cooling in the afforestation scenario RCP4.5, but warming in all other scenarios, which are the deforestation scenarios (Fig. 3.3 *b*; corresponding maps in Fig. 3.4).

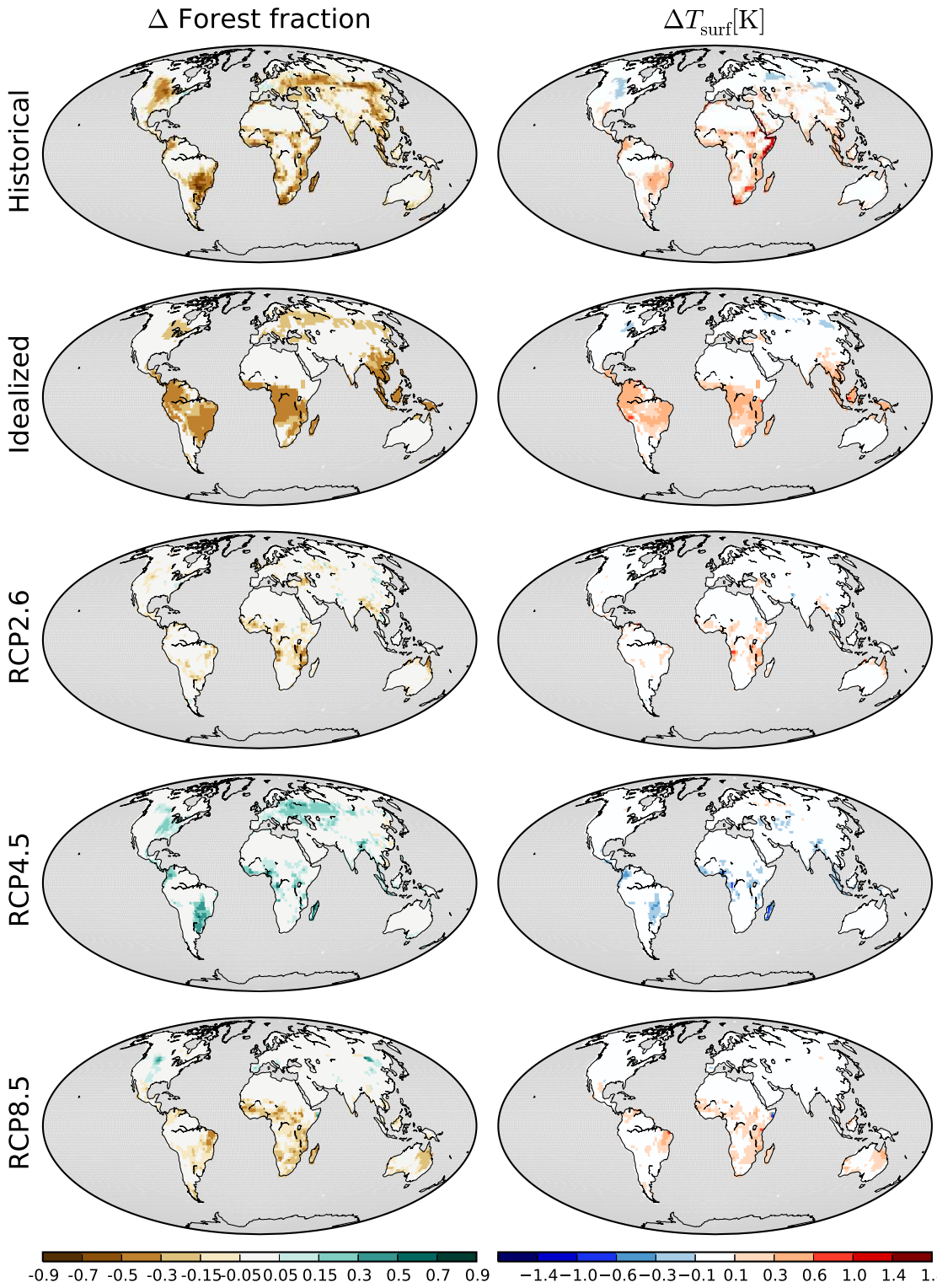

Figure 3.4: Land-use–induced land cover change (LULCC): changes in forest fraction and resulting changes in local surface temperature. The changes in surface temperature are obtained using the look-up map for present-day background climate and accounting for the nonlinearity. For a description of the idealized scenario, see Appendix B.2.

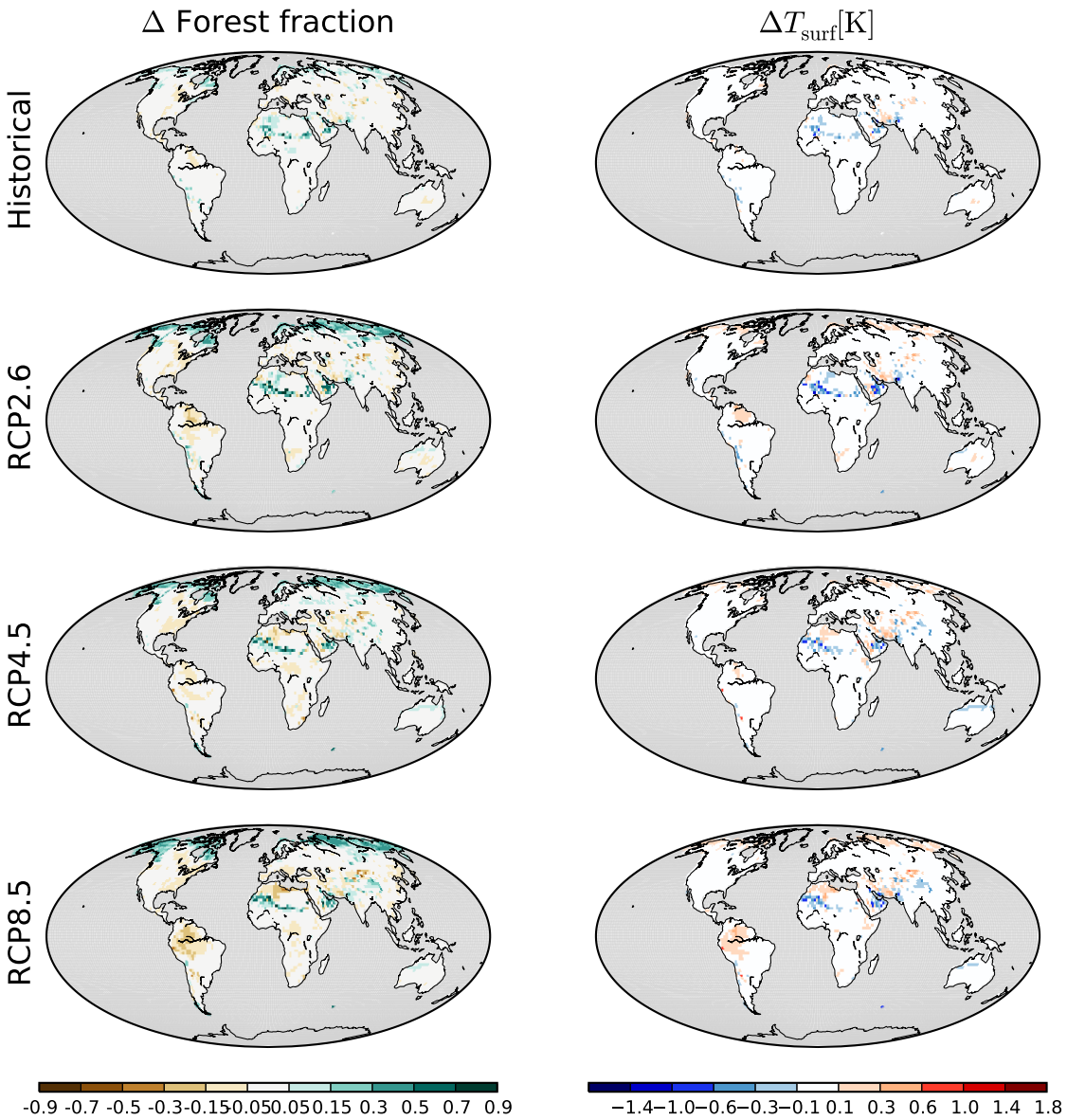

Figure 3.5: Climate–induced land cover change (CILCC): changes in forest fraction and resulting changes in local surface temperature. The changes in surface temperature are obtained using the look-up map for present-day background climate and accounting for the nonlinearity.

The temperature changes of CILCC are negligible for historical deforestation and induce a warming in all RCPs. As opposed to land-use–induced changes in forest cover, in every scenario there are both areas with forest gain and forest loss (Fig. 3.5). Large parts of these climate–induced gains and losses of forest area compensate for each other and result in a relatively small temperature signal when averaged over the land surface. Note that CILCC in semi-arid and arid regions may be overestimated because the vegetated fraction of the grid cells there is overestimated by JSBACH (Brovkin et al., 2013b). However, this overestimation has only a small impact on our globally averaged results: Warming and cooling from forest fraction decrease and increase largely cancel

each other out from these regions on a global scale. More important for the land-mean signal are a forest die-back in the Amazon (especially in RCP8.5), where forest has a cooling effect, and a northern shift of the treeline in the boreal regions (in all RCPs), where forest has a warming effect. While the likelihood of forest die-back in a warmer climate is still unclear (e.g., Sitch et al., 2008; Rammig et al., 2010), there is a broad consensus that the boreal treeline is about to shift northwards while global warming proceeds (ACIA, 2004).

3.3.2 Influence of changing background climate

In the warmer background climate, the surface warming induced locally by deforestation is stronger compared to the effects in present-day background climate. In present-day background climate, a conversion from 100% forests to 100% grasslands in an average grid cell leads to a warming of 0.61K, while the same effect in the warmer background climate is a warming of 0.75K (see maps in Appendix Fig. B.3). In the temperate and boreal regions, these changes are associated with reduced snow cover fraction in the warmer background climate (not shown), in accordance with the study by Pitman et al. (2011). Due to this reduced snow cover, deforestation leads to a smaller albedo increase, and thus deforestation in the boreal regions becomes less cooling. Also tropical deforestation in the warmer climate warms the surface more compared to deforestation in present-day climate. This additional warming results from stronger deforestation–induced decreases of turbulent heat fluxes in a warmer climate (not shown). Qualitatively, the change due to a warming background climate is in accordance with the study by Armstrong et al. (2016): In their model, deforestation leads to a cooling, and in a warmer background climate this cooling effect decreases.

The change in background climate affects the results for the RCP scenarios: The effects of LCC in the warmer background climate are more warming compared to deforestation effects in present-day background climate (yellow bars in Fig. 3.3 *b*). For instance in RCP8.5, the influence of background warming on the LCC effects is 0.0204 K. This number consists of the contributions from historical LCC (0.0128 K) and LCC occurring between the years 2006 to 2099 (0.0076 K). Note that these two time spans are summarized in the yellow bars because we assign LCC in both time spans to the future scenario where background warming might occur. In contrast, the green and black bars only contain the contributions from LCC in the respective scenario.

3.3.3 Influence of the forest fraction prior to LCC

Here, we assess whether surface temperature responds nonlinearly to the extent of deforestation within a grid cell. Such a nonlinearity is relevant for the LCC scenarios: In case of a strong nonlinearity, the LCC effect depends on the forest fraction prior to deforestation. For instance in Fig. 3.2, the change from c_1 to c_2 (black arrow) would

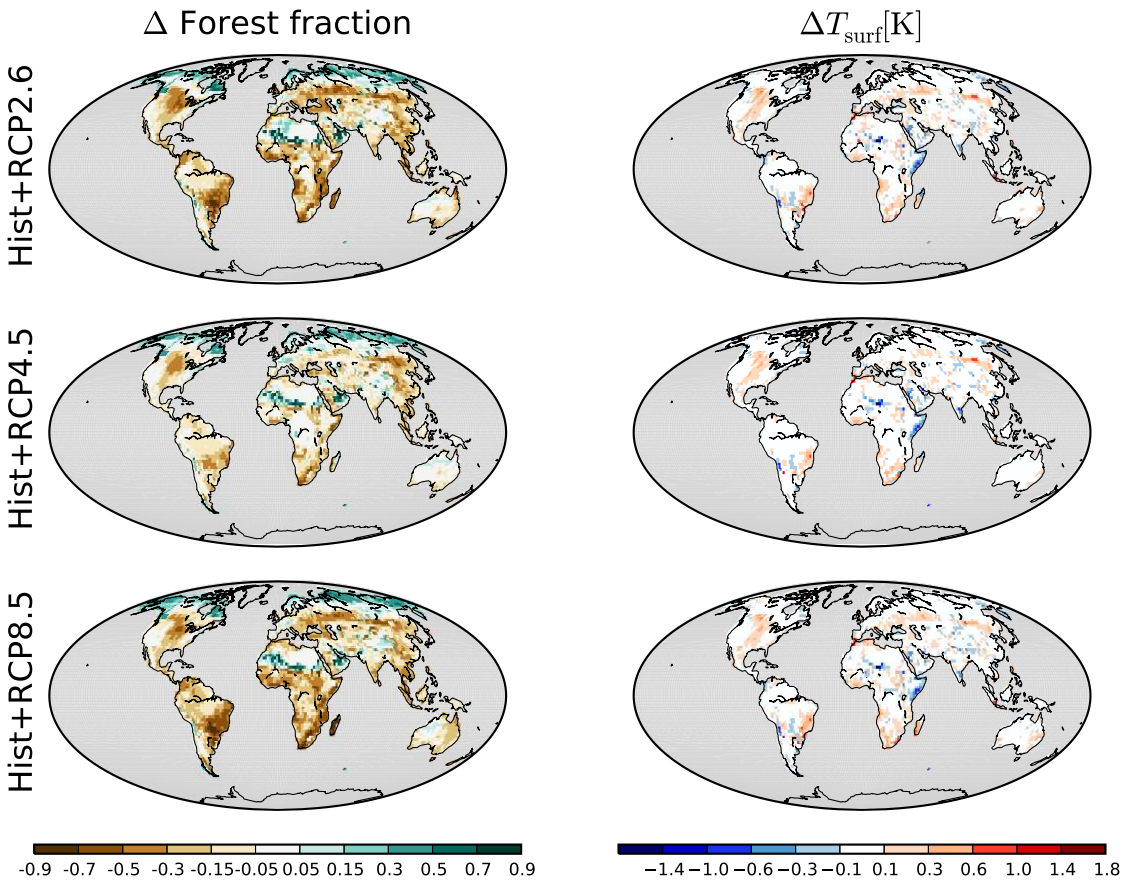

Figure 3.6: Influence of background climate warming (WARM): changes in local surface temperature, for the LCC scenarios Historical+RCP2.6, Historical+RCP4.5, and Historical+RCP8.5. These are the areas where LCC takes place cumulatively during the whole study period (years 1850 - 2100), and thus the areas that are affected by the changing background climate. The changes in surface temperature are obtained using the look-up maps for present-day and RCP8.5 background climate accounting for the nonlinearity (see Appendix Fig. B.3 for the effect of warming background climate on complete deforestation).

have caused substantially less warming if the same extent of deforestation, $c_2 - c_1$, had started from a higher forest fraction. In contrast, in case of a linear surface temperature response the deforestation effect would be independent of the forest fraction prior to LCC (gray arrow). The forest fraction prior to LCC varies across scenarios, and thus a nonlinearity, if existing, could contribute to differences in the LCC effects across scenarios.

Indeed, surface temperature responds nonlinearly to deforestation within most grid cells (Fig. 3.7). Deforestation is generally more efficient (that means, deforestation causes more temperature change per unit forest fraction change) when starting from a low forest fraction. This nonlinearity is particularly strong in the temperate, arid and tropical ecoregions, where surface temperature responds stronger to the last 25% than the first 75% of deforestation (Fig. 3.7). The nonlinearity might arise from a nonlinear response of the turbulent heat fluxes to changes in surface roughness (not shown).

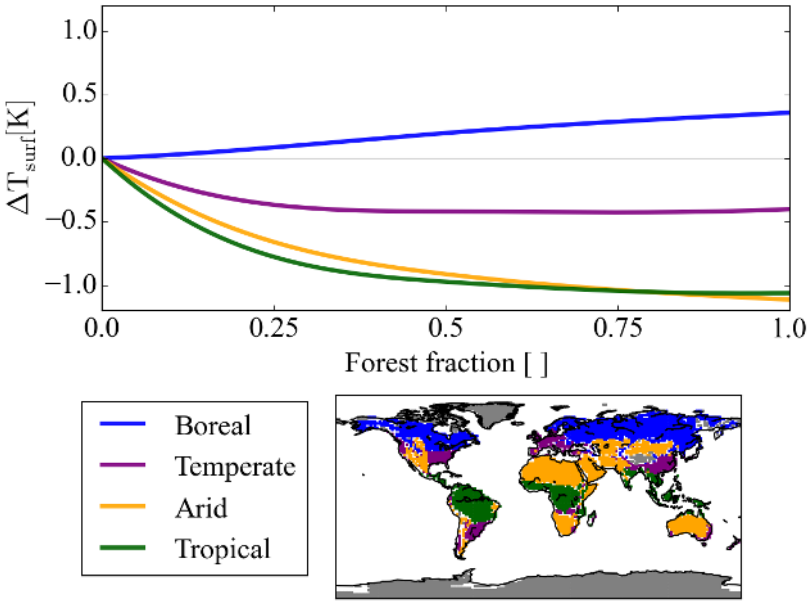

Figure 3.7: The nonlinearity differs across ecoregions. Top: Spatial averages of the already interpolated look-up maps for different ecoregions. The vertical axis denotes locally induced changes in surface temperature with respect to zero forest fraction. Bottom: Ecoregions that are used for averaging.

Similar to this study, nonlinearities have been found in a previous simulation study by Li et al. (2016). In their study, temperate and boreal changes in surface temperature were particularly strong when starting deforestation from high initial forest fractions. However, it is unclear if their nonlinearities were also present in the isolated locally induced effects, or if their nonlinearities originated from changes in global circulation due to their approach of global deforestation. Our results show that nonlinearities are not only present in the total (local plus nonlocal) effects, but can also be strong for the isolated locally induced changes in surface temperature. Thus, the deforestation impact depends on the forest fraction prior to LCC.

The nonlinearity contributes to the differences across the scenarios. To show this, we contrast our previous results (using the nonlinear look-up tables) by the results that would be obtained when ignoring the dependence on the forest fraction prior to LCC, and thus calculating surface temperature changes using linear look-up tables (black curve versus gray line in Fig. 3.2). The results are summarized in Fig. 3.3 *b*: For historical LULCC, the impact calculated using the nonlinear look-up tables is smaller than using the artificial linear look-up tables because the forest fraction prior to LCC in the historical scenario is relatively high (54% in the year 1850). The same is true for in RCP4.5, because LULCC largely consists of a reversal of historical deforestation. In the RCP2.6 scenario, the difference between the results for linear and nonlinear look-up tables becomes smaller, and in RCP8.5 the effect using the nonlinear look-up tables is even stronger compared to the results for the linear look-up tables. This is partly because the forest fractions prior to LCC are smaller than in the historical scenario

(30% in the year 2005 for both RCP2.6 and RCP8.5).

3.4 Discussion

We use a look-up approach to calculate the locally induced changes in surface temperature. Compared to other methods for isolating the local effects (Kumar et al., 2013; Malyshev et al., 2015; Lejeune et al., 2017b), this approach has two advantages: First, the look-up approach allows us to assess the relative contribution of the three factors LULCC, CILCC, and WARM, without the need to perform computationally expensive simulations for each factor and scenario separately. Second, our approach allows us to assess the importance of the nonlinearity in the response, and thus the dependence on the forest fraction prior to deforestation.

The look-up approach requires mutual independence of the LCC effects between different grid cells. For the local effects in this study, this independence is given because the local effects within a grid cell are largely independent of LCC elsewhere (chapter 2). However, the nonlocal contributions from LCC are highly dependent on the spatial extent and distribution of LCC (e.g., Swann et al., 2012; Devaraju et al., 2015). Thus, the look-up approach cannot be extended to include remotely triggered effects such as sea-ice–albedo feedbacks (e.g., Swann et al., 2010; Davies-Barnard et al., 2014).

The locally induced changes in surface temperature are relatively small when averaged over land, but can be substantial on the local scale (Figs 3.4, 3.5, and 3.6). However, we display land average values in Fig. 3.3 for the sake of comparability across factors and scenarios. Apparently, the averaging over all land areas partly obscures the fact that particularly the factors CILCC and WARM are warming locally in some regions, while they cool locally in others. Thus, their relative importance is larger than suggested by Fig. 3.3*b* because the averaging artificially attenuates some of their effects (Appendix Fig. B.5).

There is a large spread in the response to LCC across the CMIP5 models, even for the isolated local effects (Kumar et al., 2013; Lejeune et al., 2017b). Also the dependence on forest fraction prior to LCC and the three considered factors may differ across models, both concerning their relative importance and absolute quantification. Rather than giving an exact quantification, this study should be seen as illustrating that the relative contribution of the three factors can differ substantially across scenarios, up to a similar contribution of CILCC and WARM as compared to LULCC for future scenarios. Thus, our study suggests that all three factors contribute substantially to the total climate effects of LCC.

While forest fractions prior to LCC have a relatively minor effect on the considered scenarios, they can be essential in other LCC scenarios. To illustrate this, we extend our assessment of realistic LULCC scenarios by an “idealized” deforestation scenario (see Appendix B.2) similar to the experimental set-up proposed for the Land-Use Model

Intercomparison Project (LUMIP) within CMIP6 (Lawrence et al., 2016). In such an idealized scenario, surface temperature responds particularly weak because of the high forest fractions prior to deforestation (see Fig. 3.4 and Appendix Fig. B.4). These results highlight the need to be aware of the nonlinearity when comparing deforestation effects across scenarios. To evaluate whether the temperature response depends on the forest fraction prior to LCC in reality, further studies might assess the nonlinear behavior in observational datasets (e.g., Li et al., 2015; Alkama and Cescatti, 2016).

3.5 Conclusions

Previous studies found that the climate effects of LCC differ across scenarios because of differences in the spatial extent and spatial distribution of land use (e.g., Brovkin et al., 2013b). Going beyond this, we identify two reasons why the locally induced changes in surface temperature differ across scenarios:

First, the relative contribution from land use, natural vegetation dynamics and warming background climate vary across scenarios. Historically, the locally induced changes in surface temperature have been dominated by land-use–induced land cover change (LULCC). In the scenarios for future development, the more indirect factors (warming background climate (WARM) and subsequent climate–induced land cover change (CILCC) might become of equal importance compared to land use. Background climate varies across scenarios, models and ensemble members (e.g., Hawkins et al., 2009), and for a given background climate, natural vegetation dynamics can differ substantially across dynamic global vegetation models (e.g., Sitch et al., 2008). Our results suggest that both uncertainties in the development of background climate and natural vegetation dynamics might add to the uncertainty of the LCC effects across models beyond the uncertainties in the implementation of LULCC and differences in the model parametrizations.

Second, forest fractions prior to deforestation vary between the historical scenario and future projections. These initial forest fractions influence the LCC effects, because surface temperature within a grid cell responds nonlinearly to deforestation. These results have implications beyond this study: pre-LCC forest fractions differ not only across scenarios, but also across models (e.g., de Noblet-Ducoudré et al., 2012). Thus, the nonlinearity might contribute to inter-model differences of LCC effects. If observational studies confirm our findings, the nonlinearity may also be relevant for local climate change mitigation.

Chapter 4

The neglected nonlocal biogeophysical effects of deforestation[1]

Deforestation impacts surface temperature locally by altering the exchange of heat, moisture and momentum between the land surface and the atmosphere ('local effects'), but also at neighboring or remote regions ('nonlocal effects'). Observations indicate that local effects induce a warming in most locations while climate models show a global mean cooling when simulating global deforestation. Here, we show that a strong albedo-induced nonlocal cooling in climate models strongly contributes to these conflicting results. When averaged globally, we find nonlocal cooling not only when simulating the biogeophysical effects of global deforestation, but also when simulating realistic areal extents and spatial distributions of deforestation. We conclude that, because the observations cannot capture the nonlocal effects, climate models are needed to better understand and quantify the full climate effect of deforestation.

4.1 Introduction

In the recent years, global-scale datasets based on observations revealed that deforestation substantially influences surface temperature locally (Li et al., 2015; Alkama and Cescatti, 2016; Bright et al., 2017). Satellite-based observations measured the difference in surface temperature of forested versus open land either in space (Li et al., 2015) or in time (Alkama and Cescatti, 2016), and a semi-empirical approach employed in-situ observations from the FLUXNET database (Bright et al., 2017). The observation-based datasets provide valuable information not only for local mitigation and adaptation measures (Bright et al., 2017) but can also serve as a benchmark for

[1] In collaboration with C. H. Reick, Q. Lejeune, and J. Pongratz.

the evaluation of deforestation effects in climate models (Alkama and Cescatti, 2016). Although the underlying methods differ substantially (Methods), these observation-based datasets largely agree that local effects of deforestation induce a warming in most regions, especially in the low and mid latitudes while there is less agreement about a slight cooling from the local effects of high-latitude deforestation (Appendix Fig. C.1).

Similar to the observations, the biogeophysical effects of global-scale deforestation in climate models induce a warming in low latitudes and a cooling in high latitudes (Brovkin et al., 2009; Davin and de Noblet-Ducoudré, 2010; Devaraju et al., 2015). However, the latitude at which deforestation becomes cooling is shifted much further south in models (e.g., Zhang et al., 2014a), and also the oceans contribute to a cooling (e.g., Davin and de Noblet-Ducoudré, 2010). There seems to be a surprising discrepancy between a strong global mean cooling of more than 1.3 K for global deforestation in fully coupled climate models (Bala et al., 2007; Brovkin et al., 2009; Davin and de Noblet-Ducoudré, 2010; Devaraju et al., 2015) and a domination of deforestation-induced warming in the observations.

We hypothesize that the nonlocal effects are responsible for this apparent discrepancy. Large-scale deforestation in *climate models* may trigger substantial nonlocal effects via advection and changes in circulation (Swann et al., 2012; Devaraju et al., 2015). On the other hand, nonlocal effects in the **observations** cancel out by construction because changes triggered by deforestation at one location affect both forested and nearby open land at other locations in a paired-site set-up (Bright et al., 2017). Thus, the absence of nonlocal deforestation effects in observation-based datasets may explain the apparent discrepancy of 'mostly warming' in observations and 'mostly cooling' in climate models. This hypothesis could previously not be tested because until recently (see chapter 2) local and nonlocal effects in climate models could not be separated. Despite their possible importance, the nonlocal effects are still lacking a thorough understanding. For instance, it is unclear whether the nonlocal effects only exist in idealized scenarios of large-scale deforestation or also in more realistic deforestation scenarios because the nonlocal effects may depend on the areal extent (Lawrence and Vandecar, 2014) and location (Devaraju et al., 2015) of deforestation.

Here we investigate to what extent a cooling associated with nonlocal effects can explain differences between simulations and observations. In simulations of deforestation with the fully coupled climate model MPI-ESM (Giorgetta et al., 2013) we use a recently developed method (see section 2.2.3) to separate local and nonlocal biogeophysical effects. We bridge the gap between simulations of idealized large-scale deforestation and more plausible scenarios of deforestation by analyzing the local and nonlocal effects of different areal extents and different spatial distributions of deforestation. To assess the robustness of the nonlocal effects, we compare changes in surface temperature for historical and future deforestation across a wide range of climate models.

4.2 Methods

4.2.1 Separation of local and nonlocal effects in the MPI-ESM

In simulations from the MPI-ESM, we separate local and nonlocal effects as follows (see also section 2.2.3): We define the nonlocal effects as the simulated signal ad grid boxes that were not deforested. We spatially interpolate the nonlocal effects to the deforested grid cells located in between. At these deforested grid cells we then define the *local effects* as the simulated signal minus the nonlocal effects. For the local effects displayed in Figs. 4.1 and C.1, we spatially interpolate the local effects also to the un-deforested grid cells.

We apply this separation of local and nonlocal effects to simulations with the climate model MPI-ESM at about 1.9° resolution. For all simulations, we use an interactive ocean because this is essential for capturing the full biogeophysical response to deforestation (Davin and de Noblet-Ducoudré, 2010). We run each simulation experiment for 350 years and analyze the last 200 years. In order to only simulate the biogeophysical effects, we prescribe CO_2 concentrations at preindustrial level. We simulate climate in a forest world where forest cover is prescribed in the entire vegetated part of all model grid cells. In order to investigate the sensitivity of the nonlocal effects to an increasing deforestation area, we completely replace forest by grasslands in one, two, or three of four grid cells (simulations '1/4', '2/4', and '3/4') in a regularly spaced pattern (coloured grid boxes in Fig. C.2).

A better understanding of the nonlocal effects requires knowledge about the location of deforestation where the nonlocal effects are triggered. While a given nonlocal effect cannot be attributed to a specific deforestation location, we can constrain the nonlocal effects to deforestation of the high, mid, and low latitudes by simulating deforestation in these latitudinal bands separately (simulations 'low latitudes' (17° S - 17° N), 'mid latitudes'(17° - 41° S and 17° - 41° N), and high latitudes (>41° S and >41° N)). The exact latitudes were chosen such that the areal extents of deforestation (about twice the historically deforested area) are approximately equal to the areal extent in the '1/4' simulation in all three simulations. To analyze the nonlocal effects of a more realistic spatial distribution, we deforest the same areal extent but we locate deforestation grid cells near areas that were historically deforested (simulation '1/4_historical'). In these four simulations, we deforest only three of four grid cells in the respective region, so we are still able to separate local and nonlocal effects. While in these simulations all surface properties (albedo, evapotranspiration efficiency, surface roughness) are changed from forest to grass values, in an additional simulation we only change surface albedo from forest to grass values in 3/4 of all grid cells (simulation 'only albedo'). Like this, we can assess the role of changes in surface albedo for the local and nonlocal effects separately.

4.2.2 Isolation of local and nonlocal effects across models

In order to compare local and nonlocal effects across climate models, we isolate the local effects from existing simulations of the biogeophysical effects of changes in forest cover in other fully coupled climate models. For this particular set of existing simulations (historical, RCP2.6 and RCP8.5, see Table 5.1), we cannot use the separation approach described above because deforestation in these plausible scenarios deforestation does not happen in a regular spatial pattern that includes no-deforestation grid cells. Thus, we isolate the local effects by using the moving-window approach of (Lejeune et al., 2017a). We then calculate the nonlocal effects as the simulated total minus local effects, which is different from the approach above where we first isolated the nonlocal effects and then used them for obtaining the local effects. We use the last 30 years in which data are available for all models. These years are 1971 - 2000 for historical changes in forest cover, and 2070 - 2099 for changes in forest cover in the RCP simulations. Different numbers of ensemble members are available for the different models. For instance, for RCP2.6 in the MPI-ESM, there are 3 ensemble members with and 2 without deforestation. Thus, in Fig. 4.4 we show $3 \times 2 = 6$ combinations of ensemble members. For the numbers of available ensemble members in the respective models, see Appendix Table 5.1.

4.2.3 Comparison of the effects on surface temperature in the MPI-ESM to observational datasets

We compare simulated total, local and nonlocal effects on surface temperature in the MPI-ESM to two datasets inferred from satellite observations (Li et al., 2015; Alkama and Cescatti, 2016) and one semi-empirical dataset (Bright et al., 2017) based on FLUXNET observations. A these datasets should be compared with care not only because the spatial coverage and the underlying methods differ strongly. While the two satellite-based datasets (Li et al., 2015; Alkama and Cescatti, 2016) only employ observations under cloud-free conditions, the ground-based observations (Bright et al., 2017) are free of this cloud bias. Conversions between different vegetation types are analyzed in the different datasets. The dataset by (Li et al., 2015) considers differences between forests and 'open land' (grasslands and croplands). The dataset by Alkama and Cescatti (2016) considers forest cover changes related to different drivers such as forest clearings for agriculture, forestry, or disturbances such as forest fires or windstorms (Hansen et al., 2013). For the dataset by Bright et al. (2017), we average the data of their Figs. 2 *d*), *e*), and *f*) which examine the conversion between different forest types and grass. We weigh this average with the occurrence of the respective forest type in MPI-ESM.

For the observational range in Fig. 4.1, we average latitudinally over locations where values in at least one of the three datasets are available. For the dataset by Alkama

and Cescatti (2016), we weighted the data for the latitudinal average with the forest loss at the respective locations. The corresponding Appendix Fig. C.1 shows only locations where forest loss exceeds 1% in the analysis time frame (years 2003 - 2012).

4.2.4 Deforestation-induced warming due to land carbon loss

To provide a first-order estimate of the importance of biogeophysical effects to those of deforestation–related carbon emissions we estimate how much carbon would be released to the atmosphere by the deforestation applied in the '1/4_historical' simulation. For this, we scale the respective deforestation areas with carbon values of different forest types as used in a bookkeeping model for land-use emissions (Hansis et al., 2015). The range in Fig. 4.2 includes an upper estimate (starting with values for primary forest of the default dataset used in that study) and a lower estimate (starting with values for secondary forest of the alternative dataset with lower carbon values). The resulting change in carbon is then converted in a change into global mean temperature using the MPI-ESM value of the transient response to cumulative emissions (Gillett et al., 2013).

4.3 Towards an understanding of the nonlocal effects

4.3.1 Nonlocal effects exacerbate comparison against observations

We find that our hypothesis is confirmed. In regions where observations are available, the changes in surface temperature from nonlocal effects contribute to the difference between the local effects in the observation-based datasets (Li et al., 2015; Alkama and Cescatti, 2016; Bright et al., 2017) and the total (local plus nonlocal) effects in the MPI-ESM (Fig. 4.1 and Appendix Fig. C.1). The local effects from the MPI-ESM largely lie within the range of these observations. In the northern mid and high latitudes, the local effects in the model match the observations reasonably well. However, for deforestation of three of four grid cells (simulation '3/4') a nonlocal cooling of up to 0.9 K strongly contributes to the difference between total effects and observations. The nonlocal effects may depend on the areal extent of deforestation (see next paragraph) and thus even be stronger in the case of deforestation in all grid cells globally.

There are regions where even the isolated local effects in the model do not match the observations particularly well. For instance, in the southern-hemisphere tropics the

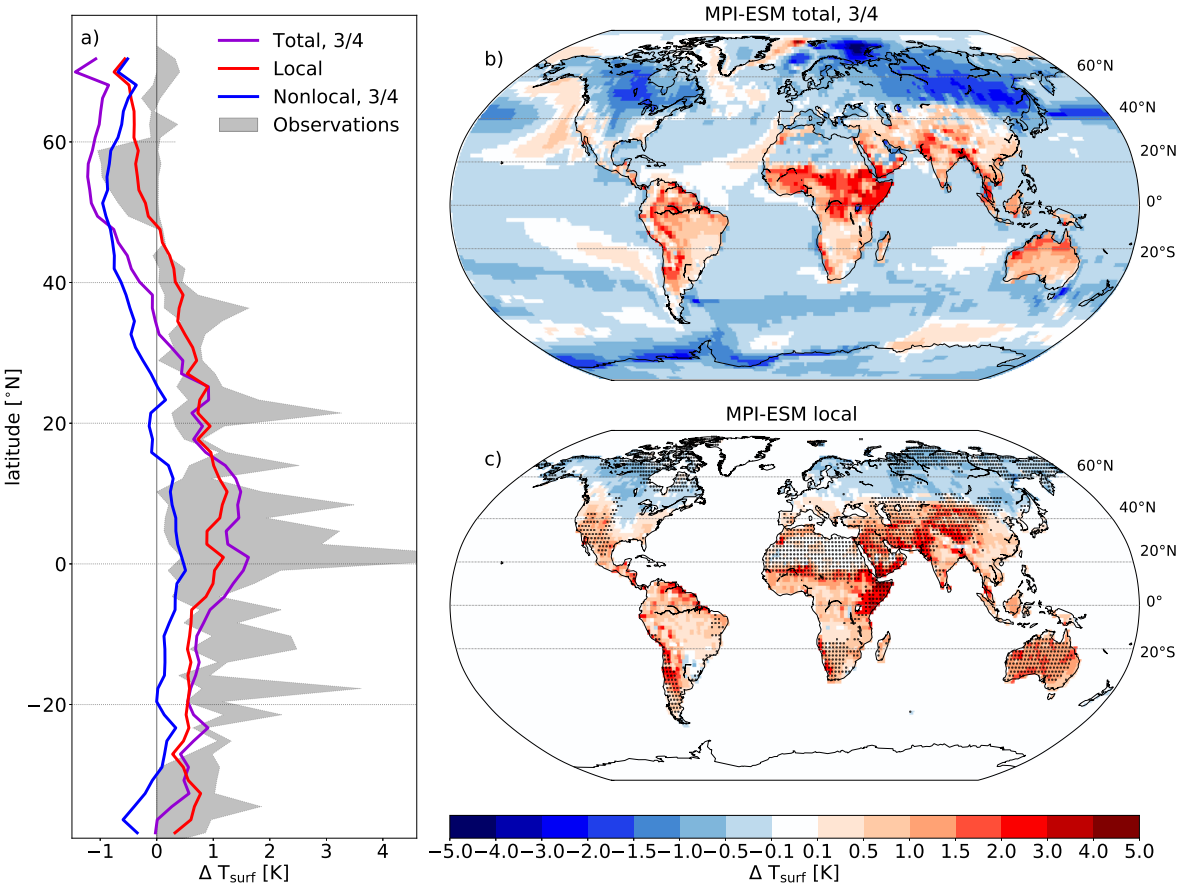

Figure 4.1: Comparison of biogeophysical effects on surface temperature in the MPI-ESM versus observations. The shaded area in the latitudinal plot indicates the range of three observation-based datasets (Li et al., 2015; Alkama and Cescatti, 2016; Bright et al., 2017), the lines indicate total, local and nonlocal effects when simulating deforestation of three of four grid cells ('3/4') in the coupled climate model MPI-ESM. For the latitudinal averages, values in the MPI-ESM are restricted to areas where values in at least one of the observational datasets is available (bottom, land grid cells that are not stippled). The results for the MPI-ESM are shown on the right. Top: total (local plus nonlocal) deforestation effects. Bottom: local effects isolated as in section 2.2.3. The map for the nonlocal effects is shown in Fig. 4.3 *a*), and maps of the observation-based datasets are shown in Appendix Fig. C.1.

deforestation-induced local warming is underestimated by the MPI-ESM. There, either the model could be biased due to a misrepresentation of processes, or the observations could be biased because of high cloud cover in the satellite-based observations (Li et al., 2015; Alkama and Cescatti, 2016) and large spatial gaps between the FLUXNET sites (Bright et al., 2017).

4.3.2 Analysis of the nonlocal effects in the MPI-ESM

The importance of the nonlocal effects becomes even more apparent when not only focusing on temperature changes in regions where observations are available but con-

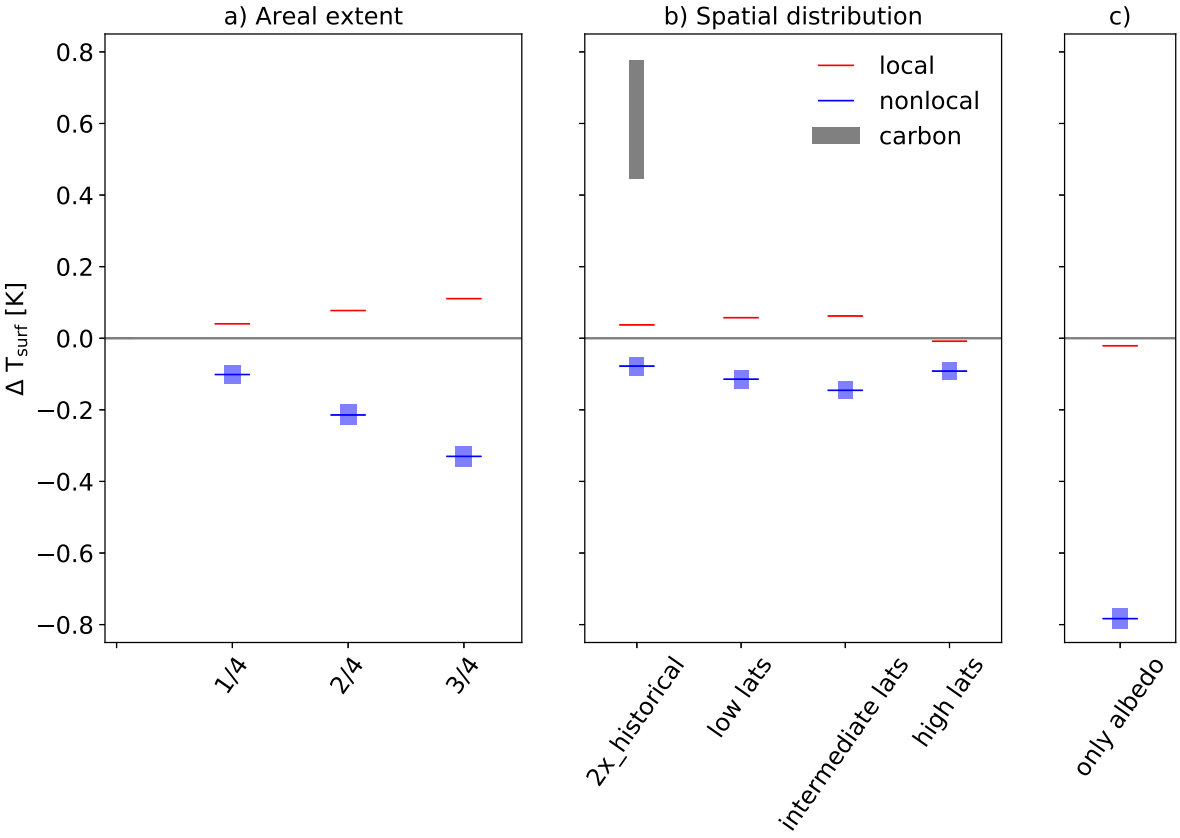

Figure 4.2: Drivers of the nonlocal cooling. The thin horizontal lines denote the globally averaged temperature changes, and the colored rectangles denote the 95% confidence intervals. The globally averaged nonlocal changes in surface temperature depend on *a*) the areal extent of deforestation (1, 2 or 3 of 4 grid cells) and *b*) the location of deforestation (near historically deforested areas or in low, mid, and high latitudes). The gray bar ('carbon') represents an estimate of the temperature increase due to land carbon loss associated with the '1/4_historical' scenario; the corresponding values are obtained using a bookkeeping approach and the transient response to cumulative emissions (Methods). *c*) the simulated processes. The effects of only changing albedo are largely restricted to the nonlocal effects.

sidering changes in global mean surface temperature (Fig. 4.2). Spatially homogeneous deforestation of three of four grid cells (simulation '3/4') results in a global mean warming of ~0.1 K for the local effects and a global mean cooling of ~-0.3 K for the nonlocal effects. The local warming is thus overwhelmed by a nonlocal cooling in our simulations. The simulated ratio of 1 : -3 between global mean local warming and nonlocal cooling remains constant when simulating deforestation of one, two, or three of four grid cells. Thus, in contrast to previous studies (Lawrence and Vandecar, 2014), we find that both local and nonlocal effects scale linearly with the number of deforested grid cells (see also maps in Appendix Fig. C.2). Thus, the nonlocal effects dominate the globally averaged response not only when simulating idealized large-scale deforestation as frequently performed in previous studies (Brovkin et al., 2006; Bathiany et al., 2010), but also when simulating smaller areal extents of deforestation closer to

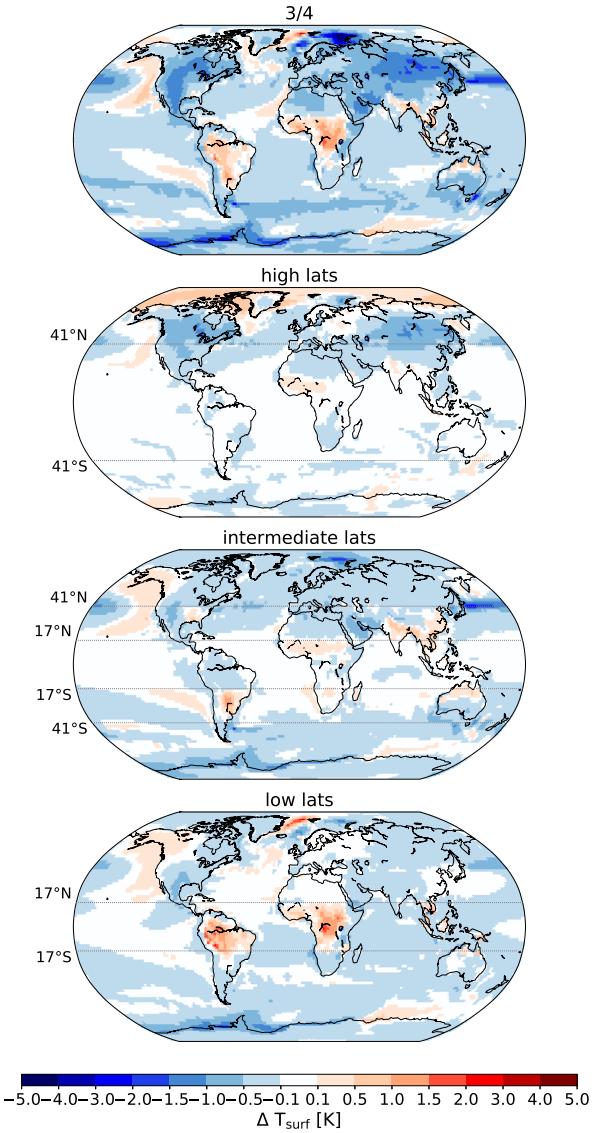

Figure 4.3: Nonlocal effects on surface temperature [K] in the MPI-ESM and the contributions from deforestation in latitudinal bands. Changes in surface temperature when simulating deforestation of three of four grid cells globally, in the high-, mid-, and low latitudes. The dashed lines denote the borders of deforestation in the respective simulations.

those altered historically or projected for the next century.

The climate effects depend not only on the areal extent, but also on the location of deforestation. While the 1 : -3 ratio was obtained by simulations in which deforestation is distributed homogeneously across the globe, the nonlocal cooling also dominates when simulating a more realistic spatial distribution of deforestation ('1/4_historical') in which deforestation is simulated in a spatial pattern similar to historical deforestation. Furthermore, the nonlocal effects exert a global mean cooling for deforestation in all three latitudinal bands. For high-latitude deforestation, this cooling is in line with the total biogeophysical effects in previous studies (Bonan et al., 1992; Betts, 2000; Mahmood et al., 2014). However, the nonlocal cooling in our simulations is even

stronger for low- and mid-latitude deforestation (Fig. 4.2 *b*).

The global mean nonlocal cooling signal of low-latitude deforestation challenges the wide-spread idea that the biogeophysical effects of tropical deforestation induce a warming (Bonan, 2008; Mahmood et al., 2014). Three aspects shed light into this apparent contradiction: First, while we consider only biogeophysical effects, some studies included the effect of land carbon losses related to tropical deforestation (Bala et al., 2007; Bathiany et al., 2010), which contribute a strong warming. Second, some studies look only at the local effects (Li et al., 2015; Alkama and Cescatti, 2016; Bright et al., 2017) or at least include the local effects (Claussen et al., 2001; Findell et al., 2006), for which the global mean effect of low-latitude deforestation is also warming in our simulations (Fig. 4.2 *b*). Third, even in our simulations the nonlocal effects cause a regional surface warming of the low latitudes (Fig. 4.3) because of a regional decrease in clouds and precipitation. However, the global average of the effects of low-latitude deforestation is dominated by the nonlocal cooling that extends much beyond the deforested regions (Claussen et al., 2001) (Fig. 4.3).

The change in surface albedo has been identified as the driver of the biogeophysical cooling in deforestation simulations (Davin and de Noblet-Ducoudré, 2010). For a better understanding of this cooling, we separate local and nonlocal effects resulting from a change in only surface albedo from forest to grass values while preserving all other surface properties. As expected, an increase in surface albedo leads to a cooling in both the local and nonlocal effects because more solar incoming radiation is reflected by the brighter grasslands. Surprisingly, the vast majority of this cooling is excluded from the local effects (Fig. 4.2 *c* and Appendix Fig. C.2): within a brightened grid box, the decrease in net solar radiation is largely balanced by latent and sensible heat fluxes (Appendix Fig. C.3) and thus the local surface cooling is small. The decrease in latent and sensible heat fluxes in the brightened grid cells leads to cooler and drier air, and this cooler air is carried to neighboring and remote grid cells via advection. Therefore the albedo-induced cooling is mostly found in the nonlocal effects and may thus be lacking in the observations. This implies that, while the local temperature response to deforestation is driven by non-radiative processes (Bright et al., 2017), the radiative processes are essential for the nonlocal (and thus also the full) temperature response.

4.3.3 Intermodel comparison of nonlocal effects

The nonlocal cooling is not only apparent in the MPI-ESM, but also in other climate models. The global mean cooling in the MPI-ESM is rather small in comparison to other models ranging between -1.3 K and -1.6 K for the biogeophysical cooling resulting from global-scale deforestation (Bala et al., 2007; Davin and de Noblet-Ducoudré, 2010; Devaraju et al., 2015). In realistic scenarios of deforestation, we assess the robustness of the nonlocal cooling across a wide range of fully coupled climate models (Fig. 4.4).

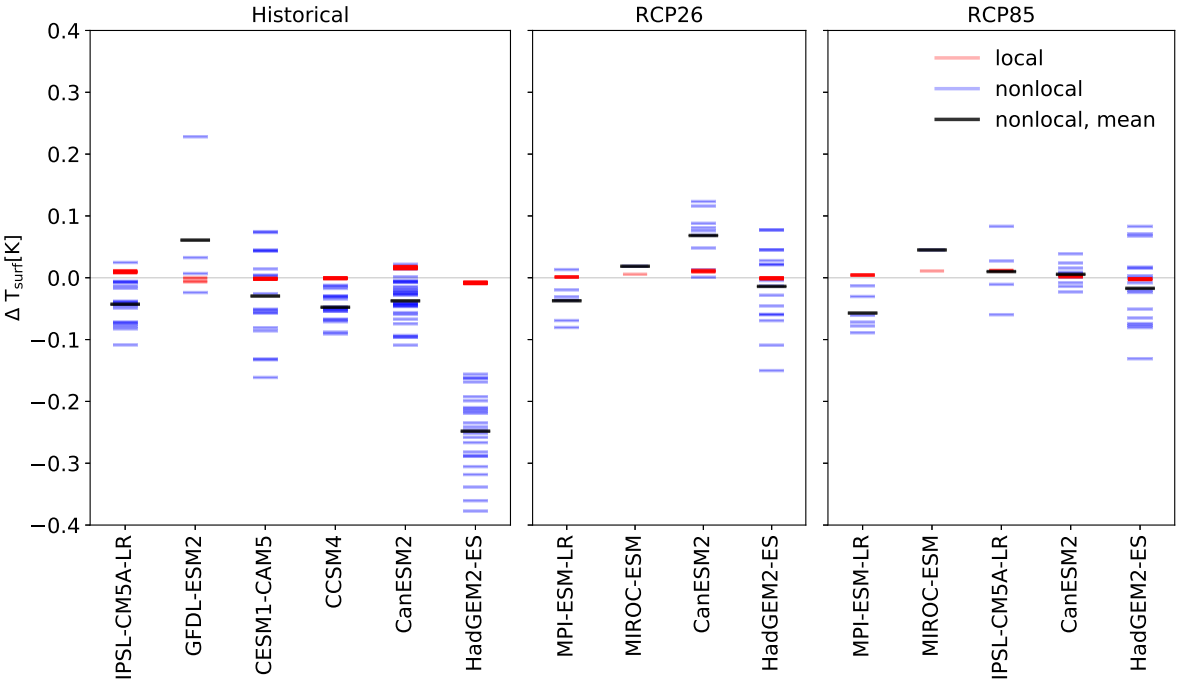

Figure 4.4: Comparison of local and nonlocal effects on surface temperature [K] across models. Changes in global mean surface temperature for (red, blue) different combinations of ensemble members and (black) the mean of all available ensemble members (Methods). Local effects are isolated as in (Lejeune et al., 2017a) (Methods). The nonlocal effects are approximated as the difference between simulated total and local effects. Shown are averages over the last 30 years of historical deforestation (years 1860 - 2000) and deforestation in the RCP2.6 and RCP8.5 scenario (years 2006 - 2100).

We use a method to isolate the local biogeophysical effects from existing simulations (Lejeune et al., 2017a) (Methods) of historical deforestation and deforestation in the scenarios RCP2.6 and RCP8.5 (Moss et al., 2010), and we define the nonlocal effects as the simulated total minus local effects. Consistently with our idealized experiments in the MPI-ESM, the nonlocal effects induce a cooling in all models except in models where only few ensemble members are available. Within one model, the spread across the ensemble members is much smaller for the local effects (most values in Fig. 4.4 happen to be plotted on top of each other) than for the nonlocal effects because the climate variability is by construction largely included in the nonlocal effects (Kumar et al., 2013; Lejeune et al., 2017b). The method that we use here to isolate the local effects across models might underestimate the local effects (Lejeune et al., 2017a) (Appendix Fig. C.4). An underestimated local warming would imply an underestimated nonlocal cooling, so we think that this underestimation of the local effects does not affect our conclusion that there is a tendency towards nonlocal cooling across the models.

4.4 Conclusions and outlook

We conclude that the local effects alone –and thus also observations– yield a highly incomplete picture of the climatic consequences of deforestation. The nonlocal effects can strongly contribute to the mismatch between models and observations because the albedo-induced nonlocal cooling may largely be excluded from observation-based datasets. When focusing on global mean surface temperature, the nonlocal cooling by far exceeds the local warming. Whether the local or nonlocal effects are considered to be more important depends on the perspective. While the local effects are important for a consistent model evaluation (Alkama and Cescatti, 2016) and may support local adaptation and mitigation strategies (Bright et al., 2017), our results show that the nonlocal effects are essential if the biogeophysical effects are considered for an implementation in policies that aim at mitigating global climate change.

Forests have been identified as a key component for the mitigation of global climate change (Grassi et al., 2017). Observation-based studies suggested that afforestation, originally intended to store carbon, might co-benefit from a local biogeophysical cooling (Li et al., 2015; Alkama and Cescatti, 2016; Bright et al., 2017). But instead, when including the nonlocal effects, we find that the biogeophysical effects may reduce the carbon-related climate benefits of afforestation (estimated as 'carbon' in Fig. 4.2, see Methods). Before the biogeophysical effects can be included in climate policies, a better understanding of the nonlocal effects is needed. Because the observations lack the nonlocal effects, climate models are essential to better understand and quantify the full climate effect of deforestation.

Chapter 5

Summary, Conclusions and Outlook

5.1 Summary of methods

This thesis focuses on the separate analysis of the local and nonlocal effects of land cover change (LCC) on surface temperature. In the following, the employed methods are briefly summarized. A more detailed description can be found in the methods section of the respective chapter.

All three main chapters of this thesis employ simulations of LCC using the Max Planck Institute Earth System Model MPI-ESM (Giorgetta et al., 2013). The effects of deforestation in the MPI-ESM is calculated by comparing climate in two simulations: In one simulation forests are prescribed in specific model grid cells, and in a second simulation grasslands are prescribed in these grid cells. In all simulations atmospheric CO_2 concentrations are prescribed to simulate only the biogeophysical effects of LCC. The local and nonlocal biogeophysical effects can be separated because LCC was only performed in specific grid cells while leaving vegetation unchanged in other grid cells in a regularly spaced pattern. For details of the separation approach, see section 2.2.3.

There are some methodological features that link all three main chapters, such as the separation method for local and nonlocal effects, or methods that are shared by two chapters, such as the comparison of local and nonlocal effects with observations in chapters 2 and 4. However, there are also some methodological features that are unique to the respective chapters:

- **Chapter 2** focuses on the local effects. All simulations for this chapter are performed using the land-atmosphere model ECHAM6/JSBACH3. Sea surface temperatures (SSTs) and sea ice are prescribed in order to prevent strong LCC-induced changes in background climate and in order to reduce climate-related noise, and thus 30 years of simulations were sufficient for an analysis of the local effects. The changes in the components of the surface energy balance are analyzed separately, e.g. as in the paper by Luyssaert et al. (2014). This energy balance

decomposition is employed separately for the local and nonlocal effects on surface temperature to enhance process understanding.

- **Chapter 3** investigates differences between the local effects between historical LCC and plausible scenarios of future LCC. The background climate may differ for LCC in the past and in the future and background climate may substantially influence the LCC effects (Pitman et al., 2011). To study this, the set of simulations from chapter 2 in present-day background climate is extended by simulations in a warmer RCP8.5 background climate. Furthermore, a look-up approach for the local effects is developed by which a change in forest cover within a grid cell can be directly converted into a resulting change in surface temperature. To assess whether locally surface temperature responds linearly to a decrease in forest cover, the experiments from chapter 2 of 100% of deforestation within the grid boxes are extended by simulations of deforestation in steps of 25%.

- **Chapter 4** focuses on the nonlocal effects. An interactive ocean model is essential to simulate the full climate effect of LCC (Ganopolski et al., 2001; Davin and de Noblet-Ducoudré, 2010), in particular for the nonlocal effects because changes in climate that are induced by changes in SSTs are felt also in model grid cells where vegetation remains unchanged. Thus, all simulations for this chapter are performed using the fully coupled climate model MPI-ESM. Because of the substantial climate variability the analysis is based on longer simulations than in chapter 2, 200-year means are analyzed instead of 30-year means. Local and nonlocal effects on surface temperature are separated not only for a regularly spaced pattern of LCC but also for LCC concentrated in specific regions. In order to improve process understanding, local and nonlocal effects are separated in a simulation where forests are replaced by a 'bright forest', so only surface albedo is increased from forest to grass values while all other surface properties of the forest areas remain unchanged. An inter-model comparison for the nonlocal effects is employed to assess the robustness of the nonlocal effects across models.

5.2 Lessons learnt from the isolation of the local effects

Chapters 2 and 3 focus on the locally induced changes in surface temperature, which could not be investigated independently of nonlocal effects (including climate variability) in most previous studies. The main findings concerning the local effects are:

1. The approach that is developed in chapter 2 to isolate the local effects is robust. Within one grid cell the local effects are largely independent of the areal extent of LCC outside of this grid cell. Thus, the local effects are largely independent of the LCC scenario.

2. Both concerning the sign and the order of magnitude, the locally induced changes in surface temperature in the MPI-ESM agree reasonably well with three observation-based datasets (Li et al., 2015; Alkama and Cescatti, 2016; Bright et al., 2017). Deforestation in the MPI-ESM locally induces an annual mean warming in the tropics and mid latitudes as well as a cooling –with a strong seasonal cycle– in the high latitudes.

3. The local effects depend on the background climate (Pitman et al., 2011), and chapter 3 shows that this substantially contributes to differences between the local effects for historical LCC and future LCC in the RCP scenarios.

4. Surface temperature in ECHAM6/JSBACH3 locally responds nonlinearly to LCC. In the low and mid latitudes, the deforestation-induced warming is only weak when reducing forest cover within a model grid cell from 100% to 25%, but removing the last 25% of forests locally leads to a strong warming.

5.3 Lessons learnt from the isolation of the nonlocal effects

Chapter 2 emphasizes that the nonlocal effects depend strongly on the areal extent of LCC and that the nonlocal effects of global LCC, which could not be isolated in previous studies, can be as large as the local effects in a set-up with prescribed SSTs. In order to capture the full nonlocal effects, chapter 4 systematically investigates the nonlocal effects of LCC in a fully coupled climate model. The main findings concerning the nonlocal effects are:

1. In the case of where deforestation is applied in a regular spatial pattern, the globally averaged nonlocal effects scale linearly with the number of deforested grid cells. Thus, nonlocal effects can also be triggered for a small areal extent of LCC.

2. The nonlocal effects depend on the spatial distribution of LCC. Deforestation in the inner tropics leads to a nonlocal warming regionally, but on a global average the nonlocal effects lead to a cooling for deforestation in the low, mid, and high latitudes.

3. The increase in albedo is responsible for this nonlocal cooling. When only increasing the albedo, the nonlocally induced cooling is even stronger compared to simulations where all surface properties are switched from forest- to grassland state.

4. The nonlocal cooling is not only apparent in the MPI-ESM but also in other climate models, although a definite conclusion is exacerbated because in most models the nonlocal effects are small compared to climate-induced variability.

5.4 Both local and nonlocal effects matter

As described in chapter 2, the separate analysis of local and nonlocal effects, which was not possible in previous studies, enables a deeper process understanding of the underlying mechanisms for the local and nonlocal effects. The local effects are mainly driven by changes in local surface properties whereas the nonlocal effects are driven by changes in atmospheric conditions that are via advection also transported to locations where no LCC happened. Because the mechanisms differ so strongly between local and nonlocal effects, there are good reasons to investigate either of the two effects in isolation. Whether the local or nonlocal effects should be considered depends on the application, as is elaborated the following two paragraphs.

An isolation of the *local effects* may be beneficial in many situations. For instance, the isolated local effects may serve as a testbed for an **inter-model comparison** of biogeophysical LCC effects (Lejeune et al., 2017b). Previous inter-model comparison studies struggled with a poor signal/noise ratio. As shown in chapter 2 and previous studies (e.g., Kumar et al., 2013), the local effects largely exclude climate-induced noise thus an isolation of the local effects is essential in inter-model comparisons, especially for variables with a particularly poor signal/noise ratio such as precipitation. In addition, even if the areal extent and spatial distribution of LCC differs across models (de Noblet-Ducoudré et al., 2012), the local effects are largely independent of the spatial distribution of LCC (see chapter 2), and this robustness warrants a consistent comparison across models. Furthermore, as shown in chapter 4, an isolation of the local effects is essential when **comparing observations against models** because the nonlocal effects substantially contribute to a mismatch between the local effects in observations and the total effects of global deforestation in climate models. Finally, a quantification of the local effects may be required for policies that aim at reducing surface temperature locally.

Some applications may not require the isolated local effects but the *nonlocal effects*. For instance, most people do not live in forests, but rather next to forests or even far away from any forest. Thus for assessing the climatic consequences of LCC on **living conditions** the nonlocal effects may be the key aspect. In particular the nonlocal effects are essential for a possible implementation of the biogeophysical effects in international policies that aim at mitigating regional to global climate change. Thus, a better understanding and quantification of the nonlocal effect is required.

To conclude, this thesis establishes a link between the biogeophysical effects of large-scale LCC and more plausible LCC scenarios. The local effects within a grid box are largely independent of LCC elsewhere, while the nonlocal effects strongly depend on the extent and spatial distribution of LCC. Furthermore, the nonradiative processes are dominating the local effects (Bright et al., 2017) but this thesis emphasizes that the radiative processes (mainly due to albedo change) are essential for the nonlocal effects and thus the total climate response. Thus, this thesis reconciles the gap between

previous estimates of deforestation-induced negative radiative forcing (e.g., Rotenberg and Yakir, 2010; Pongratz et al., 2010) and local warming in many locations in observations (Li et al., 2015; Alkama and Cescatti, 2016; Bright et al., 2017). Finally, the new method to separate local and nonlocal effects opens pathways for further research as outlined in the next section.

5.5 Pathways for further research

Expanding the understanding of LCC effects in the MPI-ESM

While this thesis contributes to clarifying how surface temperature is influenced by LCC locally and LCC elsewhere, there are still open questions regarding the local and nonlocal LCC effects in the MPI-ESM. Most of the following research questions might even be tackled with existing simulations that were performed in the context of this thesis.

1. Deforestation in the MPI-ESM influences temperature not only at the surface but also **temperature of the atmosphere**. The decrease in surface roughness that is associated with deforestation alters the redistribution of latent and sensible heat between surface and atmosphere. Thus, surface temperature and atmospheric temperature can be expected to react quite differently to deforestation. While we have shown that the local effects are much weaker for 2m-air temperature (Fig. A.3.1) compared to surface temperature (Fig. 2.2), it is not clear whether local effects exist for temperature of even the lowest layer of the atmosphere model or whether any temperature signal that reaches the atmosphere is immediately advected away into neighboring and remote grid cells.

2. While this thesis focuses on surface temperature, the focus of further studies may extend to additional variables and processes. For instance, it is unknown how LCC-induced changes in **cloud cover** and associated cloud radiative effects influence climate locally and elsewhere. Furthermore both local and nonlocal changes in cloud cover and precipitation may be sensitive to the **choice of the convection scheme** that is employed in the atmospheric part of the model. Finally, both productivity and respiration on land are influenced by temperature and the availability of soil water, both of which are influenced by the local effects. This warrants research on the influence of the biogeophysical effects on the **land carbon storage**.

3. Appendix A.2 and previous studies highlighted the strong seasonality of the local effects (e.g., Malyshev et al., 2015) and the strong mitigation potential of the local effects during heat extremes (Lejeune et al., 2017a). However, the role of the *nonlocal* effects during **heat extremes** and the **seasonality** of the nonlocal

effects remains largely unknown. Furthermore, a **changing background climate** may not only affect the land carbon storage (Schneck et al., 2015; Sonntag et al., 2016) and the local biogeophysical effects of LCC (e.g., chapter 3), but also the nonlocal effects may be substantially influenced e.g. by a decrease in snow cover.

4. Chapter 4 opens pathways for a better **understanding of the nonlocal effects**. The different length scales at which the nonlocal effects act warrant more research. For instance, Fig. 4.3 suggests that the nonlocal effects of low-latitude deforestation induce a regional warming whereas the nonlocal cooling extends much beyond the deforestation region. It remains unclear where the nonlocal effects are exactly triggered, and new methodologies are needed for the more precise attribution of nonlocal effects to originating regions. Process understanding may be improved by not only separating local and nonlocal effects of changes in surface albedo but also the other surface properties evapotranspiration efficiency and surface roughness.

5. All simulations were performed with a model version of the MPI-ESM that may over-simplify some processes. For instance, all plant types within a grid cell share one soil moisture reservoir, which may not be adequate in cases where forests and grasslands are spatially clearly separated. A more adequate representation of hydrology and the implementation of a canopy model in the MPI-ESM may **improve the inclusiveness** of the processes that are relevant for the biogeophysical LCC effects.

6. Living conditions not only depend on temperature but rather on **perceived temperature** which is also influenced by humidity, solar and thermal radiation and wind speed (e.g., Staiger et al., 2011). Future studies may focus on local and nonlocal effects of LCC on perceived temperature.

Going beyond effects in the MPI-ESM and going beyond LCC

In this thesis, the approach to separate local and nonlocal effects was applied to the biogeophysical effects of LCC with a focus on surface temperature in the MPI-ESM. The separation approach presented in chapter 2.2.3 enables a wide range of applications that reach far beyond this work.

A separate analysis of the local and nonlocal effects opens ways for **improving process understanding across models in inter-model comparison studies**. Local and nonlocal effects may be compared separately across models. Such a comparison may identify whether the large spread that was found in previous intercomparison studies (e.g., Pitman et al., 2009; de Noblet-Ducoudré et al., 2012; Boysen et al., 2014) originates from differences in land surface models or from differences in how atmosphere models react to a given change in the land forcing.

A **'cloud bias'** exists for local effects inferred from satellite-based observations. Satellites can observe surface radiometric temperature only during cloud-free conditions (e.g., Alkama and Cescatti, 2016), and the LCC effects under cloud-free conditions may be different in cloudy conditions (e.g., Li et al., 2015). In addition, the satellite observations may be biased because forests can actively influence cloud cover (Teuling et al., 2017) and thus under certain conditions satellite observations might still be available over open land but not over forests. To assess to what extent a cloud bias influences satellite observations, surface radiometric temperature from fluxnet sites – where temperature can be measured both under cloudy and cloud-free conditions– may be employed. In a paired-site set-up (one over forest, one over grassland) the LCC effects may be separately analyzed for cloudy versus cloud-free conditions. In studies that compare models and observations, the simulation results should be filtered for cloud-free conditions in order to ensure a consistent comparison.

Local and nonlocal effects may enable a deeper process understanding not only for the biogeophysical effects of land cover change but also for **land management** such as irrigation and forest management. In addition, the separation approach may shed more light onto a multitude of **other land surface processes** that may also influence climate elsewhere such as wildfires. Finally, the separation approach could be employed in studies on land-atmosphere–interactions such as the influence of soil moisture on heat extremes.

Appendix

A Appendix for chapter 2

A.1 Number of necessary simulation years for robust local effects

Throughout this chapter we use 30 years of simulations in our data analysis. To assess whether those 30 years are sufficient to identify the local contribution, we create an ensemble of 5 members for sparse LCC. For each of those members, we compare the mean of the first k years against the mean of all the years of the remaining four members, for the local effects and the total effects (local plus nonlocal), respectively. As a measure of inaccuracy, we calculate the Root Mean Square (RMS) deviation between the two maps, evaluated at all LCC cells. Fig. A.1.1 illustrates that, for sparse LCC, the RMS deviation is lower for the local effects than for the total effects. For the local effects, the RMS deviation seems to stabilize after 30 years, indicating that simulating longer than 30 years does not markedly increase accuracy of the results.

A.2 Regional analysis of seasonality for extensive LCC

Here we provide additional evidence for local and nonlocal effects being qualitatively different. For this purpose, we explore the seasonality of local and nonlocal effects separately. Local and nonlocal effects for boreal winter (DJF) and summer (JJA) are shown in Figs. A.2.1 to A.2.4 for changes in surface temperature and precipitation. The local changes in surface temperature vary seasonally: In the high northern latitudes, the local effects in winter are a cooling of up to 3 K (Fig. A.2.1 *b*), while in summer, the local effects are a warming of up to 0.5 K (Fig. A.2.2 *b*). In contrast, the nonlocal effects on surface temperature have the same sign in DJF and JJA in large parts of the boreal zone, such as northern Asia and Canada (Fig. A.2.1 *d* versus Fig. A.2.2 *d*). For precipitation, the largest difference between DJF and JJA is the location of zones in the tropics/subtropics where LCC leads to a reduction in precipitation; these zones are further north in JJA for both local and nonlocal effects (Figs. A.2.3 and A.2.4).

While the maps presented in Figs. A.2.3 to A.2.4 provide information about the seasonality of LCC-induced changes in surface temperature and precipitation, these figures

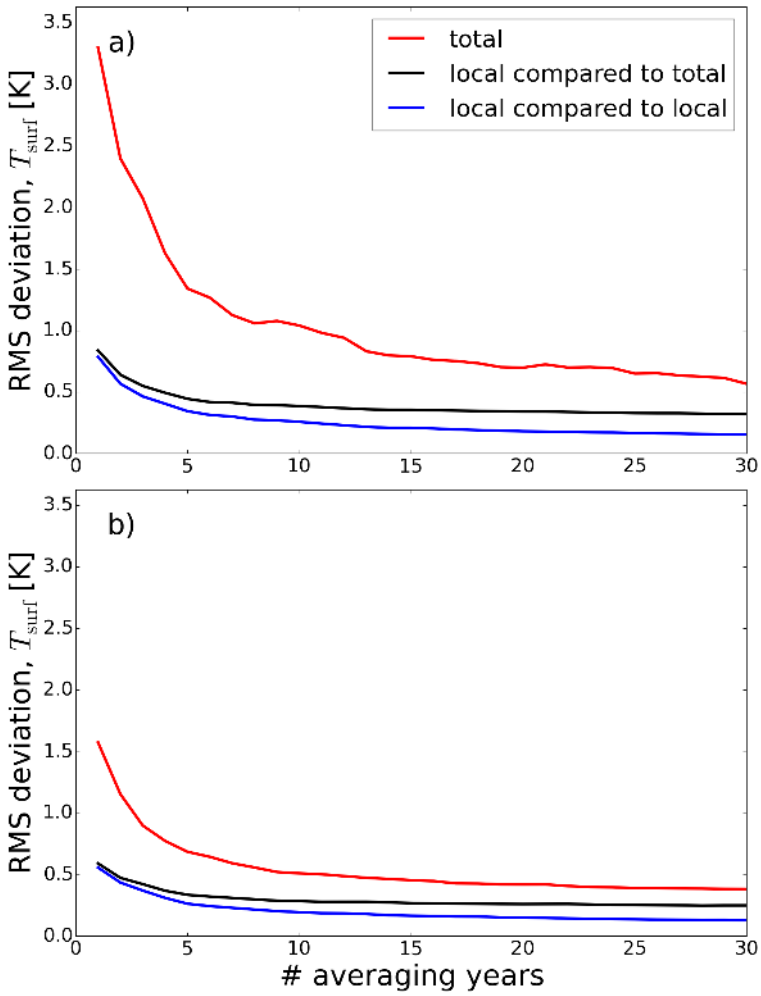

Figure A.1.1: Root Mean Square (RMS) deviation of surface temperature T_{surf} [K] for *a* January and *b* July, RMS deviation over all land areas. The lines show means of the 5 obtained values. The *y*-axis denotes the number of averaging years.

do not give insight in the underlying mechanisms. We select four regions, indicated by rectangles in Fig. A.3.1, where we identify the dominant mechanisms for local and nonlocal effects of extensive LCC in different climate regimes. To this end, we performe an energy balance decomposition in these four regions, and present the results in Fig. A.2.5.

Canada and Europe represent temperate regions with and without long-lasting snow cover. The local cooling in Canada in the winter and spring months (which is not apparent in Europe) originates from a reduction in shortwave net radiation, induced by an increase in surface albedo due to a combination of the local increase in snow cover and the loss of snow masking after deforestation. In contrast, the nonlocal effects exhibit an increase in shortwave net radiation, which partly originates from a nonlocal decrease in snow cover. The Amazon and Australia represent regions with humid and arid tropical/subtropical conditions, respectively. The local changes in latent and sensible heat in the Amazon are presumably linked to the LCC-induced changes in

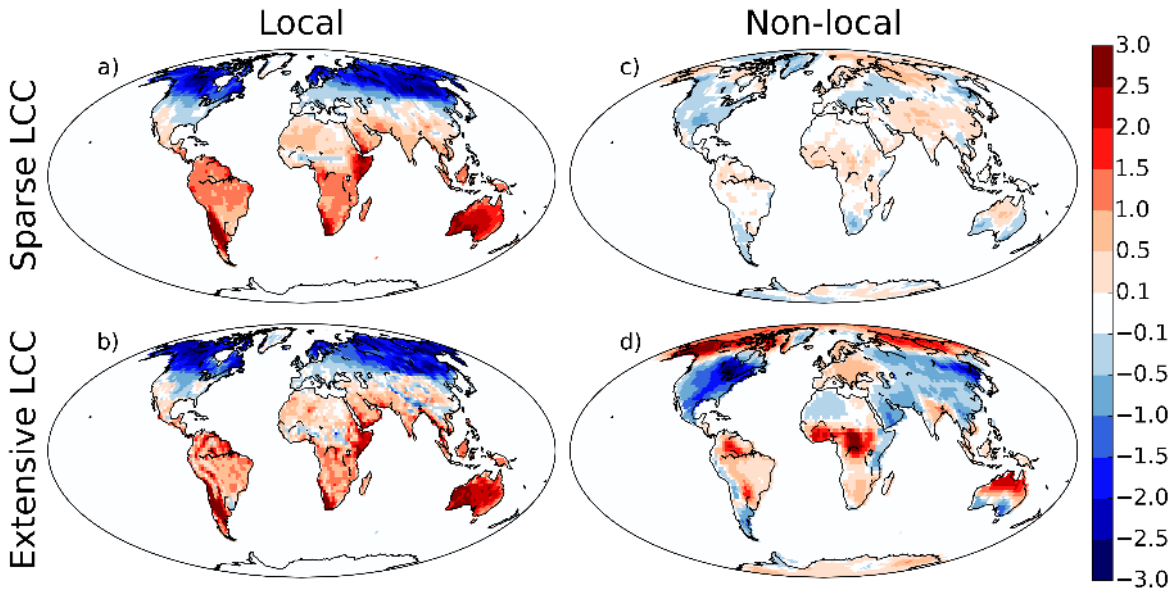

Figure A.2.1: Boreal winter (DJF) change in mean surface temperature [K] due to *a*,*c* sparse and *b*,*d* extensive deforestation. *a*,*b* local effects, *c*,*d* nonlocal effects. Mean over 30 years and another 30 years from a simulation with LCC cells shifted by two.

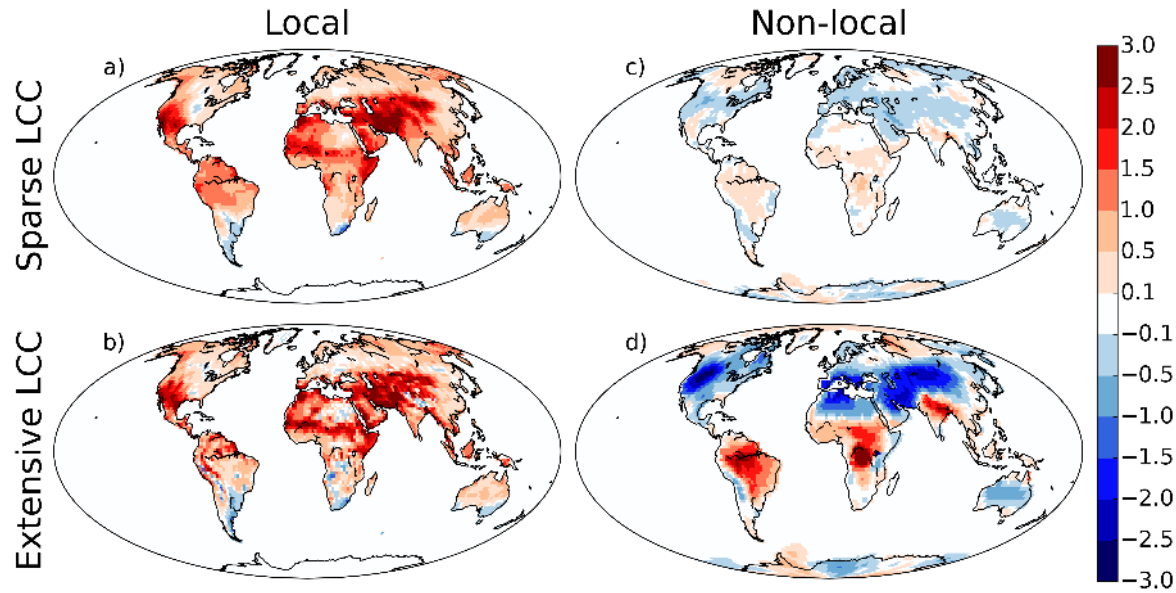

Figure A.2.2: Boreal summer (JJA) change in mean surface temperature [K] due to *a*,*c* sparse and *b*,*d* extensive deforestation. *a*,*b* local effects, *c*,*d* nonlocal effects. Mean over 30 years and another 30 years from a simulation with LCC cells shifted by two.

local evapotranspirative efficiency, but also to local changes in precipitation. The local changes in sensible heat in Australia are presumably originating from the local LCC-induced decrease in surface roughness. In contrast, the nonlocal changes in latent and sensible heat in Australia seem to be driven by the changes in precipitation. Local and nonlocal effects can differ in sign (e.g., local increase versus nonlocal decrease in

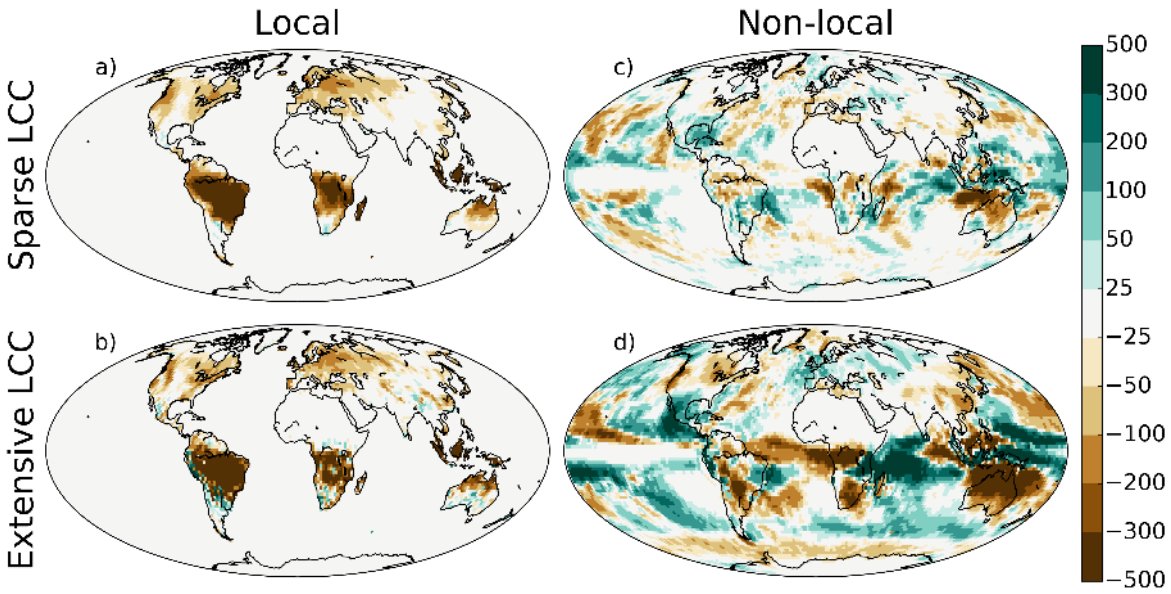

Figure A.2.3: Boreal winter (DJF) change in mean precipitation [mm/y] due to *a*,*c* sparse and *b*,*d* extensive deforestation. *a*,*b* local effects, *c*,*d* nonlocal effects. Mean over 30 years and another 30 years from a simulation with LCC cells shifted by two.

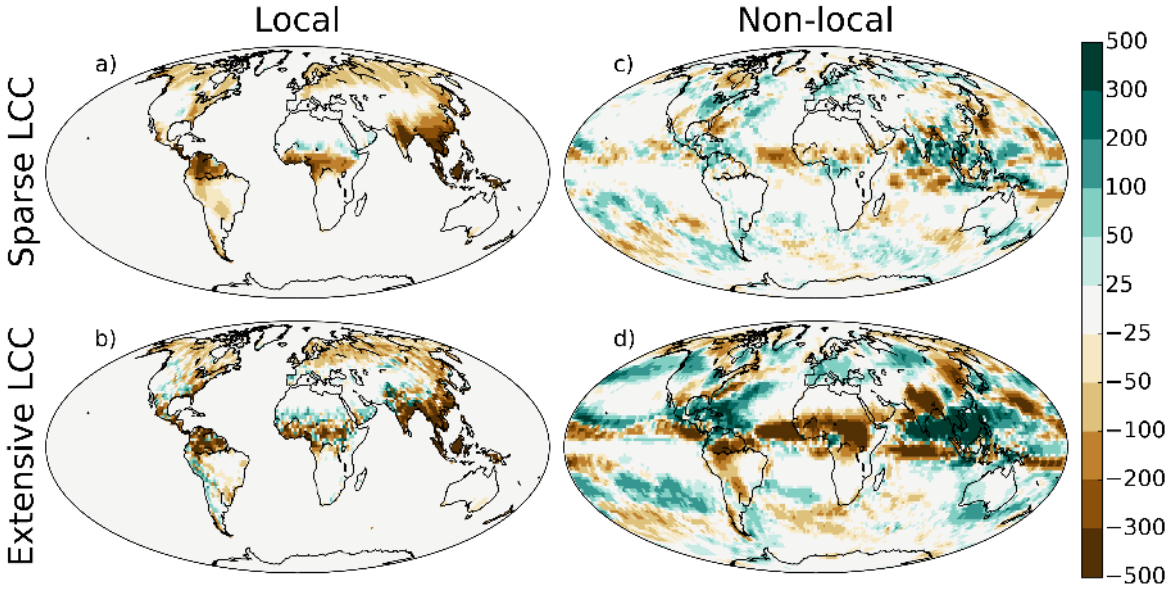

Figure A.2.4: Boreal summer (JJA) change in mean precipitation [mm/y] due to *a*,*c* sparse and *b*,*d* extensive deforestation. *a*,*b* local effects, *c*,*d* nonlocal effects. Mean over 30 years and another 30 years from a simulation with LCC cells shifted by two.

snow cover fraction in Canada) and seasonality of the respective climatic drivers (e.g., precipitation in the Amazon).

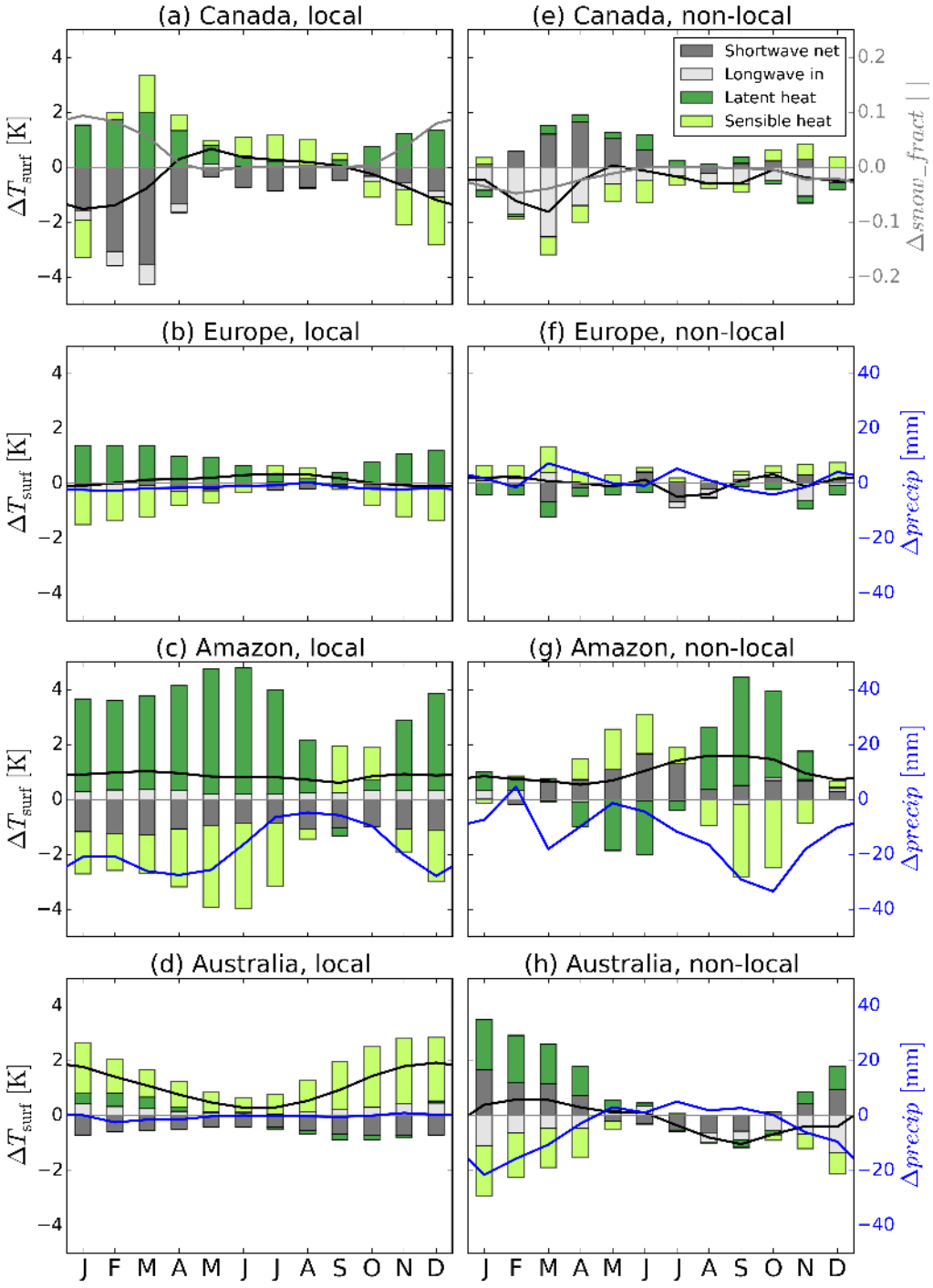

Figure A.2.5: Energy balance decomposition of monthly mean changes in surface temperature (T_{surf} [K]) caused by extensive deforestation. Shown are *a-d* local effects and *e-h* nonlocal effects as averages over regions indicated in Fig. A.3.1 *b*. The bars represent surface temperature changes due to changes in components of the surface energy budget. The black line indicates total changes in surface temperature, which is approximately the sum of the bars in the respective month. The blue and gray lines indicate changes in precipitation (*precip*) and snow cover fraction (*snow_fract*).

A.3 Results for 2m-air temperature

Fig. A.3.1 shows results analogous to Fig. 2.2 for 2m-air temperature for comparison against other published or follow-up studies. The conclusions are qualitatively the same as for surface temperature and precipitation: The two local effects are similar, while the nonlocal effects differ substantially. Note that the local effects on 2m-air temperature in our model are substantially weaker than the effects on surface temperature. In contrast to the local effects, our nonlocal effects influence 2m-air temperature and surface temperature to a similar degree (subfigures *d* of Fig. 2.2 versus Fig. A.3.1).

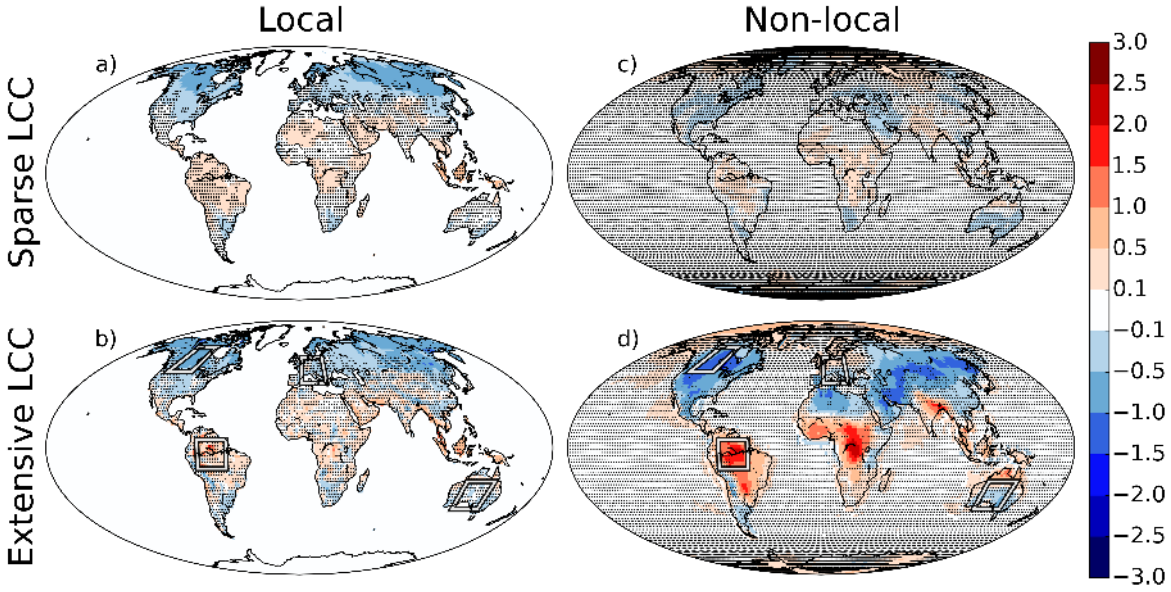

Figure A.3.1: Difference in mean 2m-air temperature [K] for *a*,*c* sparse and *b*,*d* extensive deforestation. *a*,*b* Local effects, *c*,*d* nonlocal effects. Statistical significance is calculated according to a 5 % level in a Student's t-test accounting for autocorrelation (Zwiers and von Storch, 1995). Note that we mark grid cells that are *not* statistically significant. The regions shown as rectangles in *b*,*d* denote areas selected for the regional energy balance decomposition in Fig. A.2.5.

This different impact of local and nonlocal effects on 2m-air temperature may arise from the different underlying mechanisms: The local effects originate from changes in local surface properties and the land surface directly responds, while the lowest atmospheric layer (which represents the lowest ∼40 m) mainly adjusts to these changes in surface variables. This adjustment is incomplete, because some of the temperature change is diluted by horizontal advection. In MPI-ESM, 2m-air temperature is calculated by interpolation between surface temperature and the lowest level of the atmosphere, based on Monin-Obukhov similarity theory. Thus, similar to the lowest atmospheric layer, 2m-air temperature is less affected by LCC compared to surface temperature. In contrast, the nonlocal effects (e.g., changes in global circulation patterns) are primarily affecting the atmosphere, and the land surface variables adjust to

the changed atmospheric conditions. Because the temperature change in the land grid cells is not diluted by advection to adjacent land grid cells, the surface temperature can fully adjust to the changed atmospheric conditions. Thus, the nonlocal effects on surface temperature and 2m-air temperature are almost equally affected by LCC.

A.4 Interpolation method and interpolation errors

The separation method includes horizontal interpolation between grid cells for the isolation of both local and nonlocal effects. Inland, where data points with known values are available at all four surrounding sides, we apply bilinear interpolation. At coastal regions, where values for at least one side is missing, we apply nearest-neighbor extrapolation. For simplification, we refer to this combination of interpolation and extrapolation as "interpolation" here and in the main text.

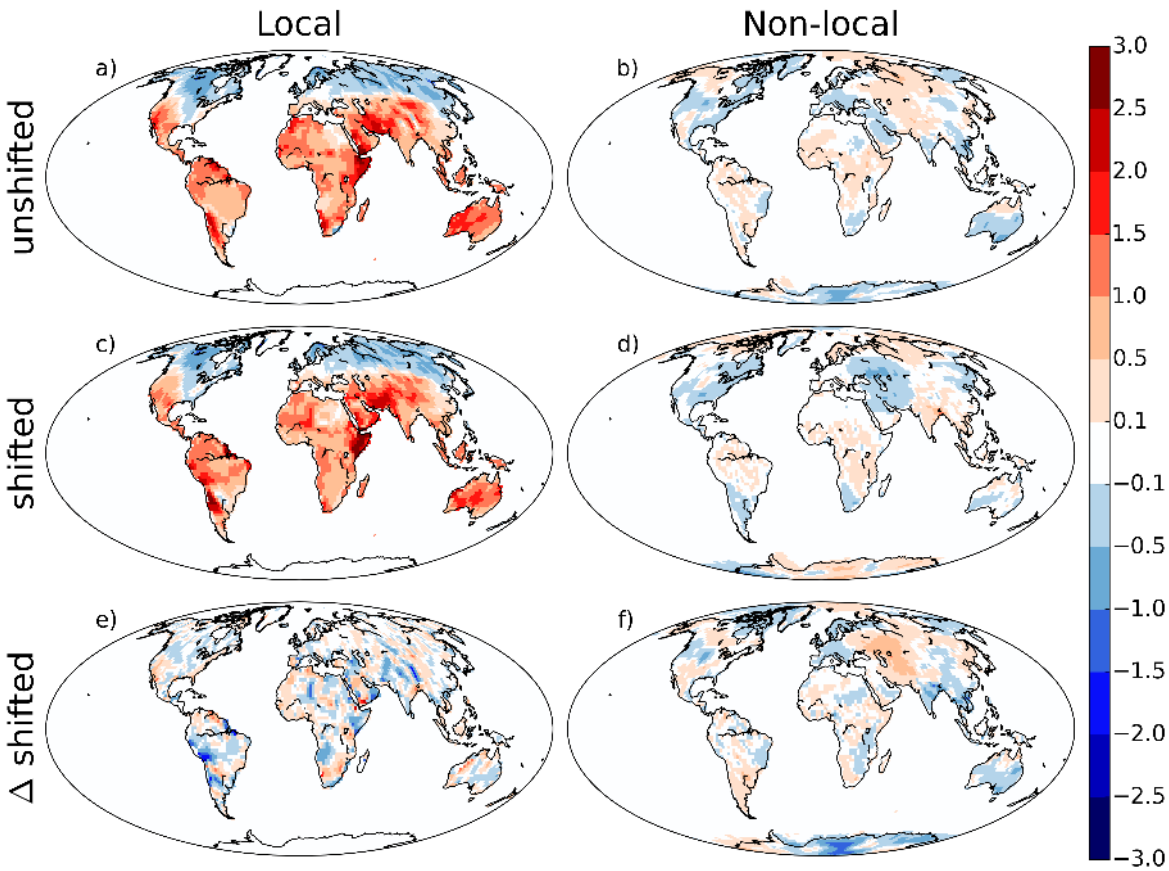

Figure A.4.1: Analysis of interpolation error for changes in surface temperature due to **sparse** LCC. The panels show a,c,e, local effects and b,d,f nonlocal effects of a,b the unshifted simulations, c,d the shifted simulations and e,f the differences between unshifted and shifted simulations.

In order to assess errors associated with this interpolation, the simulations with the LCC cells at their original location (here referred to as "unshifted") are complemented

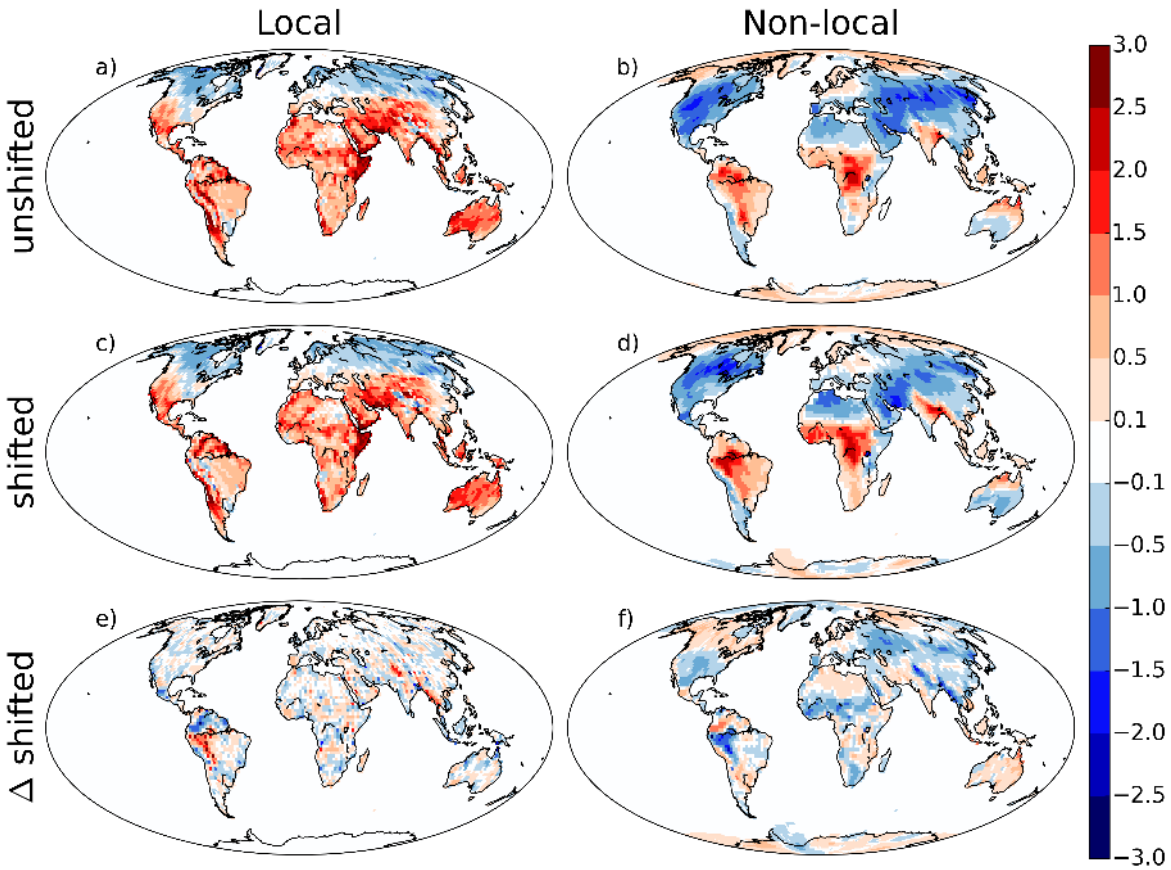

Figure A.4.2: Analysis of interpolation error for changes in surface temperature due to **extensive** LCC. The panels show a,c,e, local effects and b,d,f nonlocal effects of a,b the unshifted simulations, c,d the shifted simulations and e,f the differences between unshifted and shifted simulations.

with additional simulations. In these additional simulations, we shift the LCC cells by two (here referred to as "shifted"). We isolate local and nonlocal effects separately for the unshifted and shifted simulations, both for sparse LCC (Fig. A.4.1) and for extensive LCC (Fig. A.4.2). Considering the nonlocal effects, a fair amount of inter-annual variability can be seen in the differences between the unshifted and shifted versions (see subfigure f of Fig. A.4.1). The local effects are by construction largely free of this inter-annual variability, so the differences between unshifted and shifted local effects largely consist of interpolation errors. Furthermore, the local effects already include the interpolation errors from the nonlocal effects (via step d of the step-by-step instruction of the separation approach in the main text). Thus, when analyzing the overall interpolation errors, we focus on the local effects in the following.

The shifted and unshifted local effects are generally in good agreement (subfigures a versus c in Figs. A.4.1 and A.4.2). Globally, the interpolation errors are similar for sparse and extensive LCC: the root mean square difference over land between the unshifted and shifted local effects is 0.35 K for sparse LCC and 0.39 K for extensive LCC. In some regions, the interpolation errors can not be neglected, especially in the

surroundings of mountain ranges such as the Andes or the Himalaya (subfigures e in Figs. A.4.1 and A.4.2) where the interpolation errors are larger than 1 K. Thus, for the analysis in the main text, we consider the combined information from shifted and unshifted simulations in order to decrease the dependence on the exact location of the LCC cells.

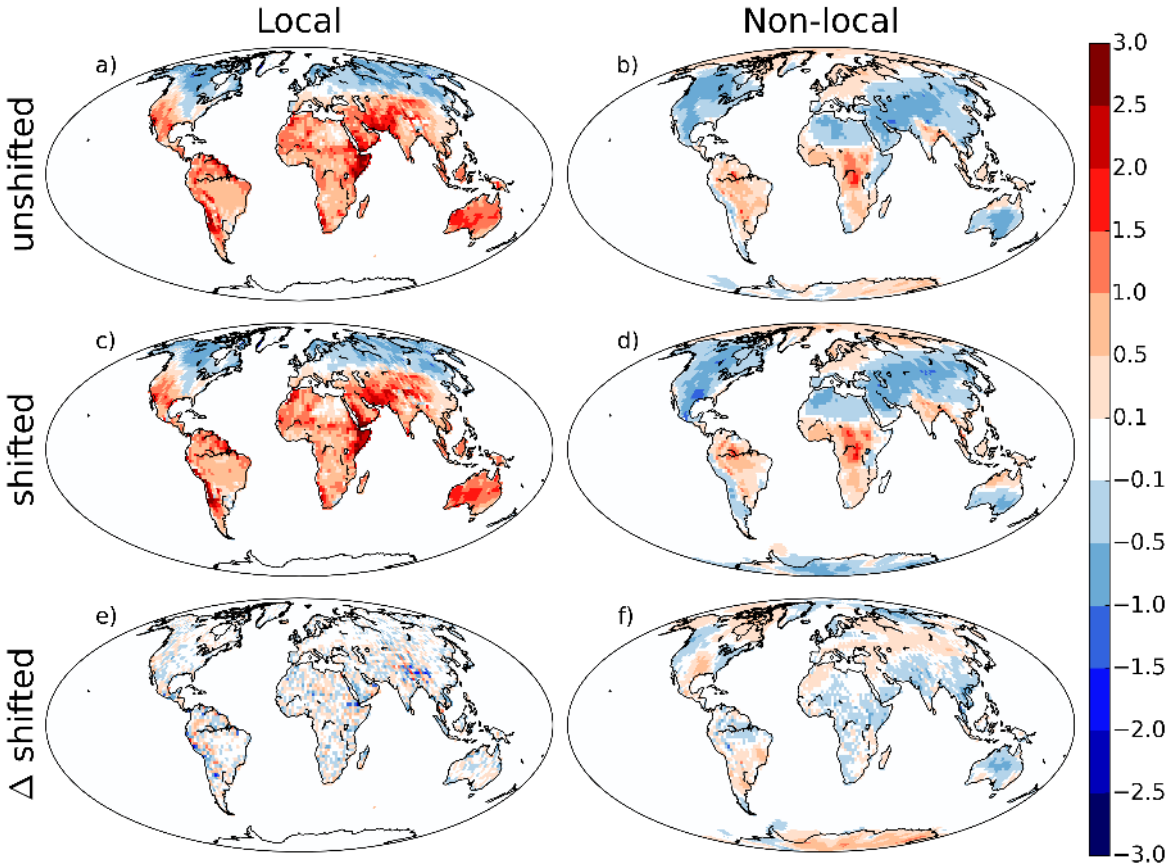

Figure A.4.3: Analysis of interpolation error for changes in surface temperature due to **chessboard** LCC. The panels show a,c,e, local effects and b,d,f nonlocal effects of a,b the unshifted simulations, c,d the shifted simulations and e,f the differences between unshifted and shifted simulations.

In follow-up studies that require an isolation of the local effects, the horizontal interpolation errors can be reduced as follows: Instead of choosing a sparse or extensive pattern in the isolation approach, a chessboard-like pattern of altering one out of two grid cells may be chosen. Thus, the calculation of both local and nonlocal effects requires horizontal interpolation only from directly adjacent grid cells. This "chessboard LCC" reduces the horizontal interpolation errors (see subfigure e in Fig. A.4.3): The root mean square difference over land between the unshifted and shifted local effects is then reduced to 0.29 K.

A.5 Total local plus nonlocal effects

To give an idea about the total (local plus nonlocal) effects of extensive deforestation, we provide the sum of local and nonlocal effects for changes in surface temperature and precipitation (Fig. A.5.1). The surface temperature change maps were obtained by adding the local and nonlocal effects of Fig. 2.2, The precipitation change maps were obtained by adding the local and nonlocal effects of Fig. 2.3. Because the nonlocal effects of sparse LCC are small, the local plus nonlocal effects of sparse deforestation are similar to the local effects alone. In contrast, the strong nonlocal effects of extensive LCC magnify the local effects in some regions, as can be seen in the inner tropics or the high northern latitudes.

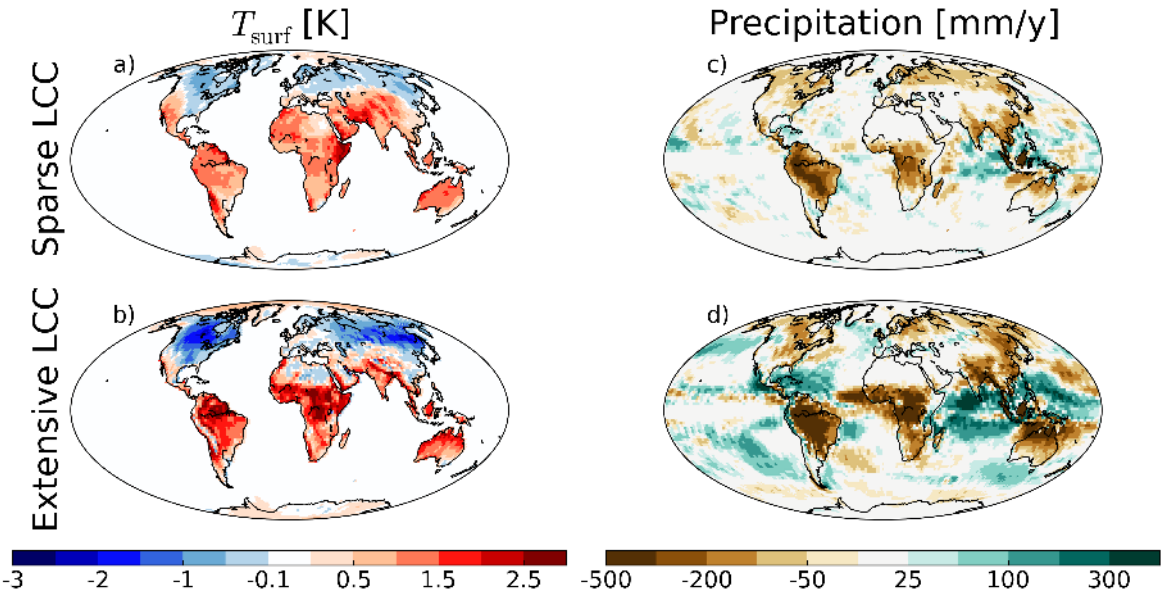

Figure A.5.1: Sums of local and nonlocal effects for *a*,*c* sparse and *b*,*d* extensive deforestation. Subfigures *a* and *b* denote changes in surface temperature [K], *c* and *d* denote changes in precipitation [mm/y].

B Appendix for chapter 3

This appendix provides additional information for chapter 3. The figures are numbered according to the order of their reference in the main text.

- Fig. B.1 shows that the synergies between land-use–induced and climate–induced land cover change are small. Thus, our choice of fist applying LULCC and then CILCC for the results in the main text does not influence our conclusions.
- In section B.1 and Fig. B.2, we assess the influence of changes in the vegetated fraction within a grid cell.
- Fig. B.3 displays the changes in surface temperature for complete deforestation in two different background climates, and the difference of the two effects. This difference is used for calculating the influence of a changing background climate on the locally induced changes in surface temperature in the LCC scenarios as described in section 3.3.2 of the main text.
- In Appendix B.2 and Fig. B.4, an idealized scenario is added to our assessment.
- Fig. B.5 shows results separately for areas where LCC leads to cooling and warming, respectively.

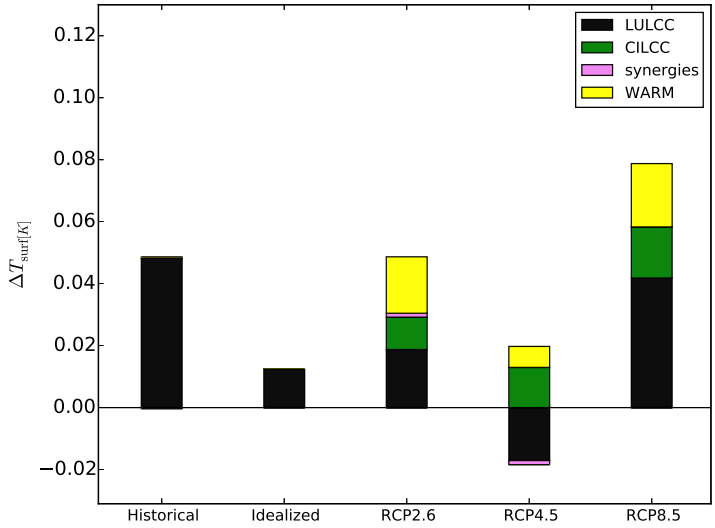

Figure B.1: Despite the nonlinearity it does not substantially matter whether we first calculate LULCC or CILCC. The synergies (pink bars) between LULCC and CILCC are small in all considered LCC scenarios, because LULCC and CILCC are active in different regions (the affected regions in Figs 3.4 and 3.5 are mostly disjoint).

B.1 Influence of changes in the vegetated fraction

In addition to changing forest cover fractions (c) within the vegetated part of each grid cell, the vegetated fraction (veg_{max}) is changing in a warmer climate due to natural vegetation dynamics, altering the total forest fraction within a grid cell. For the results in the main text, we fixed veg_{max} to the grid values of the year 2005, and only considered changes in c. Keeping this veg_{max} constant possibly leads to an underestimation of the role of climate-induced land cover change. Here we want to estimate how big the influence of changing veg_{max} can become. Note that when vegetated fraction increases, bare land is replaced by both grasslands and forests, while our method only allows calculating the effects of replacing forests by grasslands and vice versa, so the calculations here should be understood as a rough estimate for the influence of changing veg_{max}. Using the present-day look-up curve s for each grid cell, we estimate the contributions of Δc, Δveg_{max}, and the synergy term $\Delta c \Delta veg_{max}$ as follows:

$$\Delta \mathrm{T}_{\mathrm{surf}}(\Delta c) = s(c_{2100} - c_{2005}) \tag{5.1}$$

$$\Delta \mathrm{T}_{\mathrm{surf}}(\Delta veg_{max}) = s(c_{2005} + c_{2005}(veg_{max2100} - veg_{max2005})) - s(c_{2005}) \tag{5.2}$$

$$\Delta \mathrm{T}_{\mathrm{surf}}(\Delta c \Delta veg_{max}) = s(c_{2005} + (c_{2100} - c_{2005})(veg_{max2100} - veg_{max2005})) - s(c_{2005}) \tag{5.3}$$

where equation (5.1) describes the response in locally induced surface temperature due to changes in c when veg_{max} is kept constant, equation (5.2) describes the response due

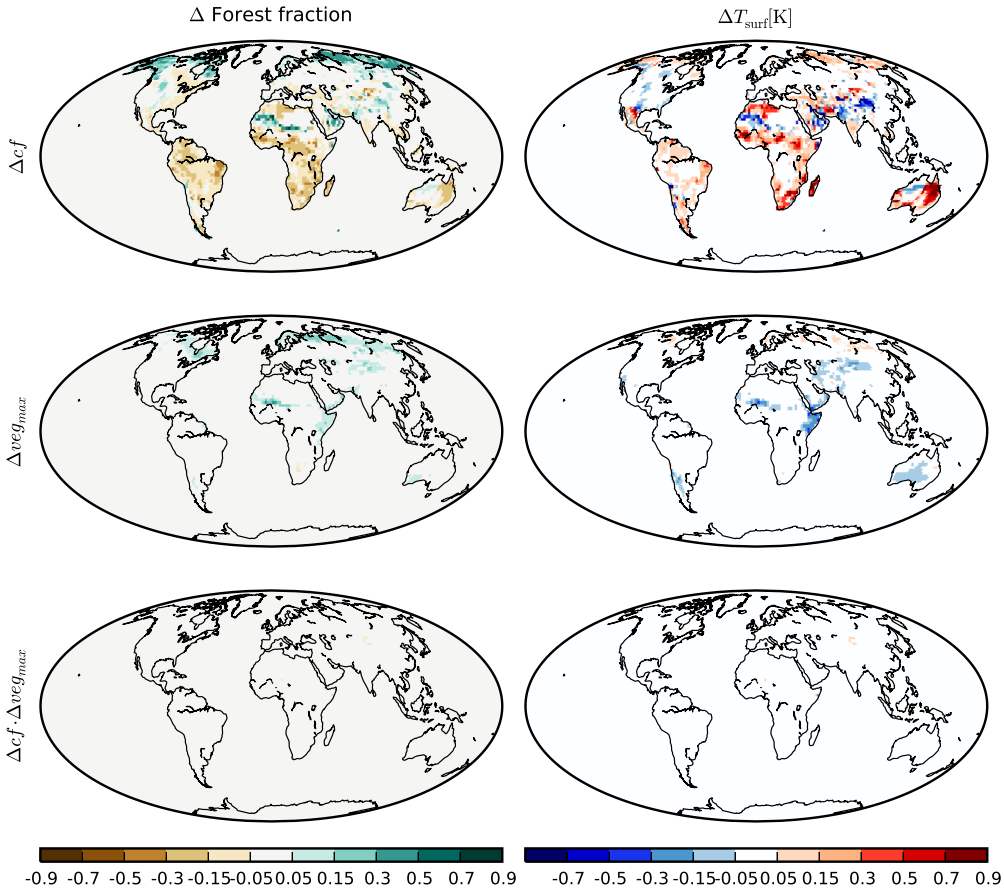

Figure B.2: Influence of the changing veg_{max} in the RCP8.5 scenario. Changes in forest fraction (left) and corresponding locally induced changes in surface temperature (right). Top, middle and bottom figures correspond to equations 1, 2 and 3 in section B.1.

to changes in veg_{max} when c is kept constant, and equation (5.3) describes the synergy between these two.

We assess the impact of the changing veg_{max} exemplary for the RCP8.5 scenario as shown in Fig. B.2. The response due to a changing c (here land-use-induced plus climate-induced land cover change) clearly dominates the response to changing veg_{max} and the synergy term.

B.2 Influence of the pre-LCC forest fraction for an idealized scenario

In section 3.3.3 of the main text, we examine the influence of pre-LCC forest fractions on the temperature response in realistic LCC scenarios. Here, we complement this assessment of realistic LULCC scenarios by an idealized deforestation scenario similar to the experimental set-up proposed for the Land-Use Model Intercomparison Project (LUMIP) within CMIP6 [Lawrence et al., 2016]: We deforest the same areal extent as for historical deforestation, but we distribute the deforestation uniformly in highly

forested areas (higher forest fraction than in 70% of all grid cells) by deforesting proportionally to the 1850 forest fraction. Like this, we redistribute historical deforestation to areas with high forest cover (see Fig. 3.4).

The deforestation-induced warming of historical and idealized deforestation is similar when using the linear look-up lines, so on average, LCC in both scenarios is located in areas which respond similarly to deforestation (see Fig. B.4). However, accounting for the nonlinearity reduces the effect of historical deforestation substantially less than idealized deforestation. This difference has two reasons: First, the pre-deforestation forest fractions differ (on average 56% for historical, 70% for idealized deforestation in the year 1850). Since deforestation is generally more efficient (that means, deforestation causes more temperature change per unit forest fraction change) when starting from a low forest fraction (Fig. 3.7 in the main text), historical deforestation is on average more efficient than deforestation in the idealized scenario. Second, historical deforestation is concentrated on comparably few grid cells, and others remain largely untouched. In contrast, idealized deforestation is distributed over many grid cells, so the deforestation of each grid cell is small (Fig. 3.4) and does not reach the low forest fractions, at which deforestation would be more efficient.

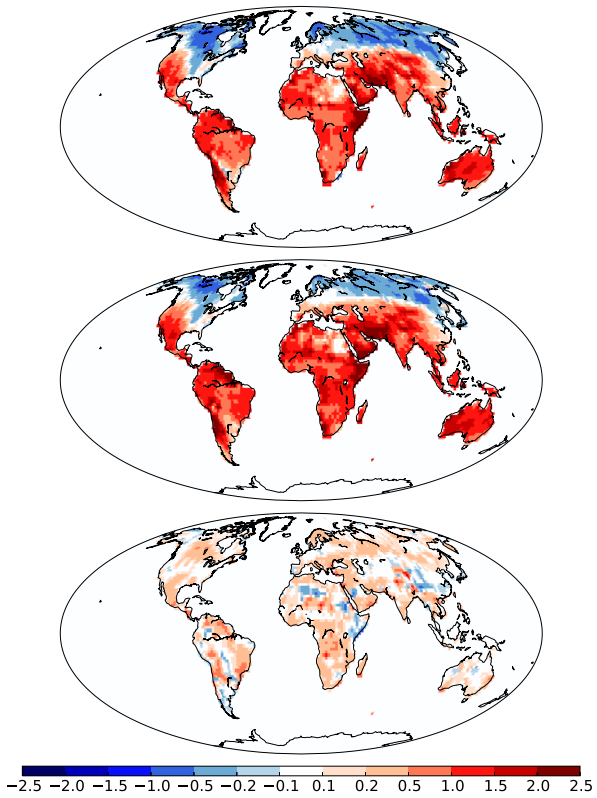

Figure B.3: Locally induced changes in surface temperature [K] for a conversion from 100% to 0% forest cover in (top) present-day (1976 - 2005) background climate, and (middle) a warmer (RCP8.5 in 2070 - 2099) background climate. Bottom: Difference of the two (in RCP8.5 minus in present-day). Surface temperature responds strongly also in semi-arid and arid regions because there the vegetated fraction is overestimated by JSBACH.

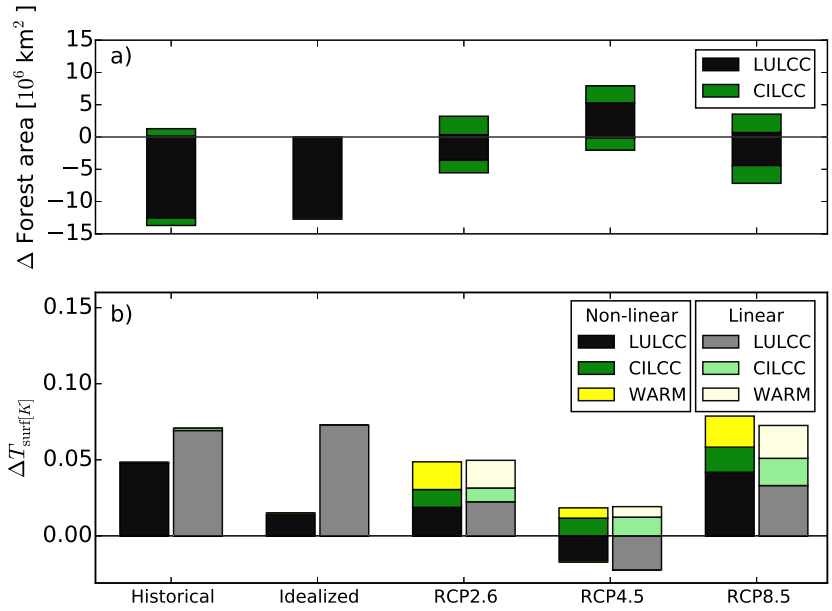

Figure B.4: Comparison of LCC effects across scenarios. Same as Fig. 3.3 but including the idealized scenario. a) Changes in forest area. b) Contributions to land-averaged local surface temperature changes [K] from land-use-induced LCC, climate-induced LCC, and warming background climate. The left bars account for the nonlinear surface temperature response, the right bars assume a linear response to deforestation.

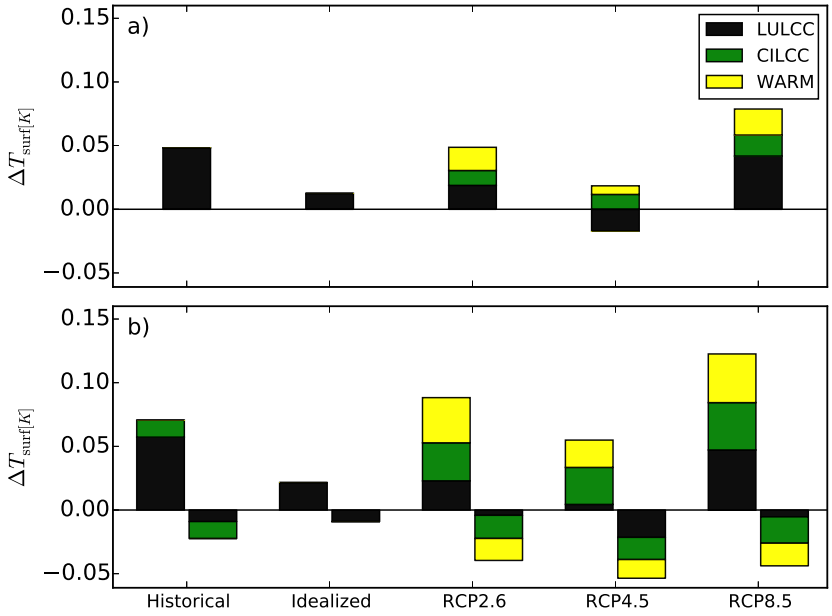

Figure B.5: Taking spatial averages over land hides some of the signal because positive and negative contributions cancel, especially for LULCC and WARM in the RCP scenarios. a) Land averages of the influence of land-use–induced land cover change (LULCC), climate-induced land cover change (CILCC) and warming background climate (WARM) on the locally induced changes in surface temperature [K]. b) These values are split into areas where the respective contribution was warming (left bars) or cooling (right bars).

C Appendix for chapter 4

This appendix provides additional information for chapter 4. The figures are numbered according to the order of their reference in the main text.

- Fig. C.1 shows the changes in radiometric surface temperature due to the local effects of deforestation in the MPI-ESM and in three observation-based datasets. These maps correspond to the latitudinal averages in Fig. 4.1 in the main text.
- Fig. C.2 shows the maps for the local and nonlocal effects on surface temperature for a selection of the global mean values shown in Fig. 4.2.
- In Fig. C.3, the mechanisms underlying local effects on surface temperature are analyzed separately for deforestation and changes in surface albedo. To this end, we decompose changes in the surface energy balance into changes in net available energy and changes in turbulent heat fluxes.
- Fig. C.4 compares the two different methods used in this thesis for calculating the local effects on surface temperature in plausible LCC scenarios.
- Table 5.1 provides an overview over the simulations used in Fig. 4.4.

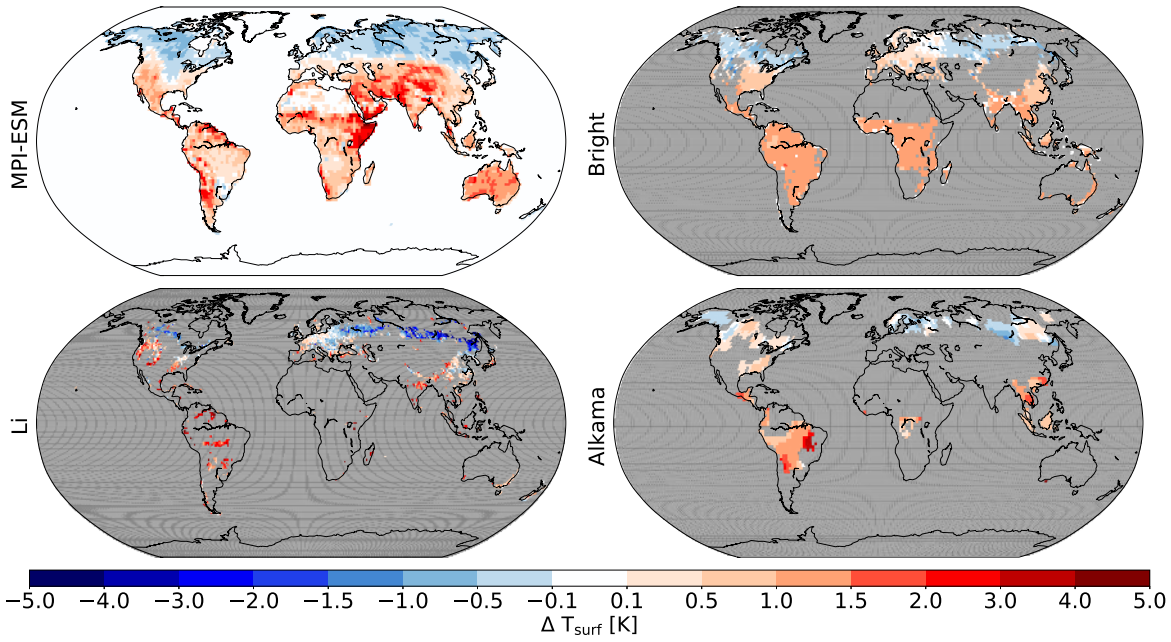

Figure C.1: Local effects of deforestation on surface temperature [K] in the MPI-ESM and observation-based datasets. These datasets comprise a semi-empirical approach based on fluxnet observations (Bright et al., 2017), and satellite-based observations on potential (Li et al., 2015) and actual deforestation (Alkama and Cescatti, 2016). These datasets are difficult to compare directly (Methods).

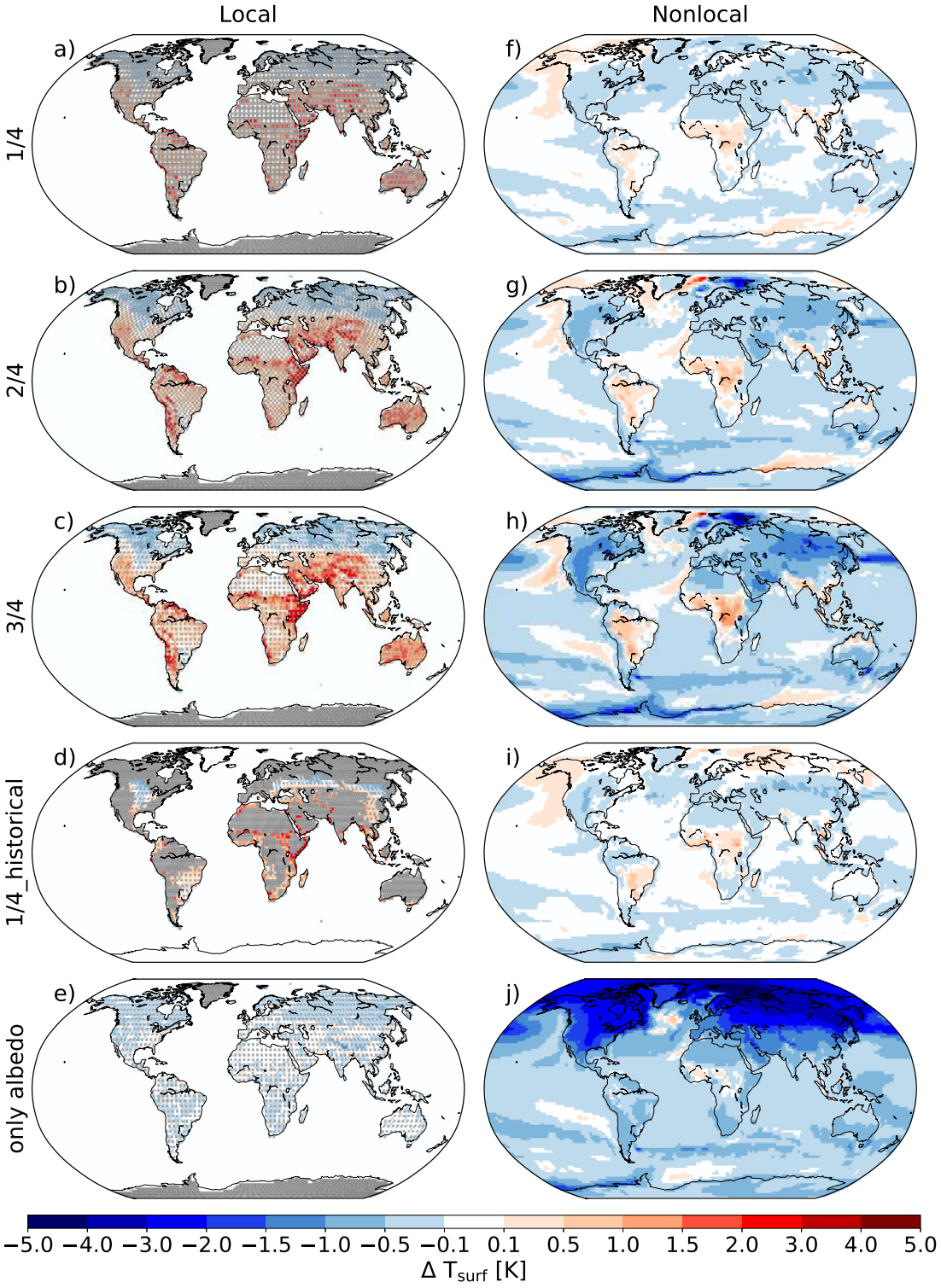

Figure C.2: Local and nonlocal effects of deforestation simulated by the MPI-ESM. See Methods section for meaning of simulation names. Shown are changes in surface temperature [K] induced by deforestation (rows 1 - 4) or induced by changes in surface albedo (last row). Land grid cells where vegetation is not changed are masked in gray.

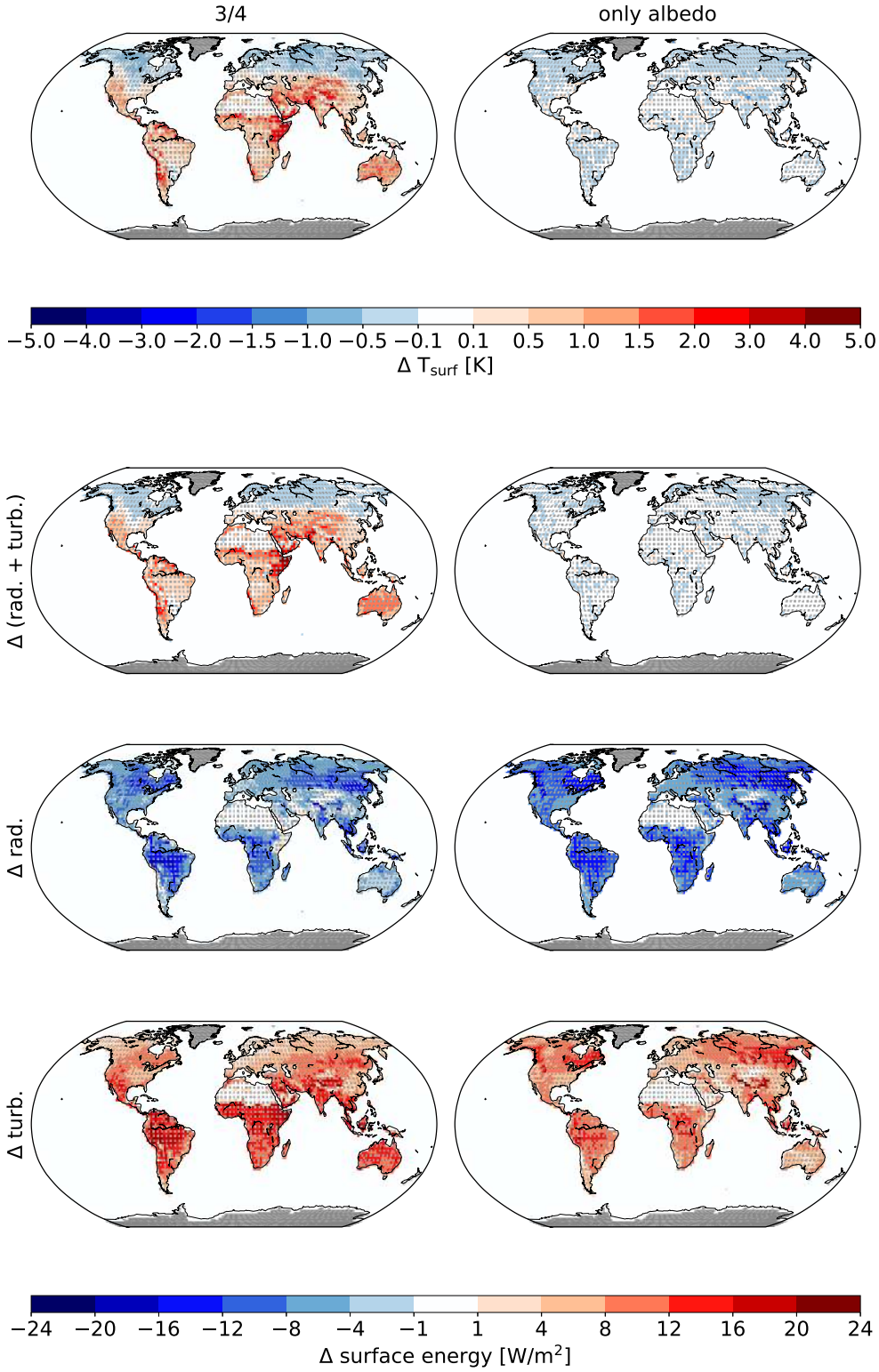

Figure C.3: Role of radiation and turbulent heat fluxes for the local effects as simulated in the MPI-ESM. Left: Local effects due to deforestation of three out of four grid cells (simulation '3/4', as in Fig. 4.1 and C.2). Right: Local effects if only albedo is changed from forest to grass values (simulation 'only albedo'). Top: Changes in surface temperature [K]. Bottom: Changes in the energy balance [W/m^2], split further into changes in radiation (longwave incoming + shortwave net radiation) and turbulent heat fluxes (latent + sensible heat). Even if only the albedo is changed, the resulting radiative cooling is largely buffered locally by the turbulent heat fluxes.

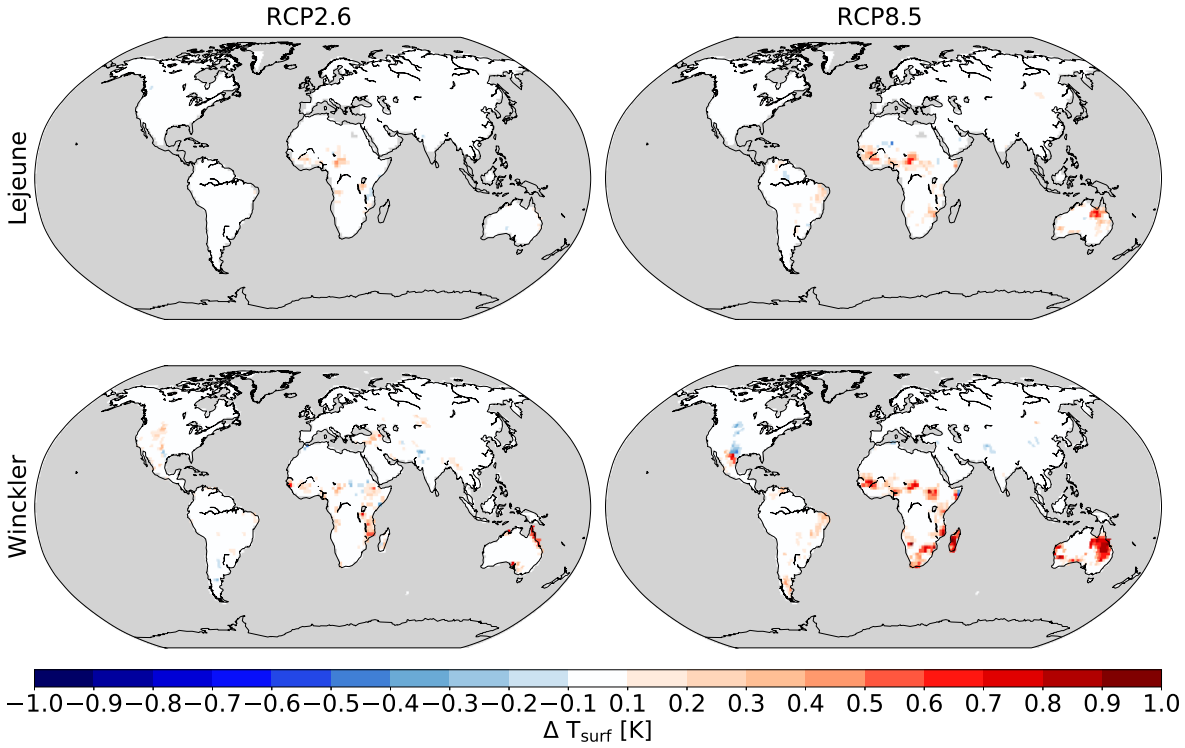

Figure C.4: Comparison of the two approaches used in the present study for the local effects on surface temperature [K] in the MPI-ESM. The local effects of RCP2.6 and RCP8.5 are calculated as in the study by Lejeune et al. (2017a) and section 3.2, respectively. The spatial patterns match well, but the magnitude of the effects differ by a factor of about two. The regression used in the first of the two approaches may lead to an underestimation of the local effects (Lejeune et al., 2017a).

Table 5.1: Overview of simulations used in the inter-model comparison in Fig. 4.4. For this comparison, simulations with two set-ups were included. In some models, the values for historical land use were obtained from the difference between land use simulations (LU) containing only the land-use forcing ('onlyLU' which is a subset of simulations of 'historialMisc' in CMIP5) and as reference (Ref.) simulations a pre-industrial control run ('piControl' in CMIP5). In another set-up, values were obtained from the difference between all-forcing runs including land use ('historical', 'RCP2.6', and 'RCP8.5' in CMIP5, respectively) and reference simulations that exclude land use ('noLU' which is another subset of 'historicalMisc', 'L2A26', and 'L2A85' respectively). Each value plotted in Fig. 4.4 is the 30-year mean of the difference between one ensemble member of LU minus one ensemble member of Ref. The numbers in the table denote the number of available ensemble members that were available for the respective model. For instance, for the historical case IPSL-CM5A-LR provides $6 \times 3 = 18$ combinations of ensemble members. The piControl runs are substantially longer than 30 years. Thus to ensure comparability across the two set-ups used for historical land use, we cut 180 years of the control run into 6 'ensemble members', each of which comprises 30 years.

	Historical							Future						
Set-up	historical - noLU			onlyLU - piControl				RCP2.6 - L2A26			RCP8.5 - L2A85			
Model	IPSL-CM5A-LR	GFDL-ESM2G	GFDL-ESM2M	CESM1-CAM5	CCSM4	CanESM2	HadGEM2-ES	MPI-ESM-LR	MIROC-ESM	HADGEM2-ES	MPI-ESM-LR	MIROC-ESM	HADGEM2-ES	IPSL-CM5A-LR
LU	6	1	1	3	3	5	4	3	1	4	3	1	4	1
Ref.	3	2	2	6	6	6	6	2	1	4	2	1	4	4

References

ACIA (2004). Impacts of a Warming Arctic: Arctic Climate Impact Assessment. *Cambridge University Press*, pages 1–140.

Alkama, R. and Cescatti, A. (2016). Biophysical climate impacts of recent changes in global forest cover. *Science*, 351:600–604.

Armstrong, E., Valdes, P., House, J., and Singarayer, J. (2016). The role of CO2 and dynamic vegetation on the impact of temperate land-use change in the HadCM3 coupled climate model. *Earth Interactions*, 20:1–10.

Bala, G., Caldeira, K., Wickett, M., Phillips, T. J., Lobell, D. B., Delire, C., and Mirin, A. (2007). Combined climate and carbon-cycle effects of large-scale deforestation. *Proceedings of the National Academy of Sciences*, 104:6550–6555.

Bathiany, S., Claussen, M., Brovkin, V., Raddatz, T., and Gayler, V. (2010). Combined biogeophysical and biogeochemical effects of large-scale forest cover changes in the MPI Earth system model. *Biogeosciences*, 7:1383–1399.

Betts, R. A. (2000). Offset of the potential carbon sink from boreal forestation by decreases in surface albedo. *Nature*, 408:187–190.

Boisier, J., de Noblet-Ducoudré, N., and Ciais, P. (2014). Historical land-use-induced evapotranspiration changes estimated from present-day observations and reconstructed land-cover maps. *Hydrol. Earth Syst. Sci.*, 18:3571–3590.

Boisier, J. P., de Noblet-Ducoudre, N., and Ciais, P. (2013). Inferring past land use-induced changes in surface albedo from satellite observations: a useful tool to evaluate model simulations. *Biogeosciences*, 10:1501–1516.

Boisier, J. P., de Noblet-Ducoudré, N., Pitman, a. J., Cruz, F. T., Delire, C., van den Hurk, B. J. J. M., van der Molen, M. K., Müller, C., and Voldoire, A. (2012). Attributing the impacts of land-cover changes in temperate regions on surface temperature and heat fluxes to specific causes: Results from the first LUCID set of simulations. *Journal of Geophysical Research: Atmospheres*, 117:1–16.

Bonan, G. B. (2008). Forests and climate change: forcings, feedbacks, and the climate benefits of forests. *Science*, 320:1444–1449.

Bonan, G. B., Pollard, D., and Thompson, S. L. (1992). Effects of Boreal Forest Vegetation on Global Climate. *Nature*, 359:716–718.

Boysen, L. R., Brovkin, V., Arora, V. K., Cadule, P., de Noblet-Ducoudré, N., Kato, E., Pongratz, J., and Gayler, V. (2014). Global and regional effects of land-use change on climate in 21st century simulations with interactive carbon cycle. *Earth Syst. Dynam.*, 5:309–319.

Bright, R. M., Davin, E. L., O'Halloran, T. L., Pongratz, J., Zhao, K., and Cescatti, A. (2017). Local temperature response to land cover and management change driven by non-radiative processes. *Nature Climate Change*, 7:296–302.

Brovkin, V., Boysen, L., Arora, V. K., Boisier, J. P., Cadule, P., Chini, L., Claussen, M., Friedlingstein, P., Gayler, V., Van den hurk, B. J. J. M., Hurtt, G. C., Jones, C. D., Kato, E., De noblet ducoudre, N., Pacifico, F., Pongratz, J., and Weiss, M. (2013a). Effect of anthropogenic land-use and land-cover changes on climate and land carbon storage in CMIP5 projections for the twenty-first century. *Journal of Climate*, 26:6859–6881.

Brovkin, V., Boysen, L., Raddatz, T., Gayler, V., Loew, A., and Claussen, M. (2013b). Evaluation of vegetation cover and land-surface albedo in MPI-ESM CMIP5 simulations. *Journal of Advances in Modeling Earth Systems*, 5:48–57.

Brovkin, V., Claussen, M., Driesschaert, E., Fichefet, T., Kicklighter, D., Loutre, M. F., Matthews, H. D., Ramankutty, N., Schaeffer, M., and Sokolov, A. (2006). Biogeophysical effects of historical land cover changes simulated by six Earth system models of intermediate complexity. *Climate Dynamics*, 26:587–600.

Brovkin, V., Raddatz, T., Reick, C. H., Claussen, M., and Gayler, V. (2009). Global biogeophysical interactions between forest and climate. *Geophysical Research Letters*, 36:1–5.

Claussen, M., Brovkin, V., and Ganopolski, A. (2001). Biogeophysical versus biogeochemical feedbacks of large-scale land cover change. *Geophysical Research Letters*, 28:1011–1014.

Davies-Barnard, T., Valdes, P. J., Singarayer, J. S., Pacifico, F. M., and Jones, C. D. (2014). Full effects of land use change in the representative concentration pathways. *Environmental Research Letters*, 9:114014.

Davies-Barnard, T., Valdes, P. J., Singarayer, J. S., Wiltshire, a. J., and Jones, C. D. (2015). Quantifying the relative importance of land cover change from climate and land-use in the representative concentration pathways. *Global Biogeochem. Cycles*, 29:842–853.

Davin, E. L. and de Noblet-Ducoudré, N. (2010). Climatic impact of global-scale deforestation: radiative versus nonradiative processes. *Journal of Climate*, 23:97–112.

de Noblet-Ducoudré, N., Boisier, J.-P., Pitman, A., Bonan, G. B., Brovkin, V., Cruz, F., Delire, C., Gayler, V., van den Hurk, B. J. J. M., Lawrence, P. J., van der Molen, M. K., Müller, C., Reick, C. H., Strengers, B. J., and Voldoire, A. (2012). Determining robust impacts of land-use-induced land cover changes on surface climate over north america and eurasia: Results from the first set of LUCID experiments. *Journal of Climate*, 25:3261–3281.

Deser, C., Knutti, R., Solomon, S., and Phillips, A. S. (2012). Communication of the role of natural variability in future North American climate. *Nature Climate Change*, 2:775–779.

Devaraju, N., Bala, G., and Modak, A. (2015). Effects of large-scale deforestation on precipitation in the monsoon regions: Remote versus local effects. *Proceedings of the National Academy of Sciences*, 112:3257–3262.

Findell, K. L., Knutson, T. R., and Milly, P. C. D. (2006). Weak simulated extratropical responses to complete tropical deforestation. *Journal of Climate*, 19:2835–2850.

Foley, J. A., Defries, R., Asner, G. P., Barford, C., Bonan, G., Carpenter, S. R., Chapin, F. S., Coe, M. T., Gibbs, H. K., Helkowski, J. H., Holloway, T., Howard, E. A., Kucharik, C. J., Monfreda, C., Patz, J. A., Prentice, I. C., Ramankutty, N., and Snyder, P. K. (2005). Global Consequences of Land Use. *Science*, 309:570–575.

Ganopolski, A., Petoukhov, V., Rahmstorf, S., Brovkin, V., Claussen, M., Eliseev, A., and Kubatzki, C. (2001). CLIMBER-2 : a climate system model of intermediate complexity . Part II : model sensitivity. *Climate Dynamics*, 17:735–751.

Gibbard, S., Caldeira, K., Bala, G., Phillips, T. J., and Wickett, M. (2005). Climate effects of global land cover change. *Geophysical Research Letters*, 32:1–4.

Gillett, N. P., Arora, V. K., Matthews, D., and Allen, M. R. (2013). Constraining the ratio of global warming to cumulative CO2 emissions using CMIP5 simulations. *Journal of Climate*, 26:6844–6858.

Giorgetta, M. A., Roeckner, E., Mauritsen, T., Bader, J., Crueger, T., Esch, M., Rast, S., Kornblueh, L., Schmidt, H., Kinne, S., Hohenegger, C., Möbis, B., Krismer, T., Wieners, K.-H., and Stevens, B. (2013). The atmospheric general circulation model ECHAM6 - Model description. Technical Report 135, Max-Planck-Institute for Meteorology, Hamburg.

Giorgetta, M. et al., (2012a), CMIP5 simulations of the Max Planck Institute for Meteorology (MPI-M) based on the MPI-ESM-LR model: The historical experiment, served by ESGF, doi:10.1594/WDCC/CMIP5.MXELHI.

Giorgetta, M. et al., (2012b), CMIP5 simulations of the Max Planck Institute for meteorology (MPI-M) based on the MPI-ESM-LR model: The RCP26 experiment, served by ESGF, doi:10.1594/WDCC/CMIP5.MXELR2.

Giorgetta, M. et al., (2012c), CMIP5 simulations of the Max Planck Institute for Meteorology (MPI-M) based on the MPI-ESM-LR model: The RCP45 experiment, served by ESGF, doi:10.1594/WDCC/CMIP5.MXELR4.

Giorgetta, M. et al., (2012d), CMIP5 simulations of the Max Planck Institute for Meteorology (MPI-M) based on the MPI-ESM-LR model: The RCP85 experiment, served by ESGF, doi:10.1594/WDCC/CMIP5.MXELR8.

Goessling, H. F. and Reick, C. H. (2011). What do moisture recycling estimates tell us? Exploring the extreme case of non-evaporating continents. *Hydrol. Earth Syst. Sci.*, 15:3217–3235.

Grassi, G., House, J., Dentener, F., Federici, S., den Elzen, M., and Penman, J. (2017). The key role of forests in meeting climate targets requires science for credible mitigation. *Nature Climate Change*, 7:220–228.

Hagemann, S., Loew, A., and Andersson, A. (2013). Combined evaluation of MPI-ESM land surface water and energy fluxes. *Journal of Advances in Modeling Earth Systems*, 5:259–286.

Hansen, M. C., Potapov, P. V., Moore, R., Hancher, M., Turubanova, S. a., and Tyukavina, A. (2013). High-resolution global maps of 21st-century forest cover change. *Science*, 342:850–853.

Hansis, E., Davis, S. J., and Pongratz, J. (2015). Relevance of methodological choices for accounting of land use change carbon fluxes. *Global Biogeochem. Cycles*, 29:1230–1249.

Hawkins, E., Sutton, R., Sutton, E. H., and Rowan (2009). The potential to narrow uncertainty in regional climate predictions. *Bulletin of the American Meteorological Society*, 90:1095–1107.

Hurtt, G. C., Chini, L. P., Frolking, S., Betts, R. a., Feddema, J., Fischer, G., Fisk, J. P., Hibbard, K., Houghton, R. a., Janetos, A., Jones, C. D., Kindermann, G., Kinoshita, T., Klein Goldewijk, K., Riahi, K., Shevliakova, E., Smith, S., Stehfest, E., Thomson, A., Thornton, P., van Vuuren, D. P., and Wang, Y. P. (2011). Harmonization of land-use scenarios for the period 1500-2100: 600 years of global gridded annual land-use transitions, wood harvest, and resulting secondary lands. *Climatic Change*, 109:117–161.

IPCC (2013). *Climate change 2013: The physical science basis. Contribution of working group I to the fifth assessment report of the intergovernmental panel on climate*

change. Cambridge University Press, Cambridge, United Kingdom and New York, NY, USA.

Kumar, S., Dirmeyer, P. a., Merwade, V., DelSole, T., Adams, J. M., and Niyogi, D. (2013). Land use/cover change impacts in CMIP5 climate simulations: A new methodology and 21st century challenges. *Journal of Geophysical Research: Atmospheres*, 118:6337–6353.

Lawrence, D. and Vandecar, K. (2014). Effects of tropical deforestation on climate and agriculture. *Nature Climate Change*, 5:27–36.

Lawrence, D. M., Hurtt, G. C., Arneth, A., Brovkin, V., Calvin, K. V., Jones, A. D., Jones, C. D., Lawrence, P. J., Noblet-ducoudré, N. D., Pongratz, J., and Seneviratne, S. I. (2016). The Land Use Model Intercomparison Project (LUMIP) contribution to CMIP6 : rationale and experimental design. *Geoscientific Model Development*, 9:2973–2998.

Le Quéré, C., Andrew, R. M., Canadell, J. G., Sitch, S., Ivar Korsbakken, J., Peters, G. P., Manning, A. C., Boden, T. A., Tans, P. P., Houghton, R. A., Keeling, R. F., Alin, S., Andrews, O. D., Anthoni, P., Barbero, L., Bopp, L., Chevallier, F., Chini, L. P., Ciais, P., Currie, K., Delire, C., Doney, S. C., Friedlingstein, P., Gkritzalis, T., Harris, I., Hauck, J., Haverd, V., Hoppema, M., Klein Goldewijk, K., Jain, A. K., Kato, E., Körtzinger, A., Landschützer, P., Lefèvre, N., Lenton, A., Lienert, S., Lombardozzi, D., Melton, J. R., Metzl, N., Millero, F., Monteiro, P. M., Munro, D. R., Nabel, J. E., Nakaoka, S. I., O'Brien, K., Olsen, A., Omar, A. M., Ono, T., Pierrot, D., Poulter, B., Rödenbeck, C., Salisbury, J., Schuster, U., Schwinger, J., Séférian, R., Skjelvan, I., Stocker, B. D., Sutton, A. J., Takahashi, T., Tian, H., Tilbrook, B., Van Der Laan-Luijkx, I. T., Van Der Werf, G. R., Viovy, N., Walker, A. P., Wiltshire, A. J., and Zaehle, S. (2016). Global carbon budget 2016. *Earth System Science Data*, 8:605–649.

Lee, X., Goulden, M. L., Hollinger, D. Y., Barr, A., Black, T. A., Bohrer, G., Bracho, R., Drake, B., Goldstein, A., Gu, L., Katul, G., Kolb, T., Law, B. E., Margolis, H., Meyers, T., Monson, R., Munger, W., Oren, R., Paw U, K. T., Richardson, A. D., Schmid, H. P., Staebler, R., Wofsy, S., and Zhao, L. (2011). Observed increase in local cooling effect of deforestation at higher latitudes. *Nature*, 479:384–387.

Lejeune, Q., Davin, E., Gudmundssohn, L., Winckler, J., and Seneviratne, S. (2017a). Historical deforestation increased the risk of heat extremes in northern mid-latitudes. *submitted*.

Lejeune, Q., Davin, E. L., Guillod, B. P., and Seneviratne, S. I. (2015). Influence of Amazonian deforestation on the future evolution of regional surface fluxes, circulation, surface temperature and precipitation. *Climate Dynamics*, 44:2769–2786.

Lejeune, Q., Seneviratne, S. I., and Davin, E. L. (2017b). Historical land-cover change impacts on climate: Comparative assessment of LUCID and CMIP5 multimodel experiments. *Journal of Climate*, 30:1439–1459.

Li, Y., de Noblet-Ducoudré, N., Davin, E. L., Zeng, N., Motesharrei, S., Li, S. C., and Kalnay, E. (2016). The role of spatial scale and background climate in the latitudinal temperature response to deforestation. *Earth System Dynamics Discussions*, 7:167–181.

Li, Y., Zhao, M., Motesharrei, S., Mu, Q., Kalnay, E., and Li, S. (2015). Local cooling and warming effects of forests based on satellite observations. *Nature Communications*, 6:1–8.

Lorenz, R. and Pitman, A. J. (2014). Effect of land-atmosphere coupling strength on impacts from Amazonian deforestation. *Geophysical Research Letters*, 41:5987–5995.

Luyssaert, S., Jammet, M., Stoy, P. C., Estel, S., Pongratz, J., Ceschia, E., Churkina, G., Don, A., Erb, K.-H., Ferlicoq, M., Gielen, B., Grünwald, T., Houghton, R. A., Klumpp, K., Knohl, A., Kolb, T., Kuemmerle, T., Laurila, T., Lohila, A., Loustau, D., McGrath, M. J., Meyfroidt, P., Moors, E. J., Naudts, K., Novick, K., Otto, J., Pilegaard, K., Pio, C. A., Rambal, S., Rebmann, C., Ryder, J., Suyker, A. E., Varlagin, A., Wattenbach, M., and Dolman, A. J. (2014). Land management and land-cover change have impacts of similar magnitude on surface temperature. *Nature Climate Change*, 4:389–393.

Mahlstein, I., Knutti, R., Solomon, S., and Portmann, R. W. (2011). Early onset of significant local warming in low latitude countries. *Environmental Research Letters*, 6:1–6.

Mahmood, R., Roger A. Pielke, S., Hubbard, K. G., Niyogi, D., Dirmeyer, P. A., McAlpine, C., Carleton, A. M., Hale, R., Gameda, S., Beltran-Przekurat, A., Baker, B., McNider, R., Legates, D. R., Shepherd, M., Du, J., Blanken, P. D., Frauenfeld, O. W., Nair, U. S., and Fall, S. (2014). Review - Land cover changes and their biogeophysical effects on climate. *International Journal of Climatology*, 34:929–953.

Malyshev, S., Shevliakova, E., Stouffer, R. J., and Pacala, S. W. (2015). Contrasting local versus regional effects of land-use-change-induced heterogeneity on historical climate: Analysis with the GFDL Earth system model. *Journal of Climate*, 28:5448–5469.

Moss, R., Edmonds, J. A., Hibbard, K. A., Manning, M. R., Rose, S. K., van Vuuren, D., Carter, T. R., Emori, S., Kainuma, M., Kram, T., Meehl, G. A., Mitchell, J. F. B., Nakicenovic, N., Riahi, K., Smith, S. J., Stouffer, R. J., and M., T. A. (2010). The next generation of scenarios for climate change research and assessment. *Nature*, 463:747–756.

Pitman, A. J., Avila, F. B., Abramowitz, G., Wang, Y. P., Phipps, S. J., and de Noblet-Ducoudré, N. (2011). Importance of background climate in determining impact of land-cover change on regional climate. *Nature Climate Change*, 1:472–475.

Pitman, A. J., de Noblet-Ducoudré, N., Cruz, F. T., Davin, E. L., Bonan, G. B., Brovkin, V., Claussen, M., Delire, C., Ganzeveld, L., Gayler, V., van den Hurk, B. J. J. M., Lawrence, P. J., van der Molen, M. K., Müller, C., Reick, C. H., Seneviratne, S. I., Strengers, B. J., and Voldoire, A. (2009). Uncertainties in climate responses to past land cover change: First results from the LUCID intercomparison study. *Geophysical Research Letters*, 36:6.

Pongratz, J., Reick, C., Raddatz, T., Claussen, M., and Caldera, K. (2011). Past land use decisions have increased mitigation potential of reforestation. *Geophys. Res. Lett.*, 38.

Pongratz, J., Reick, C. H., Raddatz, T., and Claussen, M. (2008). A reconstruction of global agricultural areas and land cover for the last millennium. *Global Biogeochemical Cycles*, 22:1–16.

Pongratz, J., Reick, C. H., Raddatz, T., and Claussen, M. (2010). Biogeophysical versus biogeochemical climate response to historical anthropogenic land cover change. *Geophys. Res. Lett.*, 37:1–5.

Rammig, A., Jupp, T., Thonicke, K., Tietjen, B., Heinke, J., Ostberg, S., Lucht, W., Cramer, W., and Cox, P. (2010). Estimating the risk of Amazonian forest dieback. *New Phytologist*, 187:694–706.

Reick, C. H., Raddatz, T., Brovkin, V., and Gayler, V. (2013). Representation of natural and anthropogenic land cover change in MPI-ESM. *Journal of Advances in Modeling Earth Systems*, 5:459–482.

Rotenberg, E. and Yakir, D. (2010). Contribution of semi-arid forests to the climate system. *Science*, 327:451–454.

Schneck, R., Reick, C. H., Pongratz, J., and Gayler, V. (2015). The mutual importance of anthropogenically and climate-induced changes in global vegetation cover for future land carbon emissions in the MPI-ESM CMIP5 simulations. *Global Biogeochem. Cycles*, 29:1816–1829.

Sitch, S., Huntingford, C., Gedney, N., Levy, P. E., Lomas, M., Piao, S. L., Betts, R., Ciais, P., Cox, P., Friedlingstein, P., Jones, C. D., Prentice, I. C., and Woodward, F. I. (2008). Evaluation of the terrestrial carbon cycle, future plant geography and climate-carbon cycle feedbacks using five Dynamic Global Vegetation Models (DGVMs). *Global Change Biology*, 14:2015–2039.

Sonntag, S., Pongratz, J., Reick, C. H., and Schmidt, H. (2016). Reforestation in a high-CO 2 world – Higher mitigation potential than expected , lower adaptation potential than hoped for. 43:1–8.

Staiger, H., Laschewski, G., and Graetz, A. (2011). The perceived temperature – a versatile index for the assessment of the human thermal environment. Part A: Scientific basics. *International Journal of Biometeorology*, 56:165–176.

Swann, A. L., Fung, I. Y., Levis, S., Bonan, G. B., and Doney, S. C. (2010). Changes in Arctic vegetation amplify high-latitude warming through the greenhouse effect. *Proceedings of the National Academy of Sciences*, 107:1295–1300.

Swann, A. L. S., Fung, I. Y., and Chiang, J. C. H. (2012). Mid-latitude afforestation shifts general circulation and tropical precipitation. *Proceedings of the National Academy of Sciences*, 109:712–716.

Teuling, A. J., Seneviratne, S. I., Stöckli, R., Reichstein, M., Moors, E., Ciais, P., Luyssaert, S., van den Hurk, B., Ammann, C., Bernhofer, C., Dellwik, E., Gianelle, D., Gielen, B., Grünwald, T., Klumpp, K., Montagnani, L., Moureaux, C., Sottocornola, M., and Wohlfahrt, G. (2010). Contrasting response of European forest and grassland energy exchange to heatwaves. *Nature Geoscience*, 3:722–727.

Teuling, A. J., Taylor, C. M., Meirink, J. F., Melsen, L. A., Miralles, D. G., van Heerwaarden, C. C., Vautard, R., Stegehuis, A. I., Nabuurs, G.-J., and de Arellano, J. V.-G. (2017). Observational evidence for cloud cover enhancement over western European forests. *Nature Communications*, 8:14065.

West, P. C., Narisma, G. T., Barford, C. C., Kucharik, C. J., and Foley, J. A. (2011). An alternative approach for quantifying climate regulation by ecosystems. *Frontiers in Ecology and the Environment*, 9:126–133.

Zhang, M., Lee, X., Yu, G., Han, S., Wang, H., Yan, J., Zhang, Y., Li, Y., Ohta, T., Hirano, T., Kim, J., Yoshifuji, N., and Wang, W. (2014a). Response of surface air temperature to small-scale land clearing across latitudes. *Environmental Research Letters*, 9(034002):7.

Zhang, W., Jansson, C., Miller, P. A., Smith, B., and Samuelsson, P. (2014b). Biogeophysical feedbacks enhance the arctic terrestrial carbon sink in regional earth system dynamics. *Biogeosciences*, 11:5503–5519.

Zwiers, F. W. and von Storch, H. (1995). Taking serial correlation into account in tests of the mean. *Journal of Climate*, 8(2):336–351.

Acronyms

CMIP5	Coupled Model Intercomparison Project, phase 5
CILCC	Climate–induced land cover change
DJF	Winter season
LAI	Leaf area index [m^2/m^2]
LE	Latent heat flux [W/m^2]
LCC	Land cover change (here mostly deforestation or afforestation)
LULCC	Land-use–induced land cover change
LUCID	"Land-Use and Climate, IDentification of robust impacts" project
LW	Surface longwave radiation
ECHAM6	Atmosphere model applied in this thesis
G	Ground heat flux
JJA	Summer season
JSBACH	Land surface model applied in this thesis
MPI-ESM	Earth system model applied in this thesis
PFT	Plant functional type
RCP	Representative concentration pathway
RMS	Root mean square
SEB	Surface energy balance
SSTs	Sea surface temperatures
SW	Surface shortwave radiation
T_{surf}	Surface temperature [K]
WARM	Influence of warming background climate on the locally induced changes in surface temperature

List of Figures

List of Tables

Ackownowledgements

I want to express great gratitude towards my highly motivated and brilliant principal advisor *Julia Pongratz* for providing both freedom and exceptional guidance throughout my PhD. Thank you for the high expectations, for great advice, networking opportunities and for teaching me to think positively about my work. I want to express great thanks to my Co-advisor *Christian Reick*, whose constructive and challenging feedback and lively discussions kept improving my manuscripts and my scientific thinking. I would like to thank *Uwe Schneider* for leading the panel meetings as my panel chair, for making his way to Julia's office on every panel meeting, and for providing scientific freedom. I would like to acknowledge *Inga Hense* and *Martin Claussen* for serving as commission members.

My thanks for fruitful scientific discussions go to the whole land department, in particular *Thomas Raddatz, Andreas Chlond and Juergen Bader*. Further, I want to say thank you for providing valuable feedback on various drafts to *Gitta Lasslop, Daniela Kracher*, all members of Dallas Murphy's writing course, *Quentin Lejeune, Sabine Egerer, Dirk Olonscheck, Raphaela Vogel, Sirsha Kalidindi,* and *Sebastian Sonntag*. Thanks to *Thomas Riddick* for valuable advice concerning the usage of the English language. I am grateful to the scientific programmers *Thomas Raddatz, Julia Nabel, Philipp de Vrese, Rainer Schnur* and *Veronika Gayler* and the guys from the CIS help desk for great technical support. Special thanks go to *Alexander Winkler* for showing me the beauty of Spyder and TeXstudio. Many thanks also to *Antje Weitz* and the IMPRS office for their cheerfulness and for great administrative support.

I would like to express my deep gratitude to all members of the "Forest Management in the Earth System" group for discussions and support. It has been a pleasure to be part of this vibrant working group. Thanks to *Sonia Seneviratne* and her group for providing insights into live and science at ETH Zurich during my one-week stay there, including the discussions with *Edouard Davin* and *Quentin Lejeune*.

I would like to thank *Sylvia Nyawira* and my other office mates, fellow PhD students, the games lunch group, and my friends for emotional support and making my time in Hamburg an enjoyable experience. I want to acknowledge the canteen cashier for providing free chocolate every Friday. Last buy not least I want to thank my family without which I could not even have started this thesis.

Aus dieser Dissertation hervorgegangene Vorveröffentlichungen

List of Publications

Winckler, J., C. H. Reick and J. Pongratz (2017), Robust identification of local biogeopysical effects of land cover change in a global climate model, J. Clim., **30**(3), 1159-1176, doi:10.1175/JCLI-D-16-0067.1.

Winckler, J., C. H. Reick and J. Pongratz (2017): Why does the locally induced temperature response to land cover change differ across scenarios?, Geophys. Res. Lett., **44**, 3833-3840, doi:10.1002/2017GL072519.

Eidesstattliche Versicherung
Declaration on Oath

Hiermit erkläre ich an Eides statt, dass ich die vorliegende Dissertationsschrift selbst verfasst und keine anderen als die angegebenen Quellen und Hilfsmittel benutzt habe.

I hereby declare, on oath, that I have written the present dissertation by myself and have not used other than the acknowledged resources and aids.

Hamburg, den 5. Dezember 2017